2012-01-01

# Constraints On The Structure Of The Border Ranges Fault System, South-Central Alaska From Integrated 3d Inversion Of Gravity/magnetic Data

Niti Mankhemthong
*University of Texas at El Paso*, niti.ace@gmail.com

# CONSTRAINTS ON THE STRUCTURE OF THE BORDER RANGES FAULT SYSTEM, SOUTH-CENTRAL ALASKA FROM INTEGRATED 3D INVERSION OF GRAVITY/MAGNETIC DATA

NITI MANKHEMTHONG

Department of Geological Sciences

APPROVED:

Diane I. Doser, Ph.D., Chair

Laura F. Serpa, Ph.D.

Terry L. Pavlis, Ph.D.

Aaron A. Velasco, Ph.D.

Eric A. Hagedorn, Ph.D.

Benjamin C. Flores, Ph.D.
Dean of the Graduate School

# CONSTRAINTS ON THE STRUCTURE OF THE BORDER RANGES FAULT SYSTEM, SOUTH-CENTRAL ALASKA FROM INTEGRATED 3D INVERSION OF GRAVITY/MAGNETIC DATA

by

NITI MANKHEMTHONG, M.S., B.S.

DISSERTATION

Presented to the Faculty of the Graduate School of

The University of Texas at El Paso

in Partial Fulfillment

of the Requirements

for the Degree of

DOCTOR OF PHILOSOPHY

Department of Geological Sciences

THE UNIVERSITY OF TEXAS AT EL PASO

December 2012

## Acknowledgements

It is the great pleasure to acknowledge Dr. Diane Doser, my graduate advisor. She proposed the research project of the investigation of the Border Ranges fault system in south-central Alaska, and offered me an opportunity to work on it. She is a great advisor giving me beneficial advice and suggestions to complete the entire dissertation and the professional publications, as well as editing my writing. Dr. Doser is my role model for my future career.

I am grateful to Dr. Terry Pavlis, Dr. Laura Serpa, Dr. Aaron Velasco, and Dr. Eric Hagedorn all on my dissertation committee, for helpful guidance and suggestions; Dr. Peter Haeussler, Dr. Mark Baker, and Rolando Cardenas, for discussions and support related to the geological background and geophysical modeling, and Dr. Gary Fuis, Dr. Richard Saltus, Dr. Dwain Butler, and Dr. Benjamin Drenth for reviewing my submitted papers. I wish to acknowledge Dr. Gary Oppliger who first taught me the fundamentals of the gravity survey method, and all faculty from the University of Texas at El Paso, the University of Nevada, Reno, and Chiang Mai University who have taught me the subjects of geology and geophysics from basic to advanced levels.

I am thankful to Dr. Mark Baker, Galen Kaip, Brian Eslick, Slade Jones, and Pawan Budhathoki for helping collect gravity data in 2009, 2010, and 2011, and Dr. Haeussler's family for housing the field crews. I would like to thank Dr. Musa Hussein, Dr. Steve Harder, Dr. Raed Aldori, Ezer Patlan, Carlos Montana, and Nisa Rhodes, for advice regarding the GIS, computer and geophysical modeling software problems and all UTEP staff from the Department of Geological Sciences, the Graduate School, and the Office of International Programs for support and help.

I also acknowledge the support of the University of Texas at El Paso, the Royal Thai Government, the American Chemical Society's Petroleum Research Fund, the Society for Advancement of Chicanos and Native Americans in Science, the American Geophysical Union, and the Geological Society of America for scholarships, teaching and research assistantships during the four years of my

Ph.D. studies. A very special thanks goes to all families, colleagues, and friends from the USA and Thailand that have greatly supported me and my work. I thank you all.

Niti Mankhemthong

December, 2012

# Abstract

I use updated gravity data, available aeromagnetic data, and other geophysical information as constraints to develop 2D and 3D structural models of density and magnetic susceptibility to better locate and determine the shape of the Border Ranges fault system (BRFS), the Border Range ultramafic and mafic assemblages and other forearc-arc boundary structures in south-central Alaska, that have previously been studied in only limited detail. There are three geophysical research projects that form the chapters of the dissertation. First, I estimated near-surface density variations in the central Kenai Peninsula based on the adaptation of the Nettleton (1939)-Parasnis (1952) method using Tarantola and Valette's (1982) inversion formulations. Results from computations showed reasonable densities and density uncertainties for regions along both sides of the fault trace. These density estimations were then used as one of several available datasets used for surface density constraints, along with other data, for the next study that performed 2D integrated gravity and magnetic modeling. In the second study, I constructed four 2D integrated density-magnetic models to determine the shape of the BRFS and other major geological structures using the GM-SYS software packages. The results helped define the extent of a serpentinized body and underplated sediments and I hypothesized about how these structures were formed. Lastly, I tested and constructed a 3D block model of density over the region of the Border Ranges fault system and the Border Range ultramafic and mafic assemblage (BRUMA). This simple 3D model was inverted and used to further examine the geometry of the BRFS and BRUMA. These results show a reasonable fit of observed and calculated free air gravity based on simple density model. The next step will be to construct more realistic complex geometrical bodies to better explore plausible subsurface geometries for the region.

# Table of Contents

# SECTION 1

## Practical Estimation of Near Surface Bulk Density Variations across the Border Ranges Fault System, Central Kenai Peninsula, Alaska.

*(Paper submitted to Journal)*

*Niti Mankhemthong[1], Diane I. Doser[1], Mark R. Baker[2]*
*[1]Department of Geological Sciences, University of Texas at El Paso, El Paso, TX 79968-0555*
*[2]Geomedia Research and Development, 6040 S. Strahan Rd., El Paso, TX 79932-1712*

### 1.1 ABSTRACT

We demonstrate a near-surface density estimation approach in an area without exposed outcrop or where outcrop occurrences do not adequately represent the subsurface rock densities based on the Nettleton (1939)-Parasnis (1952) technique as extended by Rao and Murty (1973). We applied this technique in the central Kenai Peninsula, Alaska where the region is cut by a major fault zone, the Border Ranges fault system that juxtaposes two terranes with greatly varying geological/geophysical properties. The Kenai Peninsula region can be generally divided into two different geologic settings: recent fluvial and glacial deposits of the Cook Inlet basin to the west and accreted metamorphic terranes of the Kenai Mountains to the east. Our study region includes glacial cover, deep lakes, and large topographically-driven gravity gradients between the Kenai Mountains and Cook Inlet. We selected 11 gravity loops from ~580 gravity points we collected in 2009, which have 10-20 gravity points per loop; nine loops (A to I) are located in the Quaternary glacial and alluvial deposits and two loops (J and K) are in Cretaceous metamorphic rocks of the Kenai Mountains. Inversion of the free air anomaly data gave estimates of near surface rock densities and their associated uncertainties. Our inversion results are comparable to values obtained from density logs in the Cook Inlet basin ranging from 1640 to 2600 kg/m$^3$ with an average uncertainty of 120 kg/m$^3$. Estimated densities for the accreted metamorphic terrane in the eastern peninsula of 2890±20 and 2860±10 kg/m$^3$ are slightly higher than measured densities from hand rock samples.

## 1.2 INTRODUCTION

Bulk density is a critical parameter needed to study the spatial distribution and extent of subsurface structures. Density can be estimated independently either from outcrop samples, well samples, or well logs, or far less uniquely, from analysis of the gravity field. Field samples tend to have a bias toward lower values of density because they are more weathered, less fluid-saturated, or otherwise unrepresentative of the overall density. Drilling samples and well logs provide accurate and detailed information from well-consolidated strata containing economic targets, but this information is seldom available for shallow, unconsolidated strata, or areas that do not contain deposits of economic interest.

In most places, gravity measurements themselves are the only information we have on near-surface density values and distributions. Nettleton (1939) originally pointed out that the simple Bouguer anomaly over short-scale terrain features should approach zero, if the correct subsurface density is applied in a local survey. Parasnis (1952) generalized this analysis to estimate density from a least squares line-fit between density and topography. Rao and Murty (1973) introduced the concept that Parasnis' estimate could be improved with an estimate of a planar regional anomaly.

There are several important assumptions underlying the Nettleton-Parasnis technique to estimate near-surface density from topography. First, the technique assumes that the density causing the terrain is uniform. Density uniformity is nearly impossible, as topography is usually associated with property contrasts. Second, Rao and Murty's extension assumes the gradient is linear and is not associated with shallow density variations. The assumptions of gradient linearity and deep causative source are more frequently satisfied if we use a data set with a small geographic extent. Third, the Nettleton-Parsnis method assumes the local topography is approximated by an infinite Bouguer slab.

We present a spreadsheet template (available from the authors upon request) implementation of this method where we simultaneously estimate density, and the slope coefficients of the planar anomaly. Implementing this as a generalized linear inverse problem lets us estimate solution uncertainties on these

values based on measurement accuracy, fit quality, and non-uniqueness in the model. In this implementation, a large uncertainty in the density estimate is a guarantee of inconsistency, and can arise from noisy observations, non-uniform density in the survey area, or non-planarity in the regional gravity field. A small solution uncertainty implies consistency, but does not guarantee accuracy.

We applied the analysis technique to gravity data collected from the eastern shore of Cook Inlet across the Border Ranges fault system to the Kenai Mountains in the central Kenai Peninsula. Free air gravity anomaly data were used in the inversion process. Density estimates from the spreadsheet were compared to existing density estimates obtained from density logs and rock outcrop samples.

## 1.3 GEOLOGY OF CENTRAL KENAI PENINSULA

The Border Ranges fault system (BRFS) forms an unexposed series of en echelon normal fault traces across the central Kenai Peninsula, Alaska (Haeussler and Saltus, 2011). The BRFS represents the arc-forearc boundary of the Alaska-Aleutian arc and separates the Cretaceous accretionary complex of the Kenai Mountains from younger sediments of the Cook Inlet basin (Fig. 1.1). An abrupt topographic change supports recent movement along the BRFS, maintaining the high topography in a region of active glacial and fluvial erosion (Pavlis and Roeske, 2007). We collected gravity data along several transects crossing the BRFS (Fig. 1.1).

The current topography of Cook Inlet basin results from multiple glaciations during the Holocene and Pleistocene (Reger and Pinney, 1997), recent fluvial processes (Swenson, 1997), and folding related to forearc compression (Haeussler *et al*., 2000). The recent glacial and fluvial deposits overlie the Sterling formation of the Kenai Group (Swenson, 1997). Borehole data indicate the Sterling Formation consists of cross-bedded and massive sandstones and interbedded siltstones and claystones (Haeussler *et al.*, 2000).

The Kenai Mountains form part of the Chugach terrane, an uplifted accretionary complex mainly emplaced by subduction during the Late Cretaceous (Little and Naeser, 1989). The Chugach terrane in

our study area can be divided into two major lithotectonic assemblages: a mélange of original sedimentary and volcanic rocks, and metasedimentary rocks that have been thrust beneath the mélange along the Eagle River thrust fault system (Fig. 1.1) (Plafker *et al*., 1994; Little and Naeser, 1989). Our gravity transects were selected to sample both the mélange and the metasedimentary units as well as to cross over the BRFS.

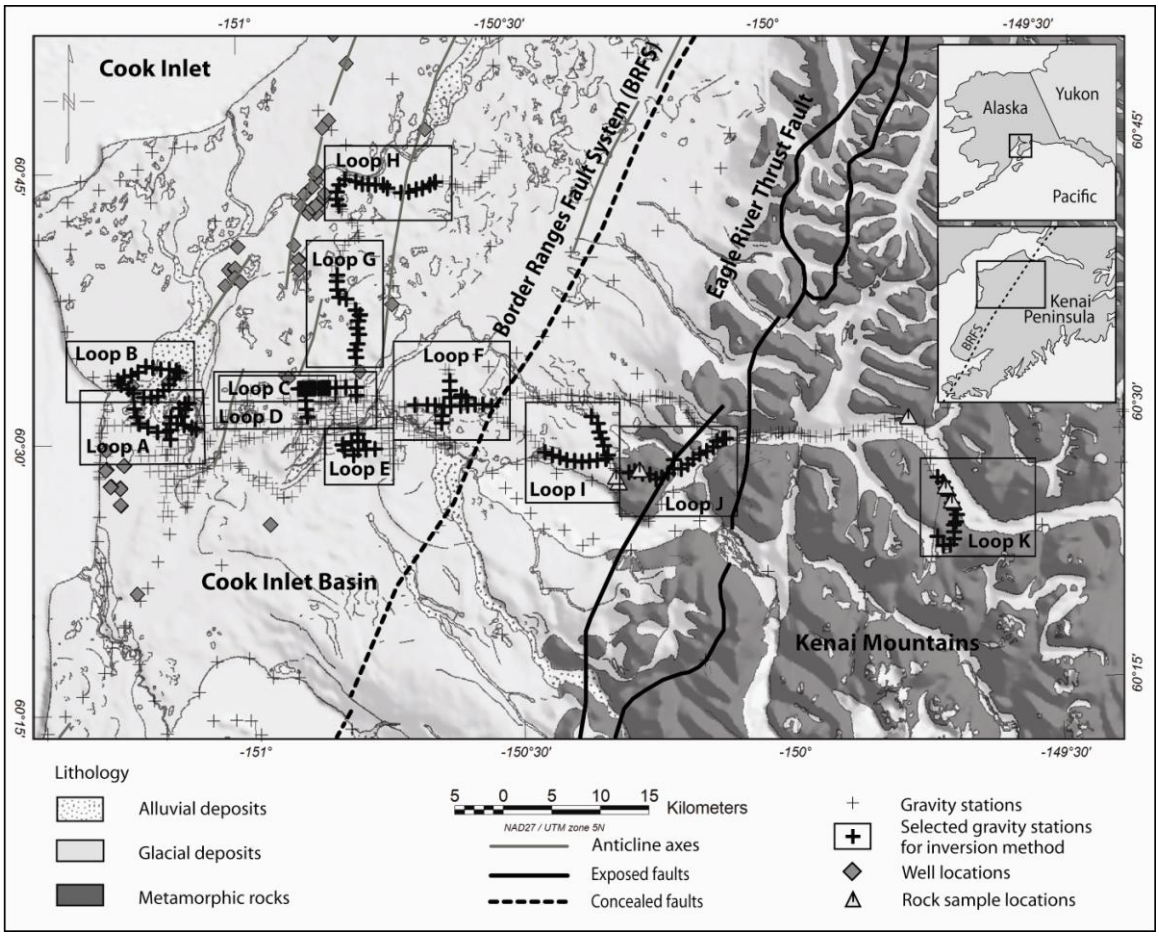


Figure 1.1: Simplified geologic map of the central Kenai Peninsula (modified from Wilson et al., 2009) showing locations of gravity measurements, well log data, and rock samples. Fault and fold data are from Haeussler et al. (2000).

## 1.3 DATA COLLECTION AND REDUCTION

A total of 580 gravity stations were collected within the central Kenai Peninsula. Measurements were acquired with a Lacoste & Romberg Model G gravimeter. Associated elevation and coordinate control were collected by a GB-100 GPS receiver with processing to achieve around 5 cm or better elevation control. The errors associated with readings taken by this gravity meter include those due to reading resolution, repeatability, and non-linear instrument drift. The nulling dial has an accuracy of 0.01 mGal. The repeatability is approximately 0.01-0.03 mGal based on numerous readings at base stations during the data acquisition stage. In addition, gravimeter drift and tidal effects from field testing are estimated to range from 0.005 to 0.04 mGal/min. We estimate the data precision is <0.3 mGal at the highest noise sites located on loose sediments.

Eleven gravity survey loops (A to K) were selected to determine the variations in surface density (Fig. 1.1). Loops J and K are located on Cretaceous metamorphic rocks of the Kenai Mountains, while Loop A to Loop I were collected on Quaternary glacial and fluvial deposits of Cook Inlet basin. The amount of gravity data collected and station distribution per loop were based on survey designs, station interval, and topographic conditions, and ranged from around 10-20 stations per loop. The survey loops were closed on local base stations every several hours. These local survey bases were tied daily into one of several regional base stations, which were tied with absolute gravity stations in Cooper Landing and Anchorage.

We compared our estimates of bulk densities to density log values in basin deposits and to density measurements of hand samples of metamorphic rocks of the Kenai Mountains. Approximately 20 well logs that had density measurements were selected for subsurface density determinations. Due to lack of well data, no comparison of results could be made for Loops G, H, and I (Fig. 1.1). Bulk density values for the Cretaceous metamorphic rock units were determined from eight selected rock hand samples.

The free air gravity anomaly values observed over the Cook Inlet basin and the Kenai Mountains range between -150 to 30 mGal (Fig. 1.2) with uncertainties of 0.1 to 0.4 mGal. Loop A, located in the Cook Inlet basin, contains the local minimum anomaly (-127 mGal). The free air anomaly increases toward the Kenai Mountains with an approximate gradient of 2 to 5 mGal/km and reaches a local maximum anomaly on Loop K (9.7 mGal). The free air anomaly variation in each loop is less than 10 mGal, except in Loops H and K that have gravity anomaly variations up to 27 and 40 mGal, respectively.

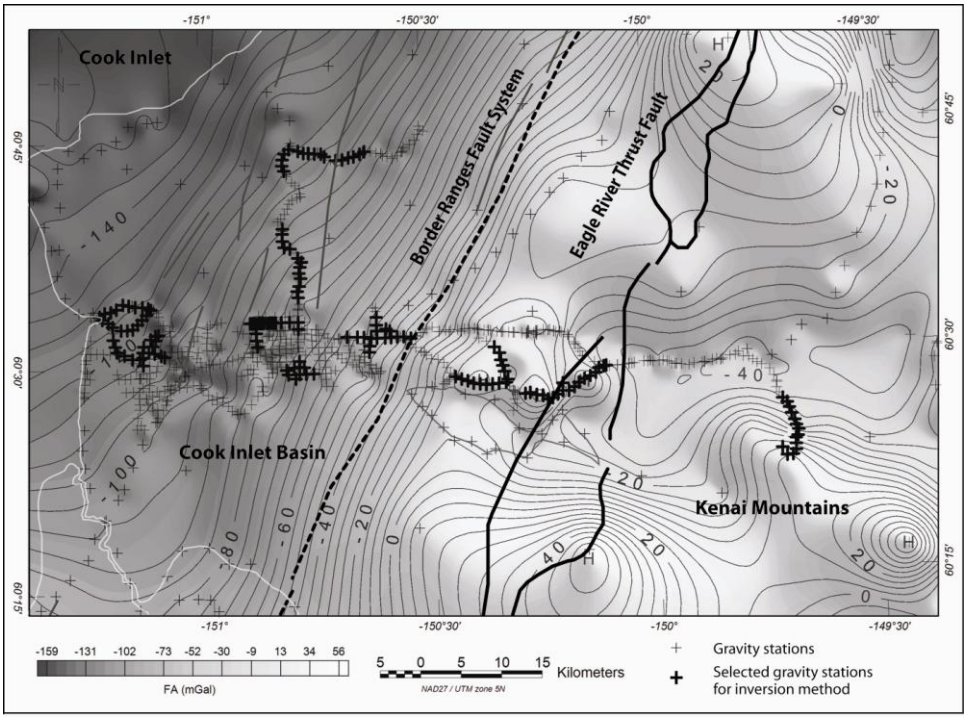


Figure 1.2: Free air gravity anomalies on the central Kenai Peninsula contoured at a 5 mGal contour interval. White line indicates the shoreline.

## 1.4 FORMULATIONS OF NETTLETON AND PARASNIS DENSITY DETERMINATION METHODS

Nettleton's method is based on the observation that over an area of constant density no terrain correlated gravity anomalies should remain after applying the Bouguer correction (Nettleton 1939 and Papp, 2009). If S and R are gravity stations at two different locations, where R is considered to be a reference station and S is any station in a station loop, then the equations for the simple Bouguer anomaly (SBA) at the two stations are:

$$SBA_S = G_{obS} - G_{lS} + G_{fcS} - G_{bcS} \quad (1)$$

$$SBA_R = G_{obR} - G_{lR} + G_{fcR} - G_{bcR} \quad (2)$$

Where,

SBA = Simple gravity Bouguer anomaly

$G_{ob}$= observed gravity

$G_l$ = Latitude correction

$G_{fc}$ = Free air correction (0.3086 mGal/m)

$G_{bc}$ = Bouguer slab correction (0.0419ρ mGal/m) where ρ is rock density in g/cm$^3$

The relative Bouguer gravity anomaly (ΔSBA) between the reference station and any station is

$$SBA_S - SBA_R = \Delta SBA = \Delta G_{ob} - \Delta G_l + \Delta G_{fc} - \Delta G_{bc} \quad (3)$$

If the Bouguer slab correction ($\Delta G_{bc}$) is ignored, Eq. (3) is equivalent to the free air anomaly formula:

$$\Delta FA = \Delta G_{ob} - \Delta G_l + \Delta G_{fc} \quad (4)$$

Where ΔFA = Relative gravity free air anomaly.

From Eq. (3); $\Delta G_{ob} - \Delta G_l + \Delta G_{fc} - \Delta SBA = \Delta G_{bc}$

$$\Delta FA - \Delta SBA = \Delta G_{bc} \quad (5)$$

According to Nettleton's observation (1939), the relative simple Bouguer anomaly (ΔSBA) should go to zero if the correct subsurface density is applied during the Bouguer slab correction.

Then from Eq. (5); $\Delta FA = \Delta G_{bc}$

$$\text{or } \Delta FA = 0.0419\rho\Delta h \quad (6)$$

Where $\Delta h$ = relative elevation change with respect to the reference station (R).

Parasnis' method is based on the fact that the Bouguer anomaly can be expressed as an equation of the form of "y = mx + b" (White, 2007). If the region between the two stations is assumed to be homogeneous in topographic relief and density ($\rho$), Eq. (6) represents a straight line with classic form of $y = mx$, where the $\Delta FA$ are the y-values and $0.0419\Delta h$ are the x-values. The calculated slope (m) corresponds to the average bulk density ($\rho$) of the near surface rocks or sediments. The Nettleton and Parasnis methods can be used to determine near surface density, if we consider a small enough distance between gravity stations so that deeper regional gravity effects do not dominate.

Rao and Murty (1973) noted that the Parasnis' method ignored the existence of any regional gravity field. They considered the existence of uniform regional gradients in the x and y directions, with a new model where $\alpha\Delta x$ and $\beta\Delta y$ are added to Eq. (6). Here $\Delta x$ and $\Delta y$ are the distances between the gravity stations and a reference station in the x and y directions, respectively, and $\alpha$ and $\beta$ are related to unknown regional gradients that are uniform along the profiles of the two points in mGal/km unit (Papp, 2009). After reducing the regional gravity, the residual gravity with respect to near surface masses becomes

$$\Delta FA = \alpha\Delta x + \beta\Delta y + 0.0419\rho\Delta h \quad (7)$$

$\Delta x$, $\Delta y$, $\Delta h$, and $\Delta FA$ are known parameters and $\alpha$, $\beta$, and $\rho$ are unknown parameters, with $\rho$ representing the density of the subsurface. Note that Eq. (7) is still a linear function of the form of "d = ax + by + cz". Thus, a least squares inversion technique can be used to determine the unknown quantities.

## 1.5 DEVELOPMENT OF INVERSION SCHEME

As described in the previous section, the unknowns in Eq. (7) can be determined using a least squares inversion method. We begin by formulating the problem in matrix form.

$$\mathbf{y} = A \tag{8}$$

Where **y** is the vector of reduced ΔFA, *A* is a matrix of perfectly known parameters containing Δx, Δy, and Δh, and represents a vector of the unknowns (α, β, and ρ).

Following the technique of Jackson (1979), Eq. (8) is weighted by the diagonal matrix of the estimated covariance uncertainties ($C_a^{-1}$) of given free air anomalies, which are approximately 0.1-0.4 mGal.

$$C_a^{-1}\mathbf{y} = C_a^{-1} A \tag{9}$$

Then, we multiply both sides by a transposed matrix ($A^T$) of *A* to begin to formulate the least squares solution.

$$A^T C_a^{-1}\mathbf{y} = A^T C_a^{-1} A \tag{10}$$

Following the method of Tarantola and Valette (1982), let $C_p^{-1}$ be the expected covariances of the unknowns. We assumed the covariances of the near surface densities were equal to the covariances of given densities from rock sample and density log measurements (~0.1 g/cm$^3$). is the vector of expected unknowns of *a priori* information. In an ideal situation, should be equal to the calculated . Thus

$$C_p^{-1} \quad - C_p^{-1} \quad = 0 \tag{11}$$

And adding Eq. (10) to Eq. (11) gives

$$A^T C_a^{-1}\mathbf{y} = A^T C_a^{-1} A \quad + C_p^{-1} \quad - C_p^{-1} \tag{12}$$

Rearranging terms we obtain

$$A^T C_a^{-1}\mathbf{y} + C_p^{-1} \quad = \quad (A^T C_a^{-1} A + C_p^{-1}) \tag{13}$$

Now, we can solve for

$$= (A^T C_a^{-1} A + C_p^{-1})^{-1}(A^T C_a^{-1}\mathbf{y} + C_p^{-1} \quad ) \tag{14}$$

Once we determine an our estimated *a posteriori* ( ) vector of unknowns, we can estimate our free air anomaly as

$$A \quad = \tag{15}$$

Following Jackson (1979; equation 20) the *a posteriori* covariance matrix, $C$ , is given by:

$$C \; = (HA - I)\, C_p\, (HA - I)^T + HC_aH^T \tag{16}$$

Where

$$\mathrm{H} = (A^T C_a^{-1} A + C_p^{-1})^{-1} A^T C_a \tag{17}$$

The square roots of the diagonal terms of the *a posteriori* covariance matrix ($\sigma_{\alpha\alpha}$, $\sigma_{\beta\beta}$, and $\sigma_{\rho\rho}$) of the model give the standard deviations (Fig. 1.3 and Table 1.1), where the $\sigma_{\rho\rho}$ are the uncertainties of the calculated densities ( ). We implemented this inversion using a popular spreadsheet software package. Note that we used an *a priori* uncertainty of 1 mgal for our observed gravity values in the inversion. This larger than the values we estimated from loop closures and repeated readings at individual stations. This higher *a priori* uncertainty reflects components of uncertainty associated with model assumptions including: 1) the Bouguer slab approximation, 2) uniform densities within the loop, and 3) linear gradients only arising from deep structure.

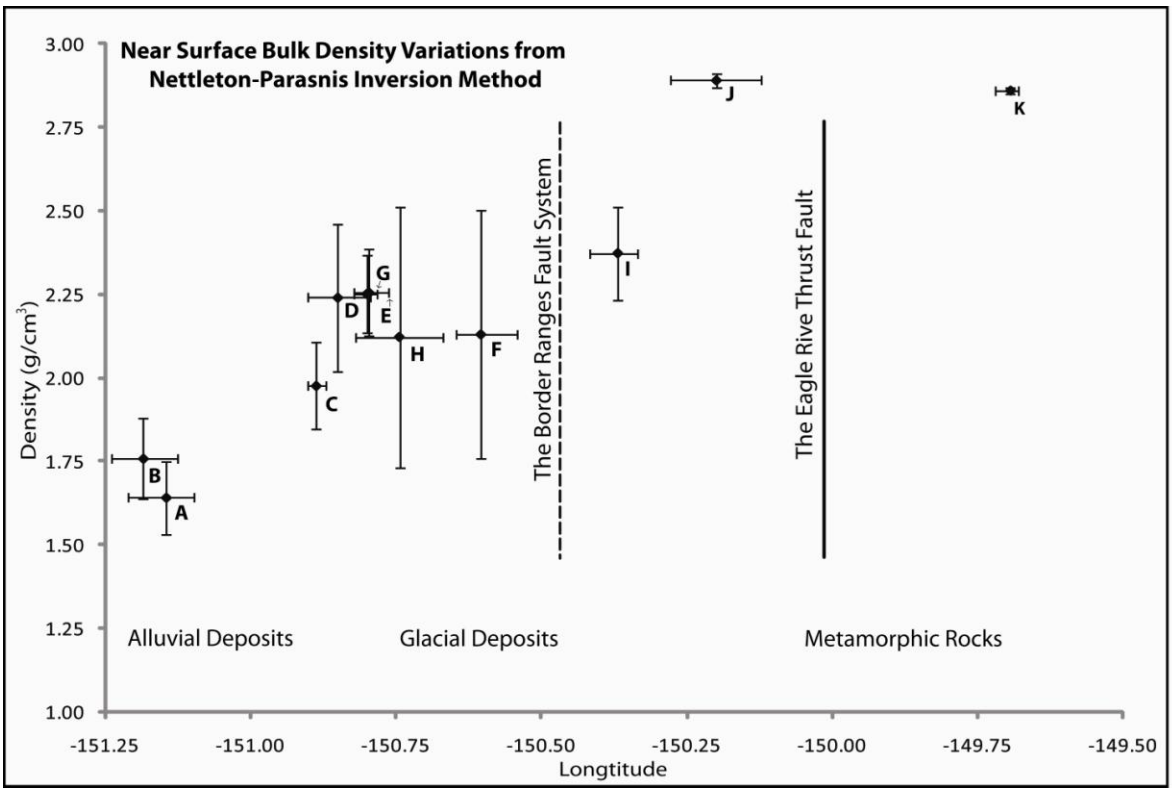


Figure 1.3: Estimates of near surface bulk density. Vertical bars indicate density uncertainties and horizontal bars the longitudinal extent of each gravity loop. The density uncertainties obtained from the model covariance matrix given in Eq. (16).

Table 1.1: Summary of calculated densities (ρ), uncertainties and standard deviations of gravity measurement distributions among selected gravity loops.

| Loop | Geology | Latitude | | Longitude | | Measured ρ | Estimated ρ | | Estimated σ | |
|---|---|---|---|---|---|---|---|---|---|---|
| | | Mean | STDV | Mean | STDV | (g/cm$^3$) | (g/cm$^3$) | | (g/cm$^3$) | |
| A | Alluvial | 60.519 | 0.010 | -151.145 | 0.036 | 2.10-2.20[*] | 1.64 | 1.70[!] | 0.11 | 0.12[!] |
| B | | 60.557 | 0.010 | -151.184 | 0.037 | | 1.76 | | 0.12 | |
| C | Glacial | 60.546 | 0.002 | -150.888 | 0.010 | | 1.98 | | 0.13 | |
| D | | 60.542 | 0.008 | -150.850 | 0.027 | | 2.24 | | 0.22 | |
| E | | 60.491 | 0.006 | -150.797 | 0.019 | | 2.25 | | 0.13 | |
| F | | 60.528 | 0.009 | -150.605 | 0.031 | 2.10-2.20[*] | 2.13 | 2.19[!] | 0.37 | 0.21[!] |
| G | | 60.612 | 0.025 | -150.801 | 0.017 | | 2.25 | | 0.11 | |
| H | | 60.726 | 0.007 | -150.745 | 0.051 | | 2.12 | | 0.39 | |
| I | | 60.482 | 0.015 | -150.370 | 0.031 | | 2.37 | | 0.14 | |
| J | Metamorphic | 60.467 | 0.018 | -150.200 | 0.047 | 2.72-2.73[#] | | [!] | | [!] |
| K | | 60.402 | 0.020 | -149.695 | 0.011 | | | | | |

[*] Determined from density log analysis.
[#] Measured from hand rock samples.
[!] Average densities (ρ) and standard deviations (σ).

## 1.6 INVERSION RESULTS

Based on the results and previous geological studies, the calculated densities are divided into four groups. The first group consists of analysis of gravity group Loops A and B. Both are located close to the mouth of the Kenai River, which is mainly covered by Quaternary alluvial and fluvial deposits. The calculated densities are 1.64±0.11 and 1.76±0.12 g/cm$^3$, respectively (Fig. 1.3). These results represent the lowest densities determined in this study due to low amount of compaction in these very young deposits.

Six density loops (Loops C, D, E, F, G, and H) are located in the Cook Inlet basin west of the concealed BRFS (Fig. 1.1). The lowland elevation ranges between 25 and 300 m with a very gentle slope from east to the west. Low-density sediments deposited during several glacial advances and retreats in the Quaternary dominate the surface geology. Calculated densities for the inversion method vary from 1.98±0.13 to 2.25±0.13 g/cm$^3$ (Fig. 1.3), which are higher than the calculated density from the fluvial deposit group, but equivalent to frequently used density values for sediments.

Loop I is also located in the transition zone between the Cook Inlet basin and the Kenai Mountains. The BRFS separates this loop from other loops located over Quaternary glacial deposits. The density for Loop I from the inversion method is 2.37±0.14 g/cm$^3$ (Fig. 1.3), which is higher than the previously discussed loops over glacial deposits. The greater densities indicate effects from shallowly buried metamorphic rocks.

Gravity Loops J and K were recorded over the metamorphic rocks of the Kenai Mountains. Loop J is located on the mélange assemblage and Loop K is located on metasedimentary rocks, which are separated by the Eagle River Thrust fault system. Densities obtained for Loops J and K are 2.89±0.02 and 2.86±0.01 g/cm$^3$, respectively (Fig.1.3).

## 1.7 DENSITY UNCERTAINTIES AND GRAVITY STATION DISTRIBUTIONS

Density uncertainties in Fig. 1.3 and Table 1.1 show the effects of both geologic complexity and elevation changes. Metamorphic terranes show the lowest uncertainty, where lithology is fairly uniform although elevation change is large (~500 to 900 m).

The alluvial and fluvial density estimates are made in fairly uniform geologic units of recent fine grained deposits of the Kenai River. Elevation differences in this area are less than 15 m. Loop A crosses the river banks and active channel of the Kenai River, so the low values reflect conditions with lowest compaction and partial water saturation. Loop B covers older alluvial terranes with more compaction. Glacial deposits show the largest ranges of variation and uncertainties, which is not unexpected given the variations in grain sizes and lithologies of these deposits. Loop C is a small detailed survey that is a subset of Loop D (Fig. 1.1). It samples small elevation changes (~10 m) in an outwash plain that appears to lie above the water table, as reflected in its lower density and uncertainty. Loop D samples a larger area and greater elevation changes (~30 m) with more water saturated material. Loops H and F are oriented across terminal moraines and sample unsaturated moraines, saturated moraines, and outwash (Fig. 1.1). These show the largest uncertainties. Loops G and E generally sample along the strike of moraines and show lower uncertainties consistent with a more uniform geology and saturation.

## 1.8 DENSITY RESULTS AND INTERPRETATIONS FROM THE WELL LOGS AND ROCK SAMPLE MEASUREMENTS

Density log measurements from approximately 20 well logs were selected for subsurface density determinations. All wells analyzed are located near gravity stations. Density log data are not available for near surface sediment; the shallowest density log starts at ~700 m depth. Two formations with markedly different densities appear on the logs. The upper formation has density values ranging between 2.10 and 2.20 g/cm$^3$ and represent clastic sedimentary rocks of the Sterling Formation (Table 1.1) that lie beneath the surficial glacial deposits. These values are similar to results from Loops C to H. The

lower formation has densities of 2.40-2.50 g/cm$^3$ and these rocks are not exposed in our survey area (Table 1.1).

Eight rock hand samples were collected at four outcrops in the Kenai Mountains for density measurements. The samples are classified as low grade metamorphic rocks. All of the collected samples were from outcrops located close to gravity stations (Fig. 1.1). Average bulk densities for the two units are equal to 2.7 ±0.05 g/cm$^3$ (Table 1.1). These bulk densities are lower than the densities calculated from the inversion method for the same rock units. This is expected for hand samples that are dried, more fractured and more weathered than rocks at depth. Another possibility is that the greater densities estimated from Nettleton-Parasnis' method may be related to the effect of sediment fill in the valleys that were not accounted for in the inversion method. For gravity data collected in extreme mountain topography we would normally expect the gravity anomaly to be lower than that predicted by the Bouguer slab, and this should consequently lead to a lower density estimate. However, if valley bases are eroded and filled by a lower density stream or lake, the change in gravity for a given topography would be increased, leading to an anomalously high density estimate. We will be conducting a complete 3-D inversion for density in a future study and can then better determine how these effects biased our results.

## 1.9 CONCLUSIONS

Estimates of near surface densities range from 1.64±0.11 to 2.25±0.13 g/cm$^3$ over gravity anomaly lows in the Cook Inlet basin and increase to 2.88±0.02 g/cm$^3$ over anomaly highs in the Kenai Mountains. The greater density (2.37±0.14 g/cm$^3$) on the eastern basin rim (Loop I) indicates effects from shallowly buried metamorphic rocks. The near surface densities determined from the inversion method are reasonable when compared to other two density determination methods: 1) rock hand samples and 2) density log analysis. The calculated density uncertainties reflect the complexities of near surface lithology beneath selected gravity stations and provide valuable information on the range of

acceptable densities that can be used in further 2D and 3D forward or inverse modeling in a region. More homogeneous rocks over the mountains gave significantly lower average uncertainty values compared to values over young sediment deposits. Thus, near surface density determinations based on the Nettleton-Parasnis inversion method can be utilized for estimating representative surface densities where no outcrop or log data may exist. We also note the inversion can be implemented using one of several inexpensive spreadsheet software packages.

## 1.10 ACKNOWLEDGEMENTS

The authors thank G. Kaip, B. Eslick, and S. Jones for helping collect gravity data in 2009 and 2010, and P. Haeussler for discussions related to the geophysical background of Kenai Peninsula. We thank reviewers D. Butler and B. Drenth for their many comments and suggestions that helped improved this manuscript. This research is funded through the American Chemical Society's Petroleum Research Fund (grant no. 48312-AC8 to D. I. Doser).

## 1.11 REFERENCES

Haeussler, P.J., and Saltus, R.W., 2011, Location and extent of Tertiary structures in Cook Inlet Basin, Alaska, and mantle dynamics that focus deformation and subsidence: *in* Studies by the U.S. Geological Survey in Alaska 2008–2009, Dumoulin, J.A., and Galloway, J.P. (ed.), U.S. Geological Survey Professional Paper, **1776–D,** pp. 26.

Haeussler, P.J., Bruhn, R.L., and Pratt, T.L., 2000, Potential seismic hazards and tectonics of the upper Cook Inlet Basin, Alaska, based on analysis of Pliocene and younger deformation: Geological Society of America Bulletin, **9**, 1414-1429.

Jackson, D.D., 1979, The use of *a priori* data to resolve non-uniqueness in linear inversion: Geophysical Journal of the Royal Astronomical Society, **57**, 137-157.

Little, T.A., and Naeser, C.W., 1989, Tertiary tectonics of Border Ranges fault system, Chugach Mountains, Alaska: deformation and uplift in a forearc setting: Journal of Geophysical Research, **B4**, 4333-4359.

Nettleton L.L., 1939, Determination of density for reduction of gravimeter observations, Geophysics, **4**, 176-183.

Papp, G., 2009, Simultaneous determination of terrain correction and local average topographic density, Acta Geodaetica et Geophysica Hungarica, **44**, 191-202.

Parasnis, D.S., 1952, A study of rock densities in English Midlands: Geophysical Journal International, **6**, 252-271.

Pavlis, T.L., and Roeske, S.M., 2007, The Border Ranges fault system, southern Alaska: *in* Tectonic growth of a collisional continental margin: Crustal evolution of south-central Alaska, Ridgway, K.D., *et al*. (ed.), Geological Society of America Special Paper, **431**, 95–128.

Plafker, G., Moore, J.C., and Winkler, G. R., 1994, Geology of the southern Alaska margin: *in* The geology of Alaska, Plafker, G. and Berg, H.C. (ed.), Geological Society of America, The Geology of North America, **G1**, 389-449.

Rao, V.B., and Murty, B.V.S., 1973, Note on Parasnis' method for surface density: Pure and Applied Geophysics, **110**, 1927-1931.

Reger, R.D. and Pinney, D.S., 1997, Last major glaciations of Kenai lowland: *in* 1997 guide to the geology of the Kenai Peninsula, Alaska, Karl, S.M., Vaughn, N.R. and Ryherd, T.J. (ed.), Alaska Geological Society, 54-67.

Swenson, R. F., 1997, Introduction to Tertiary tectonics and sedimentation in the Cook Inlet basin: *in* 1997 Guide to the Geology of the Kenai Peninsula, Alaska, Karl, S. M., Vaughn, N. R., and Ryherd T. J. (ed.), Alaska Geological Society,18-27.

Tarantola, A., and Valette, B., 1982, Generalized non-linear inverse problems solved using least squares criterion: Review of Geophysics and Space Physics, **20**, 219-232.

White, S.M., 2007, In situ density determination using Nettleton's method: University of South Carolina, Columbia, USA, unpublished document (http://serc.carleton.edu/NAGT Workshops/geophysics/activities/18922.html).

Wilson, F.H., Hults, C.P., Scholl, H.R., Haeussler, P.J., Schmidt, J.M., Yehle, L.A., and Labay, K.A., 2009, Preliminary geologic map of the Cook Inlet region, Alaska: U.S. Geological Survey Open-File Report 2009-1108 (http://pubs.usgs.gov/of/2009/1108/).

# SECTION 2

## Interpretation of Gravity and Magnetic Data and Development of 2D Cross-Sectional Models for the Border Ranges Fault System, South-Central Alaska.

*(Paper submitted to Journal)*

*Niti Mankhemthong[1], Diane I. Doser[1], Terry L. Pavlis[1]*
*[1]Department of Geological Sciences, University of Texas at El Paso, El Paso, TX 79968-0555*

### 2.1 ABSTRACT

Extensive Quaternary glacial cover and lack of dense geophysical data within the Cook Inlet basin (CIB) of south-central Alaska make locating and determining the geometry of the Border Ranges fault system (BRFS), a major feature of the Alaska-Aleutian forearc region, difficult. We use recently collected gravity data, available aeromagnetic data, and other geophysical information as constraints to develop plausible 2D cross-section models that better image the BRFS and related geologic structures of the CIB. Our integrated models show a thick sequence of Late Mesozoic sedimentary rocks and the Peninsular Terrane basement (6 to 20 km depth) overlying a serpentinized body at a depth of 16 to 34 km. The Late Mesozoic rocks and serpentinite are interpreted as possible sources of the south Alaska magnetic high over the CIB. The CIB's eastern boundaries are characterized by gravity and magnetic highs of the emplaced Border Range ultramafic and mafic assemblages (BRUMA). Formation of the BRUMA may be related to the serpentinized rocks that comprise a Jurassic oceanic arc. Our models constrain the BRFS as a structural boundary between the overthrusted BRUMA and the Chugach Terrane to the east. The BRFS dips $50^{o}$ to $70^{o}$ toward the west-northwest and extends to at least 15 km. The BRFS may penetrate steeply or shallow to a form a décollement at greater depths. A model that includes underplated sediments at the base of the accretionary complex (12 to 40 km) is consistent with the observed gravity low over the Chugach Mountains (Chugach Terrane). The underplating may be associated with the process of subducting and shortening Yakutat microplate in south-central Alaska.

## 2.2 INTRODUCTION

The Border Ranges fault system (BRFS) has played a major role in the development of the forearc basin system of south-central Alaska since Jurassic time Pavlis and Roeske, 2007 , serving as the boundary between the forearc of Cook Inlet basin (CIB) and the Chugach Terrane accretionary complex (Fig. 2.1; Shellenbaum et al., 2010). Surface exposure of the BRFS is limited, and only a few geophysical surveys (e.g., Burns, 1982; Fisher and von Huene, 1984) have been conducted across it. Thus we know little about the subsurface structure of this feature or how it has influenced the past and present day tectonics of the region. The goal of this study was to use new gravity data collected across the BRFS to develop integrated geophysical/geological models of regional structure that could be used as a starting point both for understanding how the BRFS has influenced regional tectonics, and for planned 3D modeling studies.

The focus of this study is along the inferred trace of the BRFS extending from the central Kenai Peninsula to the Castle Mountain Fault (Fig. 2.1), which includes the western Kenai Peninsula, the Anchorage area, and the eastern Susitna-Matanuska Valley. Throughout much of the region, the BRFS is marked by a pronounced change in topography from the CIB to the Chugach Mountains. However, no seismicity or recent fault scarp appears to be associated with the BRFS (Pavlis, 1982; Fisher and von Huene, 1984; Pavlis and Roeske, 2007).

In this study, we used a new dense set of gravity data collected between 2009 and 2011 and existing aeromagnetic data to model plausible geometries for the inferred BRFS. We first produced new corrected anomaly maps to distinguish different geologic features based on density and magnetic susceptibility properties. We then used the updated geophysical potential field data to construct 2D density-magnetization cross-section models. Other geological and geophysical data (e.g., well logs, seismic tomography, and surficial geology) were used to help constrain the model parameters and address problems of non-uniqueness related to tradeoffs between modeled thicknesses, depths, densities,

and magnetic susceptibilities in order to minimize model uncertainties (Saltus et al., 2001). We also compared our results to geological processes found in other, well studied subduction zones, such as serpentinization and underplating of sediments to help explain the possible causes of anomalies present in our new interpretations.

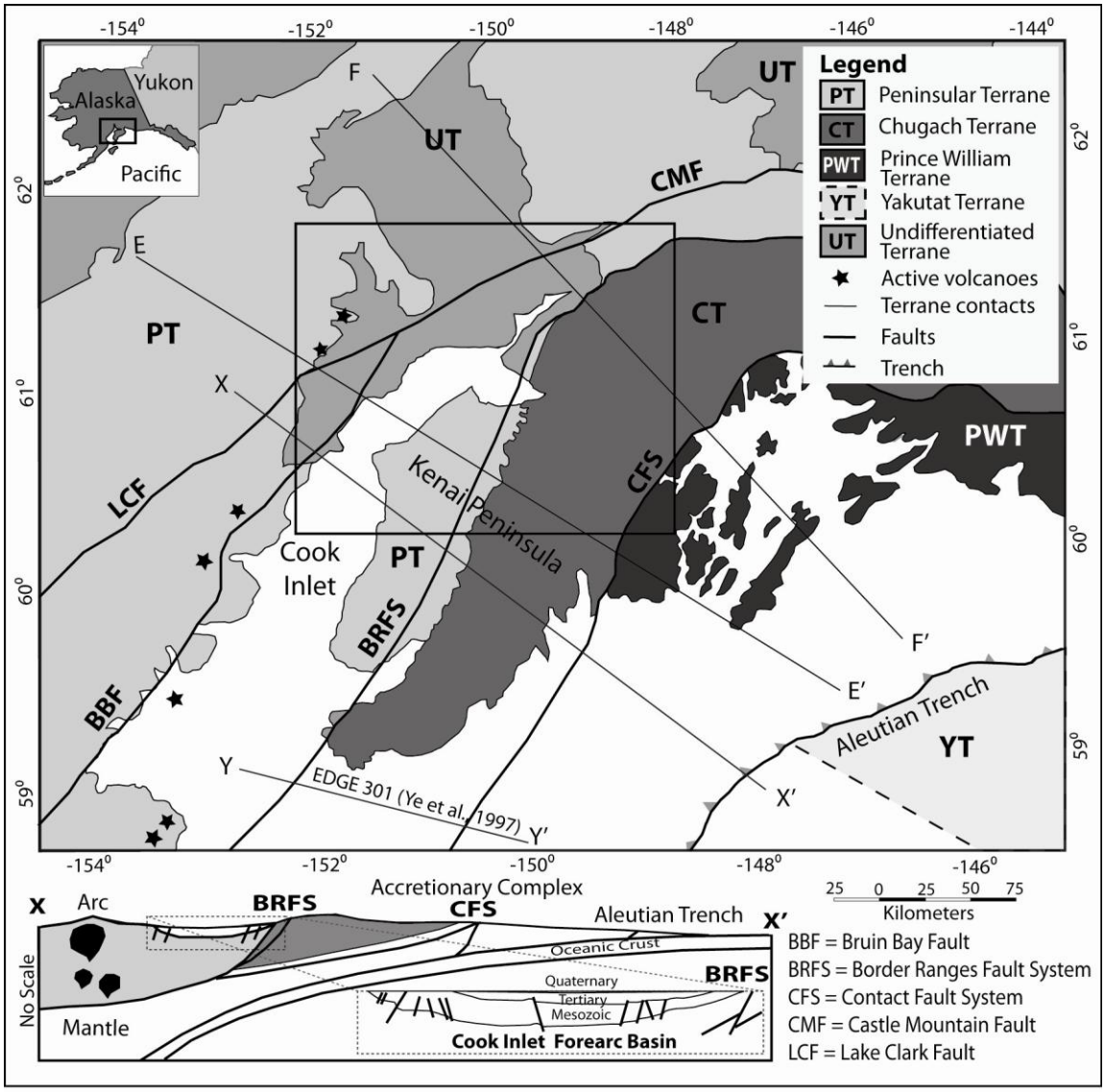


Figure 2.1: Simplified tectonic terrane map across south-central Alaska and cross-section along X-X' (without vertical exaggeration). Small rectangle within lower cross-section shows details of structures within Cook Inlet basin. E-E' and F-F' are the locations of 2D gravity forward models shown in Fig. 2.11). Y-Y' shows the location of the seismic cross-section (EDGE 301) in Fig. 2.13. The study area is indicated by the solid rectangle (geology based on Fisher and Magoon, 1978; Pavlis and Bruhn, 1983; Haeussler et al., 2000).

## 2.3 BACKGROUND GEOLOGY

The BRFS spans the region between the eastern CIB and topographically higher Kenai and Chugach Mountains. The CIB is bounded to the north by the Castle Mountain Fault and to the west by the Bruin Bay Fault (Figs. 2.1 and 2.2) (Fisher and von Huene, 1984; Shellenbaum et al., 2010). The three major sub-regions of the CIB are the Anchorage Lowland, Kenai Lowland, and Cook Inlet itself. The CIB is filled with continent derived sediments ranging in age from Mesozoic to Quaternary which collectively define the forearc basin stratigraphy and the cover sequence of the Peninsular Terrane (Plafker et al., 1994; Trop et al., 2005). The small-scale topography of the basin is affected by multiple Quaternary glaciations and recent alluvial and tidal processes (Swenson, 1997; Haeussler and Saltus, 2011). Glacial deposits have an average thickness of 180 m (Plafker et al., 1989) and may reach a thickness of 1200 m in the basin axis (Swenson, 1997).

The Quaternary glacial deposits lie unconformably over Late Eocene to upper Pliocene sedimentary rocks, termed the Kenai Group, a terrestrial section deposited in a forearc setting (Fig. 2.1; Haeussler and Saltus, 2011; Swenson, 1997). According to borehole data, the Kenai Group contains cross-bedded to massive sandstones, siltstones, claystones and shale with an estimated total thickness of ~2 km near the basin axis and thins radically to both the basin edges (Plafker et al., 1989). Five non-marine formations are classified including Sterling, Beluga, Tyonek, Hemlock, and West Foreland Formations (Swenson, 1997). The Kenai Group lies over non-marine facies of Paleogene age, which record an initial Tertiary uplift and cessation of Mesozoic depositional patterns (Swenson, 1997). Seismic reflection profiles of Tertiary formations show folded and faulted structures that initially formed during Early Eocene to Late Oligocene time (Little and Naeser, 1989), some of which may be active to the present (Haeussler et al., 2000). Paleogene sequences are underlain by Late Mesozoic sequences to the west but onlap crystalline basement to the east.

The Late Mesozoic sequences are widely recognized as a succession of shallow marine sedimentary rocks of Early Jurassic-Cretaceous age with an approximate thickness of ~8500 m (Plafker et al., 1989). The Late Mesozoic sedimentary rocks extend well east of the present CIB across the trailing edge of the Peninsular Terrane. At least 3000-m of clastic, volcanic, and volcaniclastic rocks of Late Triassic to Early Jurassic Talkeetna Formation lie underneath this succession and comprise the volcanic cover coeval with the Early Jurassic intrusive assemblages of the Peninsular Terrane basement (Trop et al., 2005; Saltus et al., 2007; Clift et al., 2012). In the Anchorage area the Mesozoic rocks, as well as their Late Mesozoic-Paleogene cover, emerge from beneath Neogene sediments and are well exposed to the east in the Matanuska Valley and northern Chugach Mountains (Pavlis and Roeske, 2007).

The Border Ranges ultramafic-mafic assemblage, or BRUMA, is identified as the Peninsular Terrane basement rocks along the eastern forearc boundary (DeBari and Coleman 1989; Plafker et al., 1989). It is stratigraphically overlain by Middle Jurassic to Paleogene sedimentary sequences to the east of the CIB, but the primary depositional relationships are complicated by younger structures (Trop et al., 2007). The BRUMA is comprised primarily of plutonic rocks that range in composition from gabbro to tonalite with local occurrences of ultramafic rocks (e.g., Burns, 1982; Plafker et al., 1994) and a fragmented crustal section of an Early Jurassic oceanic arc system (Plafker et al., 1989; Pavlis and Roeske, 2007). The ultramafic rocks of the BRUMA are interpreted as the upper mantle roots of the arc overlain by lower-crustal mafic rocks (e.g., Burns, 1982; DeBari and Coleman 1989) that pass upward to lower-Jurassic volcanic cover of the Talkeetna Formation along the Chugach Mountain fronts (e.g., Pavlis and Roeske, 2007). Outcrop exposures in the northern Chugach Mountains and previous aeromagnetic data show the BRUMA forms a 5 to 20 km wide outcrop belt (Burns, 1982; Burns et al., 1991) that is mostly concealed, except for a small part along the boundary between the eastern CIB and western Kenai and Chugach Mountains.

The BRFS separates the BRUMA from the Chugach Terrane throughout the Kenai and Chugach Mountains (Nokleberg et al., 1989). The Chugach Terrane represents a subduction complex that was accreted by northwest-directed subduction (modern coordinates) along the margin (Plafker et al., 1994), but the BRFS itself is overprinted complexly by younger fault systems (Pavlis and Roeske, 2007). The Chugach Terrane consists of two major lithotectonic assemblages separated by the Eagle River Thrust Fault (ERTF): the older McHugh Complex mélange assemblage, and the younger Valdez Group metasedimentary rocks (Fig. 2.2) (Pavlis and Roeske, 2007). Tertiary intrusions that are related to Eocene ridge subduction are found within the Chugach Terrane but are limited to small intrusions in the Anchorage area (Hill et al., 1981; Fuis et al., 1991; Plafker et al., 1994). The younger accreted deep sea fan complex that forms the Prince William Terrane is separated from the Chugach Terrane by the Contact fault system (Fig. 2.1) (Plafker et al., 1989; Fuis et al., 1991).

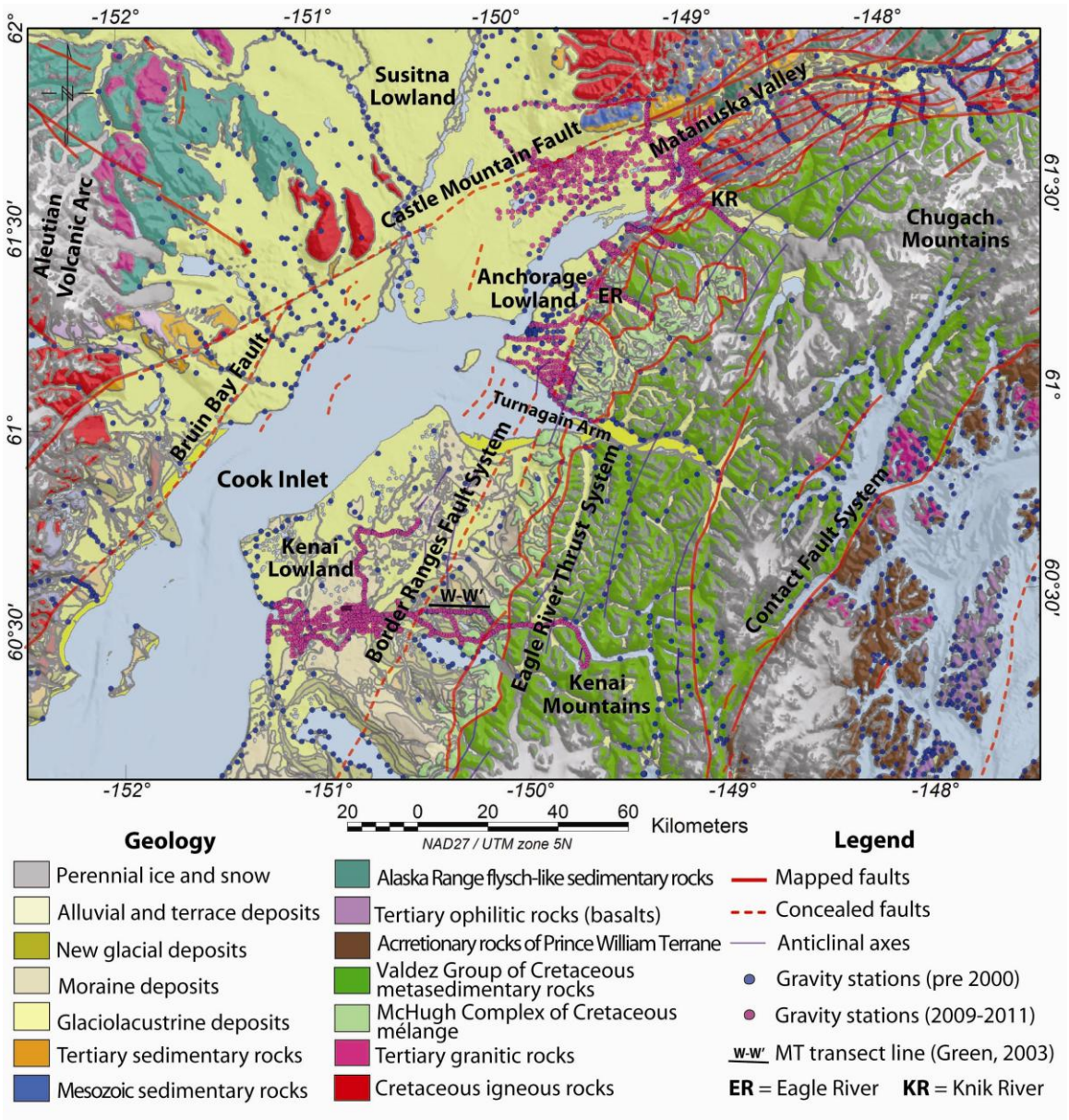


Figure 2.2: Geologic map of the central Kenai Peninsula showing locations of all gravity measurements (simplified from Wilson et al., 2009). Fault and fold data are digitized from Haeussler et al. (2000). W-W' is a location of the MT transect line from Green's (2003) study.

### 2.3.1 The Border Ranges Fault System

MacKevett and Plafker (1974) first defined the BRFS as a major structural feature extending over 1300 km from Kodiak Island on its southwestern end to Baranof Island on its northeastern end. The southwestern segment of the BRFS is the focus of this study and is defined as an arc-forearc boundary of the modern Alaska-Aleutian subduction zone (Pavlis and Roeske, 2007). The BRFS is exposed extensively in the western and northern Chugach Mountains (Pavlis and Roeske, 2007). The buried location of the BRFS beneath the Cenozoic fill has been inferred from shallow and deep geophysical data (e.g., Shellenbaum et al., 2010). Previous studies in the Cook Inlet area suggested that the BRFS forms a 2-10 km wide suture zone (Burns 1982; Fuis and Plafker, 1991) that dips steeply to vertically toward the north or northwest (Fisher and von Huene, 1984).

The history and sense of fault movements on the BRFS from the Jurassic to Middle Cenozoic are debated because of the complexities of the deformational history of the southern Alaska subduction complex (Little and Naeser, 1989; Fuis et al., 1991). The Jurassic history of the BRFS is poorly defined, in large part due to overprinting and a Middle Jurassic period of subduction erosion (e.g., Clift et al., 2005). Recent work (e.g., Amato and Pavlis, 2010) indicates episodes of accretion and subduction erosion during the Jurassic and Early Cretaceous, followed by Middle Cretaceous accretion of part of the McHugh Complex further followed by accretion of the Valdez Group. Cretaceous subduction accretion was followed by dextral motion on the BRFS in the northern Chugach Mountains which appears to have been transferred westward to the Castle Mountain Fault in Early Cenozoic age (Clift et al., 2005; Pavlis and Roeske, 2007). The timing of the lateral motion may be associated with the onset of oroclinal bending and right-oblique subduction of the Kula Plate in southern Alaska (Little and Naeser, 1989; Pavlis and Roeske, 2007). Most recently, high-angle normal movement toward the northwest appears to have occurred on the southwestern-most segment of the BRFS (Pavlis and Bruhn, 1983; Little and Naeser, 1989) that is correlated to Late Neogene forearc basin development (Pavlis and Roeske, 2007).

An absence of evidence for Neogene reactivation of the BRFS suggests it has not acted as a reverse fault after the Late Cretaceous period (Fisher and von Huene, 1984). Haeussler and Saltus (2000) presented two observations based on contrasts of topography and magnetic amomalies across the BRFS to support the hypothesis of Pavlis and Bruhn (1983) that the BRFS was reactivated by normal faulting in the Neogene. However, inferred normal faulting remains controversial (Haeussler and Saltus, 2000) faults are not well imaged on several noisy seismic reflection profiles across the BRFS, and no evidence for normal fault offsets have been observed on exposed fault scraps (Haeussler and Anderson, 1997).

## 2.4 GEOPHYSICAL DATA COLLECTION AND PROCESSING

We collected a total of ~1400 gravity stations across the BRFS within the Kenai and Anchorage Lowlands from 2009 to 2011 using a Lacoste & Romberg Model G gravimeter (Fig. 2.2). Associated elevation and coordinate control information were collected by a GB-100 GPS receiver with processing implemented in steps to achieve less than 0.1 m elevation control. The errors associated with readings taken by this gravity meter include those due to reading resolution, repeatability, and non-linear instrument drift. The nulling dial has an accuracy of 0.01 mGal. The repeatability is approximately 0.02-0.03 mGal based on numerous readings at base stations during the data acquisition stage. All acquired gravity values were tied to known local absolute gravity stations and corrected to free air and simple Bouguer anomalies. These recent data were combined with approximately 3000 existing land and marine regional gravity observations from U.S. Geological Survey and University of Texas at El Paso databases collected before 2000 (Fig. 2.2).

We employed aeromagnetic data which were compiled and reprocessed from Saltus and Simmons (1997) to show magnetic intensity that are related to magnetic material distributions and structural features across the BRFS and south-central Alaska. The selected aeromagnetic data are based on four separate surveys conducted between 1954 and 1977 with variable flight directions (N-S and E-

W), altitudes (120 to 760 m), and flight line spacings (1600 m to 16000 m). The Cook Inlet survey was covered by a coarser line spacing range and data sampling grid compared to the land surveys. The flight spacing ranges and altitudes of the original survey grids were adjusted to minimize differences at the boundaries by applying upward or downward continuation and converted from level to drape as necessary to produce a consistent survey specification of 305 m above ground (Saltus and Simmons, 1997).

We used Geosoft's Oasis montaj software to process reduced gravity and aeromagnetic anomalies with the same grid size of 1000 m and applying a minimum curvature gridding technique. A standard density of 2670 kg/m$^3$ was chosen for the Bouguer correction (Burger et al., 2006) to remove the gravity slab effect (Fig. 2.3). A terrain correction was not applied to the gravity data since this study is focused on deeper geologic structures related to long wavelength signals that will serve as starting models for the next step in our analysis, a 3D inversion of the free air gravity data. In the 3D analysis we will build a model that explicitly incorporates topography with surficial variations in geology/density, eliminating the assumption of an average near surface density that is used in most terrain correction algorithms. Total intensity aeromagnetic data were reduced-to-pole filtered to view all magnetic sources produced vertically and symmetrically (Blakely, 1995) with an inclination of 73$^o$ and declination of 25$^o$ (Fig. 2.5), presumable averages of values over 1954 and 1977 time interval (Saltus and Simmons, 1997). A horizontal gradient analysis was performed to delineate geologic contacts or faults across which rock density or magnetic susceptibility differs (Figs. 2.4 and 2.6) (Blakely, 1995). We also used Fast-Fourier Transform Gaussian low and high pass filtering analyses to distinguish residual and regional magnetic sources at different depths (Figs. 2.7 and 2.8).

## 2.5 INTERPRETATION RESULTS

### 2.5.1 Gravity Anomaly Interpretations

Northeast striking gravity anomalies show two prominent features over the study area: 1) gravity lows within the CIB, and 2) gravity highs within the surrounding mountains. The deep gravity lows (-100 to -160 mGal) extend from the Kenai and Anchorage Lowlands into Cook Inlet that corresponds well with the boundaries of the CIB (Fig. 2.3). The minimum gravity lows lie within northern Cook Inlet and the northwestern Kenai Peninsula (Fig. 2.3). The maximum gravity highs (19 mGal) are found in a belt along the eastern margin of the CIB (Fig. 2.3). This belt likely represents buried high density rocks of the BRUMA (Burns, 1982). Strong gravity gradients are observed at the northwestern edges of the CIB that are correlated to the locations of the Bruin Bay and Castle Mountains Faults, respectively (Fig. 2.4). Even stronger gravity gradients are observed to the east of the CIB that may be related to possible locations of the BRFS (Fig. 2.4).

The BRFS appears to be associated with two regions of strong gravity gradient between the CIB and the BRUMA, and between the BRUMA and McHugh Complex (Figs. 2.4 and 2.9). The gravity anomaly over the accretionary complex generally increases southeastward towards the Aleutian Trench (area denoted by "H" in Fig. 2.3), but decreases ("L" in Fig. 2.3) northeastward towards the central Chugach Mountains (Fig. 2.3). The change between higher gravity over the Kenai Mountains and lower gravity over the Chugach Mountains occurs near Turnagain Arm (Fig. 2.3). We suggest this observed change in gravity anomaly over the same accreted terrane may be related to the southwestern edge of the subducted Yakutat microplate (shown by "SEY" in Fig. 2.9) whose location is inferred by the tomographic studies of Eberhart-Phillips et al. (2006) (Figs. 2.3 and 2.9). This gravity low is also seen on a recently released free air anomaly map obtained from airborne gravity studies of the Cook Inlet region (GRAV-D Science Team, 2012) supporting the idea that this low is not an artifact of sparse data coverage or improper data correction in this region.

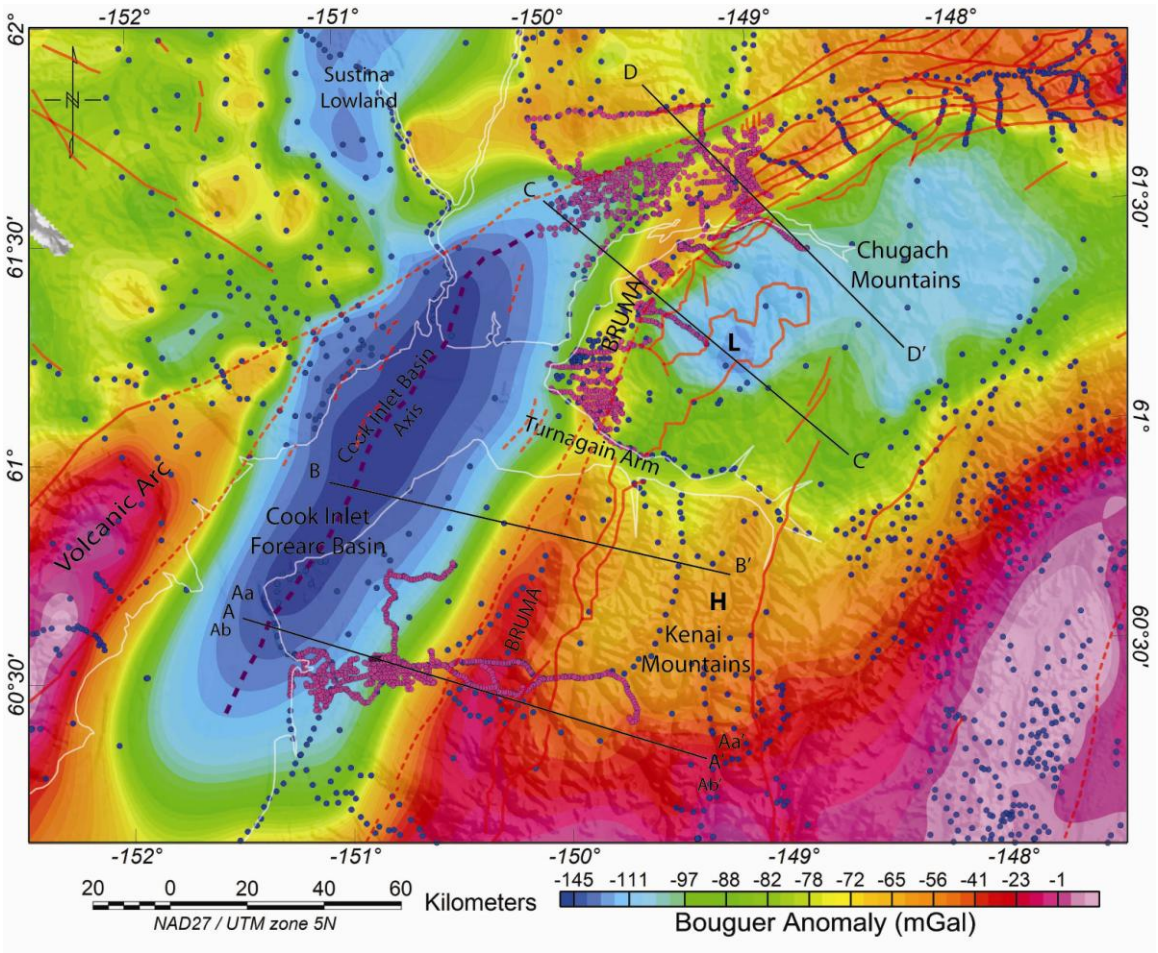


Figure 2.3: Simple Bouguer anomaly map using a reducing density of 2670 kg/m$^3$, gridded at 1000 m. Purple dashed lineament indicates the lowest gravity values which represent the center of the Cook Inlet forearc basin. The Border Range ultramafic and mafic assemblages (BRUMA) represent the highest gravity values along the east rim of the forearc basin. "H" denotes a region where gravity increases southeastward towards the Kenai Mountains and Aleutian Trench, and "L" is a region where gravity decreases northeastward towards the Chugach Mountains. The white line is the shoreline. Gravity points and fault symbols are explained in Fig. 2.2. Black lines represent four 2DGAM models analyzed in this study (Fig. 2.10).

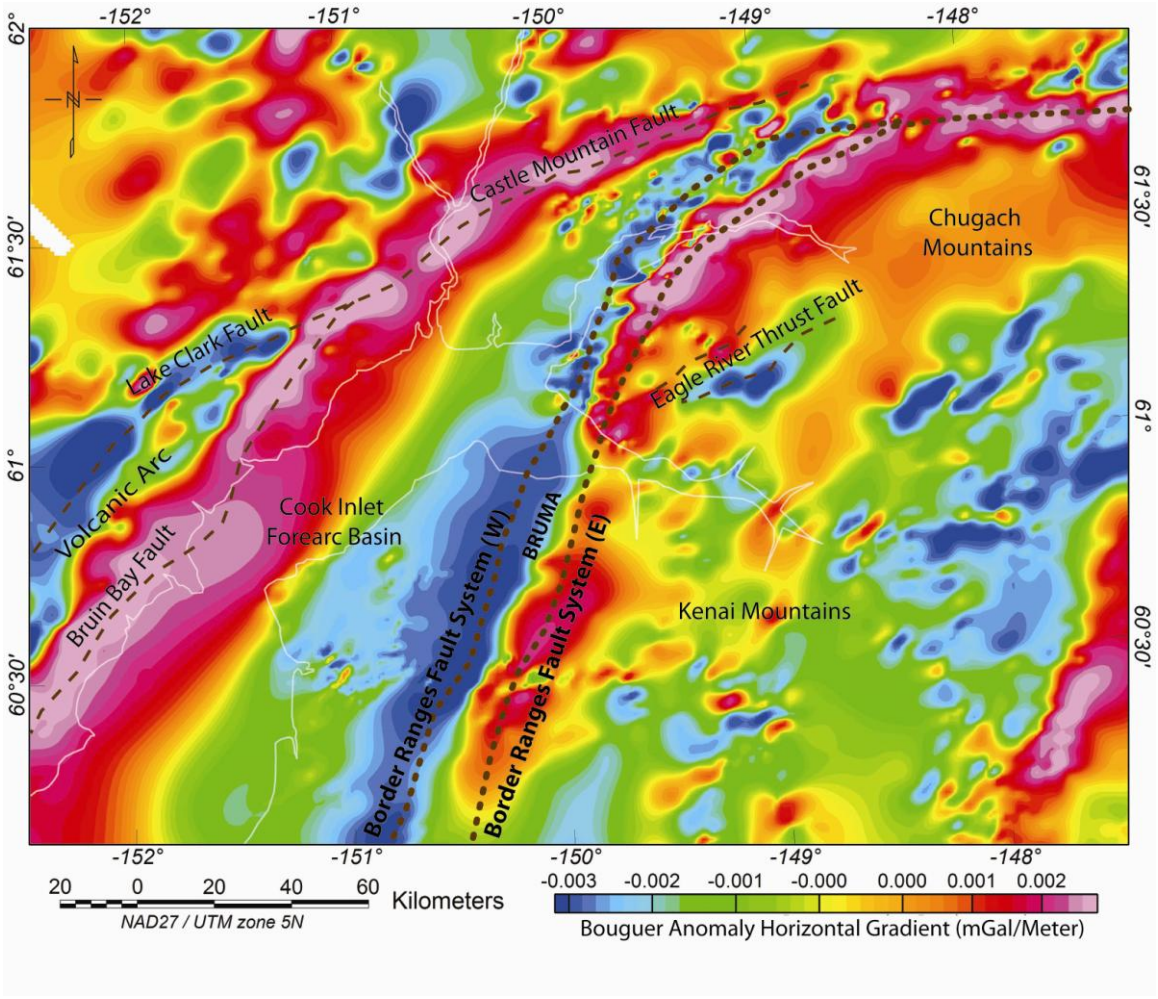


Figure 2.4: Color shaded relief map of the horizontal gradient derived from the simple Bouguer anomaly map (Fig. 2.3). Lineaments define largest gravity positive and negative gradients associated with interpreted dip-slip faults. Brown dotted lines labeled with E and W are gradients associated with the edges of the BRFS. Brown dashed lines are interpreted as other major faults. Small bull eye type anomalies reflect the effects of rugged mountain topography due to lack of terrain correction in the gravity reduction process.

### 2.5.2 Magnetic Anomaly Interpretations

Magnetic intensity lows striking northeast-southwest are subparallel to the structural fabric of the CIB and strike in the same direction as the gravity anomalies, but they have different anomaly characteristics. The magnetic anomaly map expresses an abnormal feature for basin fill with prominent magnetic highs over the basin, termed the south Alaska magnetic high (Godson 1984) (Fig. 2.5). The low-pass-filtered map shown in Fig. 2.7 supports the hypothesis that the south Alaska magnetic high may correlate with fluid serpentinization of the altered lower forearc crust/mantle at 16 to 34 km depth (Saltus et al., 2001; Hyndman and Peacock, 2003). Shallow sediments and rocks (<15 km) is not a likely a source of the magnetic highs because high-pass-filtered maps show no broadly strong magnetic highs (Fig. 2.8). The magnetic intensity highs to the west of Cook Inlet are likely related to intrusive and extrusive bodies associated with the active volcanic arc (Figs. 2.1 and 2.5) (Haeussler and Saltus, 2000). A linear contact between the long wavelength highs of Cook Inlet and these smaller highs of the arc occurs at the position of the Bruin Bay Fault. The eastern flank of the CIB is bordered by narrow magnetic highs (200-230 nT), termed the Knik Arm anomaly (Fig. 2.4; Grantz et al., 1963; Fisher and von Huene, 1984) that are in the same locations where gravity highs are observed. The BRUMA is presumably responsible for the Knik Arm anomaly. This hypothesis is supported by exposed ultramafic bodies along the mountain front between Knik River and Eagle River (shown by “KR” and “ER” in Fig 2) (Burns, 1982). The width of the Knik Arm anomaly based on the magnetic intensity gradient is narrower than the width estimated from gravity gradient analysis (Figs. 2.4 and 2.6). This difference may indicate that there is a less magnetic source, such as a mafic assemblage, located at the edges of the BRUMA (Burns, 1982). Strong gradients on the eastern flank of Knik Arm correlate to the eastern edge of the BRFS (E), which is interpreted from gravity data (Figs. 2.4 and 2.6). Relative magnetic lows are observed over the topographically high regions of the Chugach Terrane that reflect to less/no magnetic source rocks of the accretionary complex (e.g., Saltus et al., 2007). .

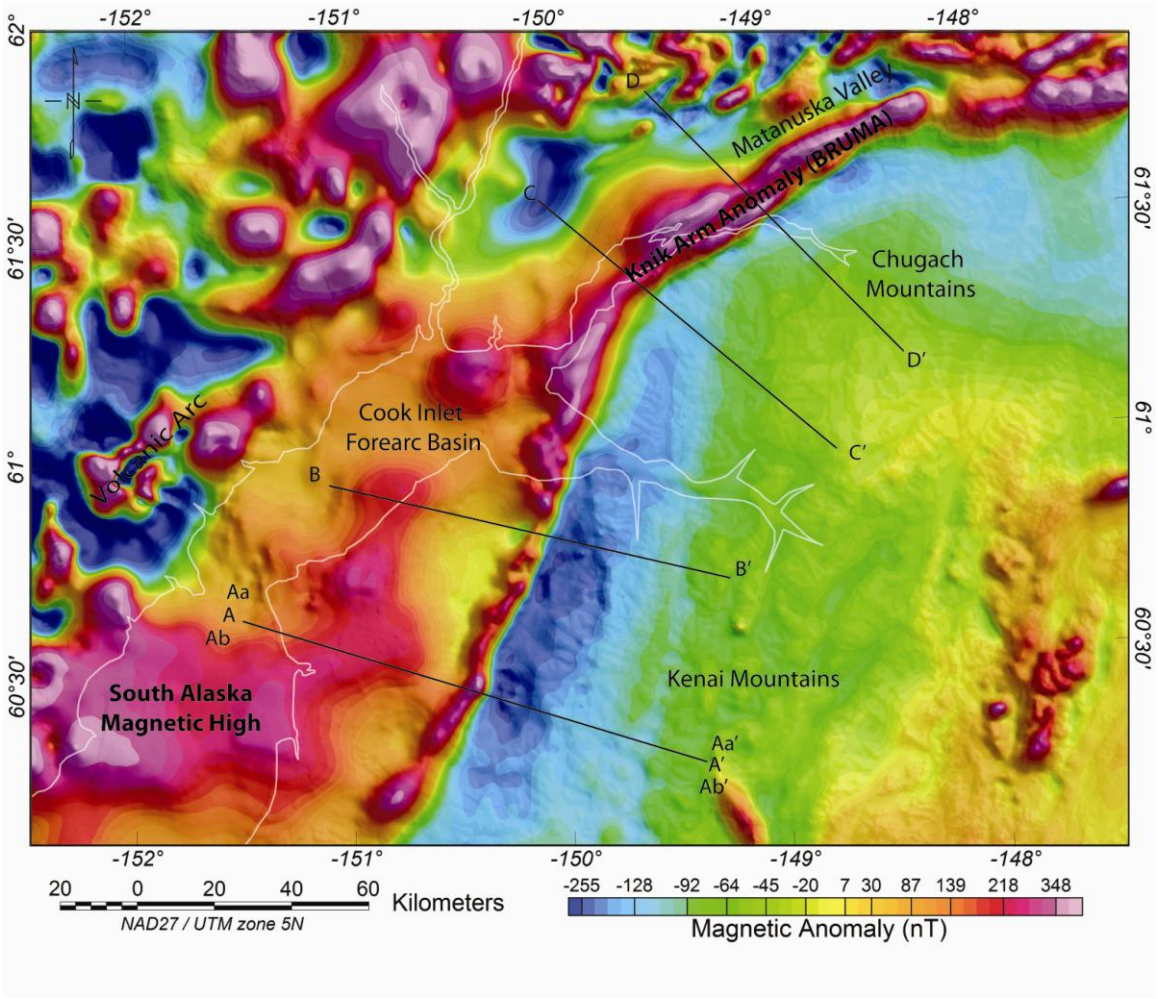


Figure 2.5: Total intensity aeromagnetic map of the study area which has been "reduced-to-pole", showing magnetic intensity highs over the Cook Inlet basin (data reprocessed from Saltus and Simmons, 1997). The Knik Arm anomaly is from Grantz et al. (1963). Black lines represent four 2DGAM models analyzed in this study (Fig. 2.10).

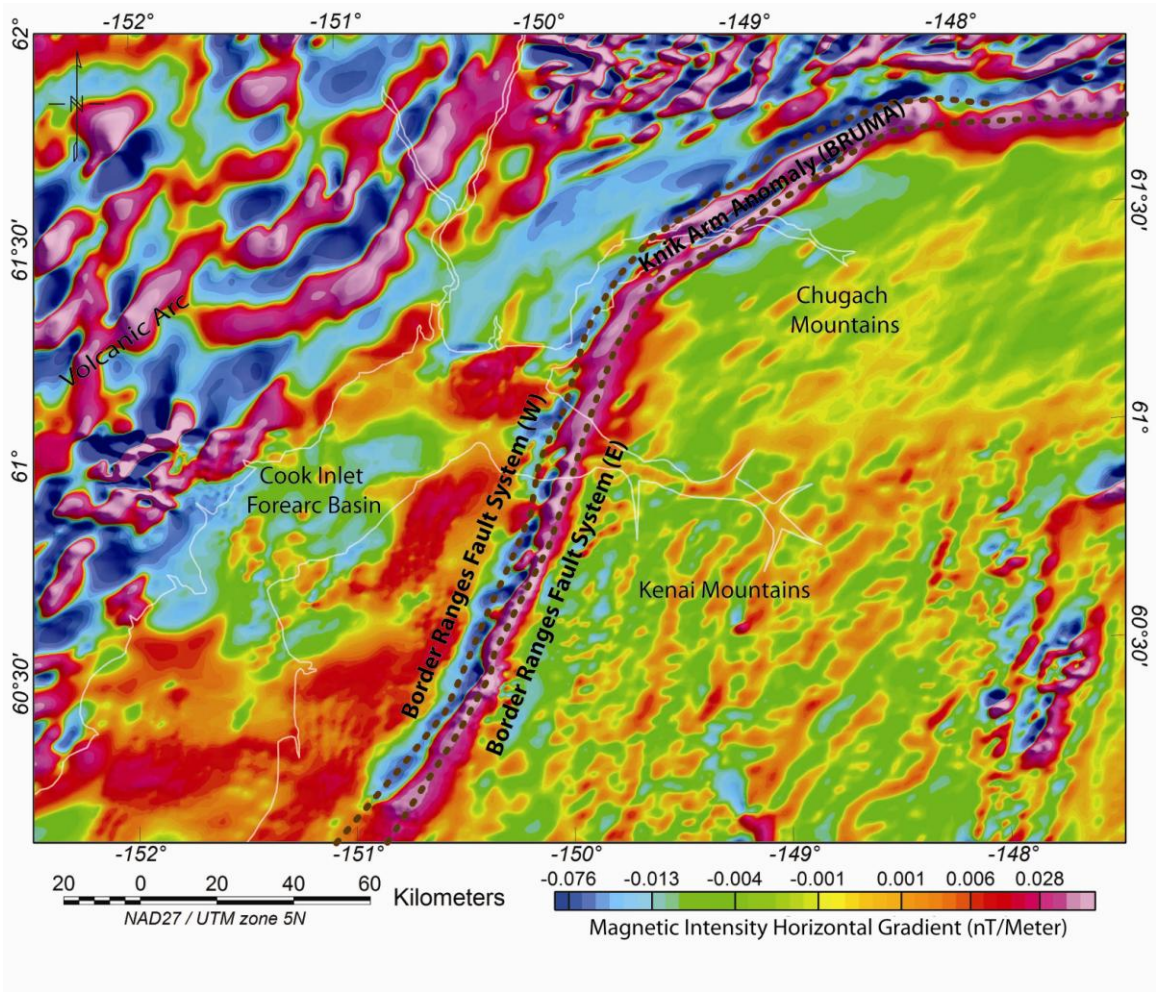


Figure 2.6: Color shaded relief map of the horizontal gradient derived from the aeromagnetic map (Fig. 2.5). Lineaments define largest gravity positive and negative gradients associated with interpreted dip-slip faults. Brown dotted lines labeled with E and W are gradients associated with the edges of the BRFS.

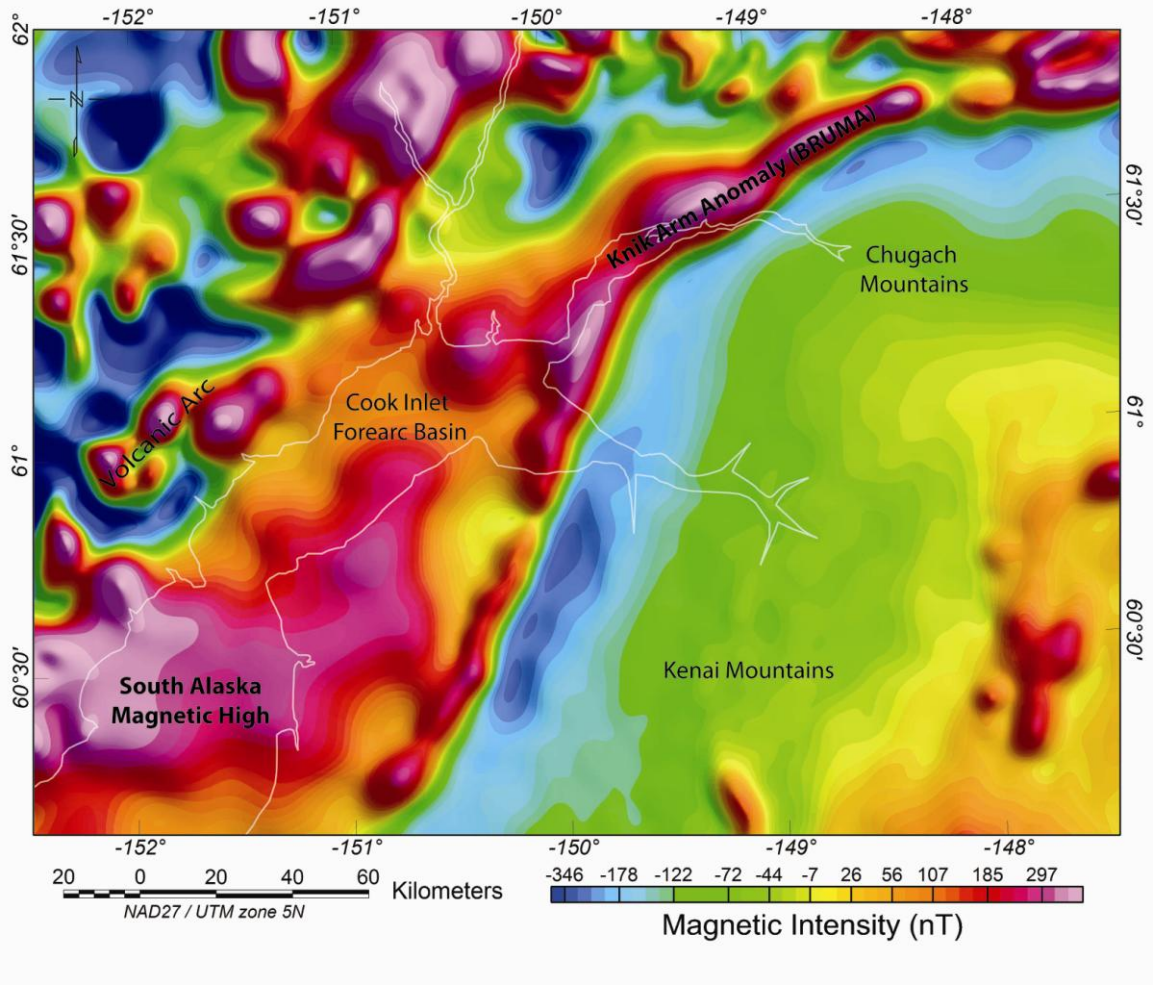


Figure 2.7: Long wavelength (>20 km) magnetic feature map obtained from Gaussian low pass filtering analysis of the total intensity aeromagnetic map (Fig. 2.5). These anomalies are primarily related to deep sources.

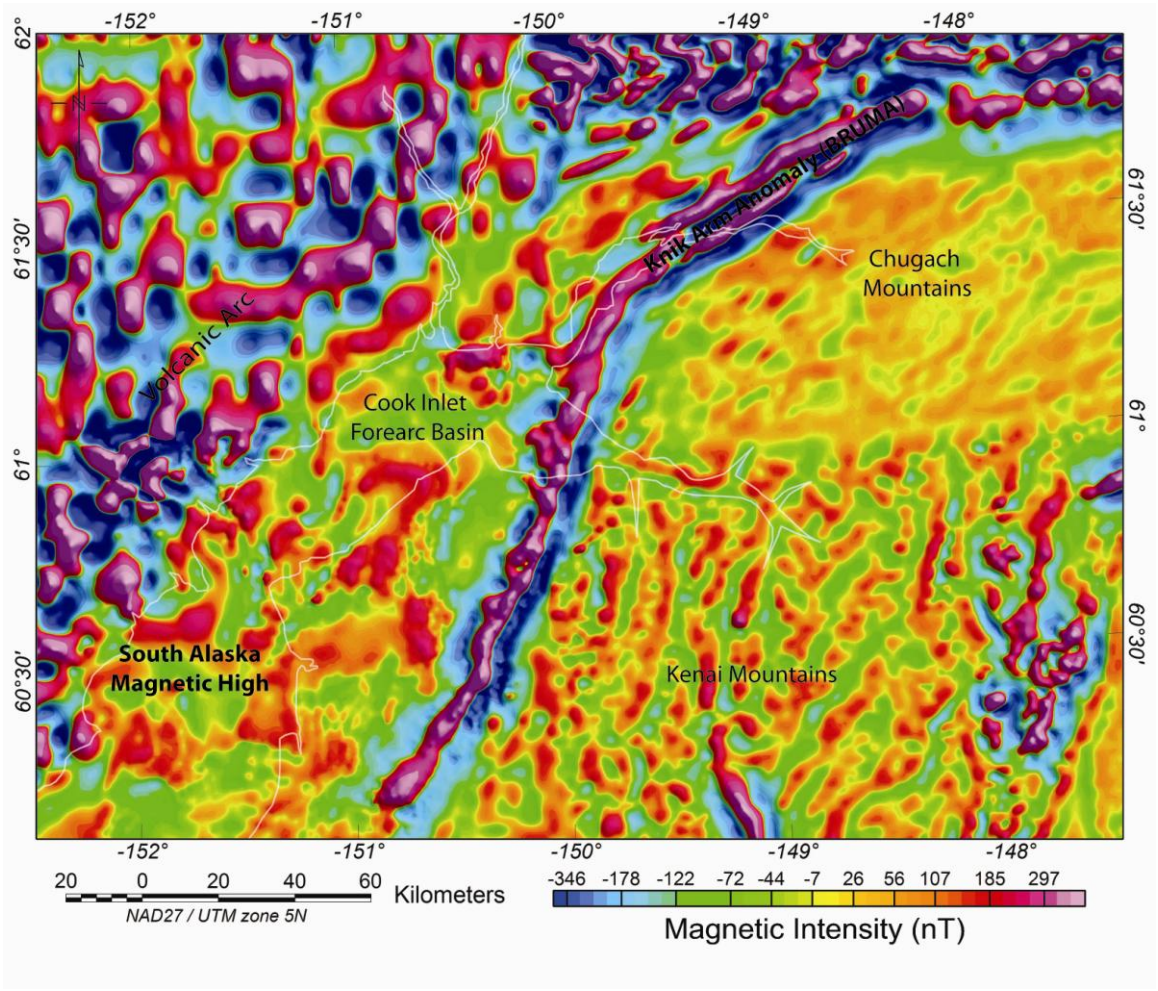


Figure 2.8: Short wavelength (<20 km) magnetic feature map obtained from Gaussian high pass filtering analysis derived of the total intensity aeromagnetic map (Fig. 2.5). These anomalies are primarily related to shallow sources.

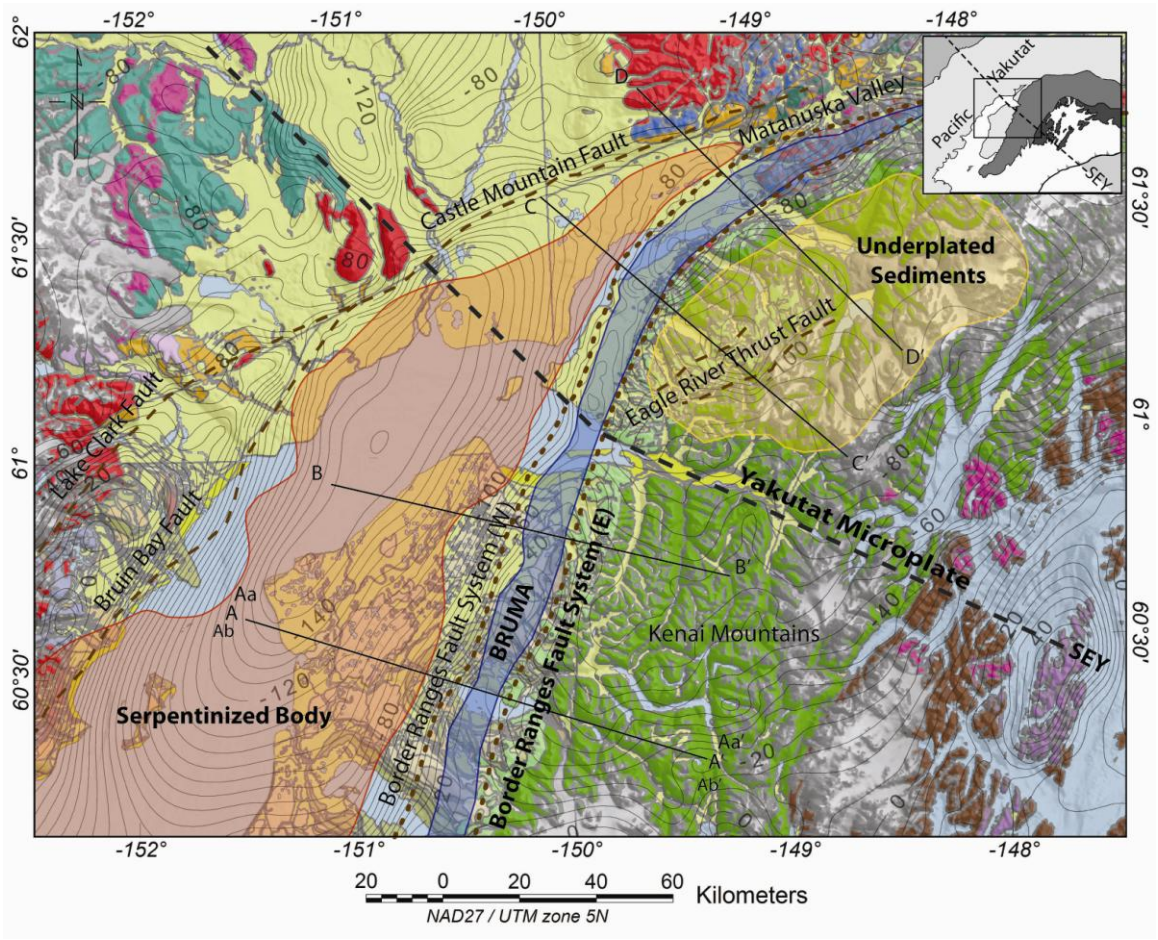


Figure 2.9: Simple geologic map overlain by Bouguer anomaly gravity contour lines (contour interval of 5 mGal) and estimated boundaries of concealed structural features located at uncertain depths based on gravity and magnetic anomaly analyses (Figs. 2.3 and 2.5). The shaded blue region indicates gravity and magnetic highs associated with the Border Range ultramafic and mafic assemblages (BRUMA); the shaded yellow region indicates gravity lows possibly related to underplated sediments; the shaded orange region indicates themagnetic highs related to a serpentinized crustal body. Dashed gray line labeled SEY represents the southern edge of the Yakutat microplate as inferred by Eberhart-Phillips et al. (2006) which separates gravity high and low zones (Fig. 2.3). Black lines represent four 2DGAM models analyzed in this study (Fig. 2.10).

## 2.6 DATA CONSTRAINTS FOR 2D INTEGRATED FORWARD MODELS

We used the GM-SYS software package to produce 2D forward models of the geologic structures over the study area at both local and regional scales, respectively. Four sub-parallel local transects (profiles A-A', B-B', C-C', and D-D' in Figs. 2.3, 2.5, and 2.9) were selected for the 2D forward modeling. All profiles strike NW-SE in a direction perpendicular to geological structures in order to illustrate the subsurface BRFS and related geologic features. Most profiles, except the northernmost profile (D-D'), start from the western flank of the forearc basin and extend eastward across the CIB, the BRFS, and end at the Chugach-Kenai Mountain ranges., We modeled structures to a depth of ~50 km and assumed homogeneous bodies extending orthogonal to the profiles to distances effectively of infinity (±30000 km). Because input data observations were derived from gridded simple Bouguer gravity anomaly and reduced-to-pole aeromagnetic anomaly data, the 2D integrated forward models discussed here are termed 2D integrated gravity and magnetic (2DGAM) models. We also modeled two longer regional transects (profiles E-E' and F-F' in Fig. 2.1) that cross the entire subduction zone from the trench to the arc and extend to depths of 120 km (Fig. 2.11). E-E' is a southern profile where more normal subduction of the Pacific Plate is occurring while F-F' is a northern profile that crosses the region of flat slab subduction of the Yakutat microplate (Fuis and Plafker, 1991).

To minimize errors of non-unique solution between the observed and calculated potential fields, the modeling programs require reasonable initial estimates of model parameters such as topography, depth, body shape, density, and magnetization of suspected sources. Several geologic maps from the U.S. Geological Survey database compiled by Wilson et al. (2009) were used for geologic contacts and fault constraints. Two digital elevation model datasets: 1) The National Elevation Dataset last updated by Gesch et al. (2002) and Gesch (2007), and 2) the Alaska Coastal Digital Elevation Model (Lim et al., 2009) were used for topographic and bathymetric constraints, respectively. Published geophysical cross-section models from Ehm (1983), Fisher and von Huene (1984), Yi et al. (1997), Haeussler et al. (2000),

Saltus and Haeussler (2001), Fuis et al. (2007) and Saltus et al. (2007), and Romero (2011) were used to guide the initial depth and thickness estimates for shallow and deep geologic features constructed in our 2DGAM models.

Table 2.1 provides information on density and magnetic susceptibility variations used in the 2DGAM models. A density of 2100-2200 kg/m$^3$ was selected for Late Tertiary sediments and sedimentary rocks of the lowland, and 2700-2740 kg/m$^3$ was chosen for metamorphic rocks of Chugach Terrane based on an estimation method outlined in Mankhemthong et al. (2012) and measurements of collected hand rock samples. Shallow densities for the basin deposits were derived from density logs obtained from the Alaska Oil and Gas Conservation Commission (2002). These gave a density of 2400-2500 kg/m$^3$ for Early Tertiary sedimentary rocks within the CIB. Previous studies (Fisher and von Huene, 1984) give a density of 2670-2700 kg/m$^3$ for Late Mesozoic rocks. Gardner's (1974) velocity-density conversion formula was used to convert from the seismic velocity models of Fuis et al. (1991) and Fisher and von Huene (1984) to rock densities for deeper geology. For example, 2900-3000 kg/m$^3$ were used for the BRUMA body, 2550-2600 kg/m$^3$ were chosen for a low velocity-density layer (LVDZ), and 3300 kg/m$^3$ was used for unaltered mantle. Based on several previous studies e.g., Christensen (1966); Coleman (1971), densities of 2750-2800 kg/m$^3$ were chosen for a serpentinized body beneath the Peninsular Terrane.

Magnetization values used in the 2DGAM models were based on measured magnetic susceptibilities for the Cook Inlet (Altstatt et al., 2002; Saltus et al., 2005; Saltus et al, 2007) and Talkeetna Mountains regions (Sanger and Glen, 2003), and geophysical magnetic surveys covering the Kenai Peninsula (Table 2.1) (e.g., Burns, 1982; Saltus and Haeussler, 2001). Altstatt et al. (2002) classified magnetic source rocks into three groups based on susceptibility measurements including low (<0.01 SI), moderate (0.01-0.10 SI), and high (>0.10 SI) magnetic sources. Thus high sources were used for a serpentinized body beneath the CIB (0.03-0.13 SI) (Godfrey and Klemperer, 1998; Carlson

and Miller, 2003). Moderate magnetic sources were correlated with the BRUMA (0.010-0.05 SI) and the volcanic arcs (0.025 SI). Magnetic susceptibility lows were associated with the metamorphosed rocks of McHugh Complex and Valdez Group (0.001-0.006 SI). Very weak magnetic or non-magnetic sources, such as stratified sedimentary formations, were assigned values 0-0.001 SI. Among the basin sedimentary groups the Late Mesozoic sediment sequences contain the highest magnetization. This high value may be related to its high amount of mafic-ultramafic mineral components (e.g., Burns, 1982).

The interpretations of integrated gravity and magnetic anomaly data yield non-unique solutions between rock density and magnetic susceptibility and modeled geometry. Several model families can be constructed to fit the observed data. The most geologically reasonable models that exhibit the least structural complexities and minimum misfit values were selected for the final models shown in Fig. 2.10. Fig. 2.12 is an alternative models used to test the sensitivity of the modeling process to variations in geologic structure or magnetic susceptibility. In this study, we accepted a RMS misfit error on the 2DGAM models when it was not over four mGal for gravity and thirty nT for magnetic forward models (Figs. 2.10, 2.11, and 2.12).

Table 2.1: Densities and magnetic susceptibilities used in the 2D integrated forward modeling

| Model bodies | Densities ($kg/m^3$) | Data sources | Magnetizations (SI) | Data sources |
|---|---|---|---|---|
| BRUMA | 2900-3000 | FV, SH | 0.030-0.063 | A |
| Basement rocks of Peninsular Terrane | 2700-2750 | FV, EP, SG | 0.005#, 0.027* | SH#, Sb* |
| Granitic intrusions | 2500-2700 | SH, A | 0.010 | A |
| Late Mesozoic rocks | 2670-2700 | FV | 0.005#, 0.027* | A#, SH#, Sb* |
| Underplated sediments | 2550-2600 | FV,Y | 0.001 | A |
| Early Tertiary sedimentary rocks | 2400-2500 | DL, SH | 0.001 | A |
| Mantle | 3300 | Sb | 0.000 | Sb |
| McHugh Complex of Chugach Terrane | 2700-2740 | HS, NP | 0.001-0.006 | A, Sa |
| Accretionary rocks of Prince William Terrane | 2600-2700 | FV | 0.002 | SG |
| Serpentinization | 2750-2800 | FV, SH | 0.03-0.13#, 0.04-0.09* | CM#,Sb* |
| Subducting Pacific Plate | 2900-3000 | Y | 0.07-0.09 | Sb, SH |
| Late Tertiary sedimentary rocks | 2100-2200 | DL, SH | 0.001 | A, Sa |
| Valdez Group of Chugach Terrane | 2690-2720 | HS, NP | 0.001-0.006 | A, Sa |
| Volcanic arcs | 2800 | FV, EP | 0.025 | A |
| Yakutat microplate | 2850 | FV | 0.017 | A |

| | | | |
|---|---|---|---|
| NP | Calculated from Nettleton-Parasnis' inversion method (Mankhemthong et al., 2012). | | |
| FV | Converted from seismic tomography data (Fisher and von Huene, 1984). | | |
| Y | Converted from seismic tomography data (Ye et al., 1997). | | |
| EP | Converted from seismic tomography data (Eberhart-Phillips et al., 2006). | | |
| HS | Measured from hand rock samples. | DL | Determined from density logs. |
| SH | Based on Saltus and Haeussler (2001). | SG | Based on Sanger and Glen (2003). |
| A | Based on Altstatt et al. (2002). | Sa | Based on Saltus et al. (2005). |
| CM | Based on Carlson and Miller (2003). | Sb | Based on Saltus et al. (2007). |
| # | Values for the best fit models (A-A' to D-D', Fig. 10) | * | Values for an alternative model (Ab-Ab', Fig. 12). |

## 2.7 2D CROSS-SECTION RESULTS

The 2DGAM models across the central CIB show Cenozoic and Mesozoic sedimentary rock sequences as deep as ~10 km filling the forearc basin along the southern profiles and ~6 km along the northern profiles (Fig. 2.7). Based on previous geological and geophysical studies (e.g., Ehm, 1983; Haeussler, 2000; Green 2003; Shellenbaum et al., 2010) and well log analysis, we modeled three sediment/sedimentary rock formations with different densities: 1) Late Tertiary, 2) Early Tertiary, and 3) Late Mesozoic rock sequences (Table 2.1). Approximate thicknesses of these units in the center of the CIB are ~1800, ~4000, and ~4500 m, respectively. Thickness changes observed on well logs provide evidence for normal faulting and reverse faulting associated with anticlinal structures (Shellenbaum et al., 2010), but cannot be modeled accurately on the 2DGAM models because of the coarse grid size (1000 m). These sedimentary rock sequences are modeled as overlying the basal crust of the Peninsular Terrane (Figs. 2.10 and 2.11).

An ultramafic (BRUMA) block is added to match the gravity highs adjacent to the eastern flank of the CIB and ultramafic surface exposures in the northern Chugach Mountain fronts (C-C', Fig. 2.11) (Pavlis and Roeske, 2007) and to the eastern flank of the Chugach Terrane (E-E' and F-F', Fig. 2.11). Misfits between observed and calculated anomalies over the ultramafic body, especially along the eastern margin of the body, may be related to mixed assemblages of mafic-intermediate composition rocks, changes in the thickness/composition of overlying sediments, and/or fault thickening/thinning of units (Bruns, 1982; Little and Naeser, 1989; Haeussler and Saltus, 2011).

A serpentinized body is added to constrain a broad south Alaska magnetic high over the CIB as inferred in models by Saltus and Haeussler (2001). According to our models, the serpentinized body is also part of a lithospheric section of an ancient oceanic arc system, as is the adjacent BRUMA block. We modeled the serpentinized body as a half wedge shape with a thickness of >20 km under the eastern CIB and ~10 km under the basin center (A-A' and B-B', Fig. 2.10). Due to westward thinning of the

serpentinized body, it probably pinches out under the western edge of the CIB (D-D', Fig. 2.10). Our serpentinization model is consistent with models of Blakely et al., (2005) that suggest the source of the magnetic highs continues farther eastward. From the southern profile (A-A', Fig. 2.10) to northern profile (D-D', Fig. 2.10), the serpentinized body was modeled as decreasing in size in order to constrain the observed decreasing magnetic intensity amplitude toward the northern CIB (D-D', Fig. 2.10). We also considered the possibility that the Talkeetna Formation could be part, or all, of the source of the high magnetic anomaly (Ab-Ab', Fig. 2.12).

The 2DGAM models show that the Chugach Terrane is comprised of two metamorphosed assemblages with slightly different density and magnetic susceptibility; the McHugh Complex and the younger Valdez Group. The two assemblages are separated by the $20^{o}$ to $50^{o}$ dipping Eagle River Thrust Fault (D-D', Fig. 2.10 and F-F', Fig. 2.11). A shallow intrusion is included on Profile C-C' to decrease misfits between observed and calculated anomalies that may be caused by heterogeneous lithologies and multiform granitic intrusions in the accretionary complex (Pavlis and Roeske, 2007).

A homogenous low velocity-density zone (LVDZ) on Profiles C-C' and D-D' is required at the base of the accretionary complex to match observed gravity lows along the northern profiles (Figs. 2.10 and 2.11). The top of the LVDZ extends to within ~12 km of the surface on C-C' and gently dips downwards to the NW and SE. The thickness of this layer is uncertain. Based on the seismic cross-sections of Ye et al. (1997), the LVDZ appears to be at least 10 km thick (Fig. 2.11). A trenchward increase in the gravity anomaly along Profiles A-A' to D-D' (Fig. 2.10) is constrained by a gently dipping oceanic slab with density highs beneath the LVDZ and the accretionary complex.

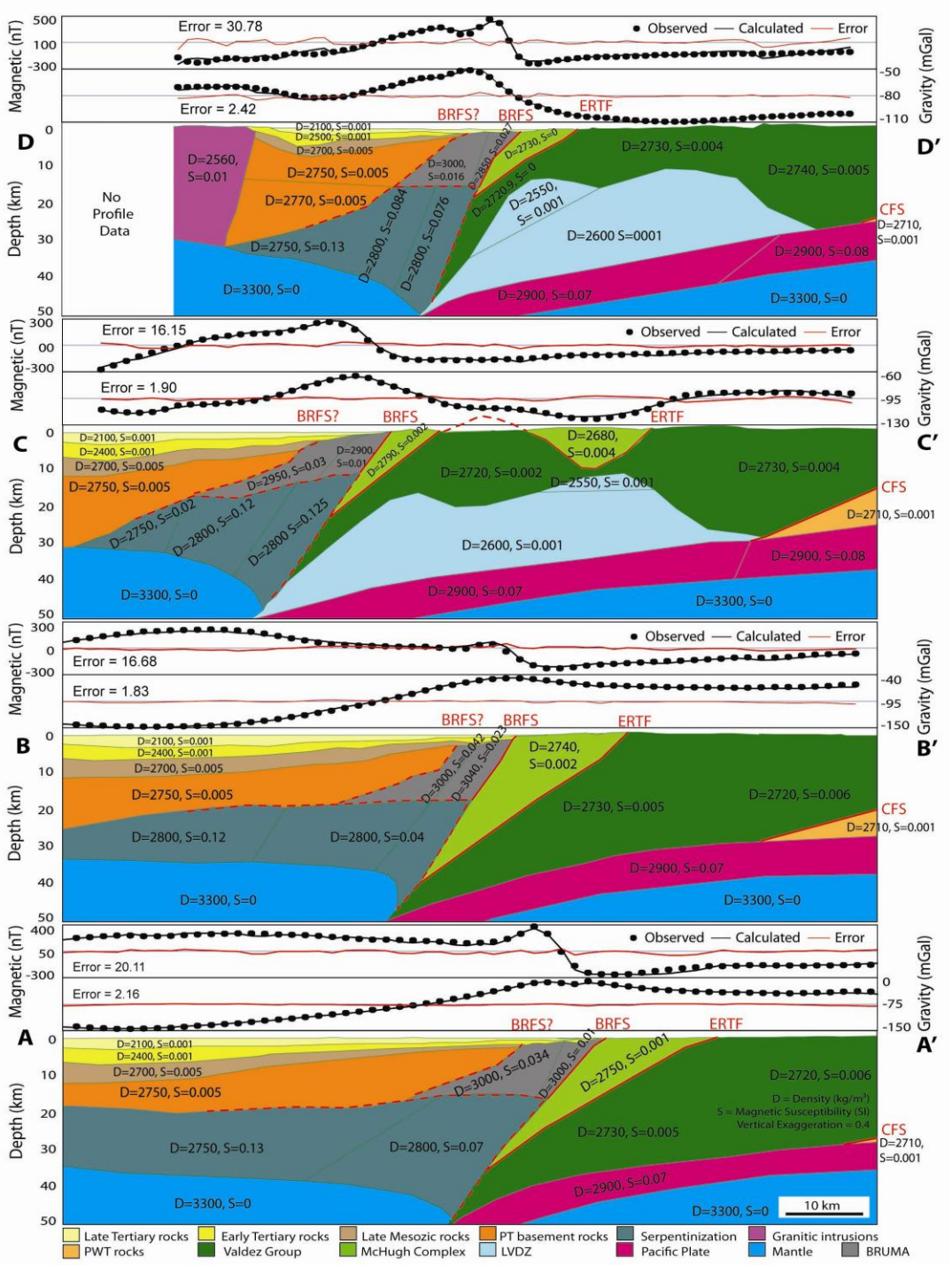


Figure 2.10: 2DGAM models arranged from south to north (A-A', B-B', C-C', to D-D') across the Cook Inlet forearc basin. The profile locations are shown in Figs. 2.3, 2.5, and 2.9. Density and magnetization constraints are given in Table 2.1. Solid red lines indicate known faults that extend to the surface; dashed red lines indicate possible subsurface faults. The BRFS is the Border Ranges fault system; CMF is the Castle Mountain Fault; ERTF is the Eagle River Thrust Fault; PT is Peninsular Terrane; PWT is Prince William Terrane. LVDZ is a low velocity-density zone (see text for details).

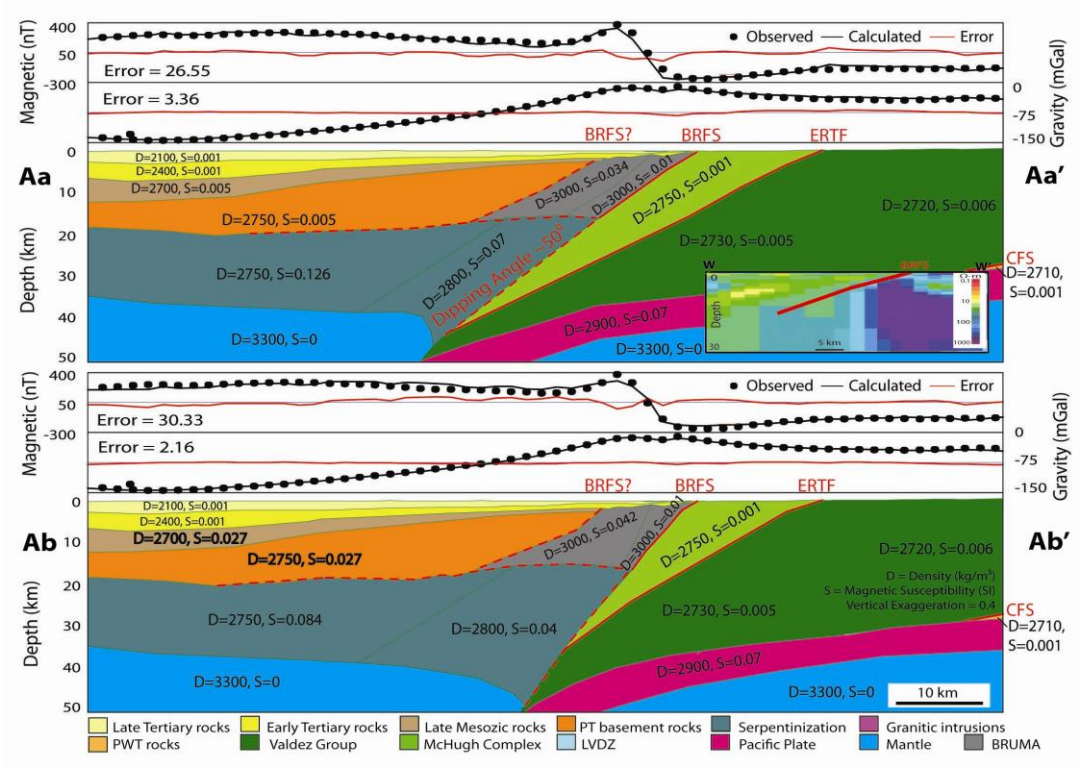


Figure 2.11: 2DGAM models (E-E' and F-F') across the broader subduction zone, south-central Alaska overlain by earthquake data (white cross symbols) collected by Alaska Earthquake Information Center (2011) which are projected up to 20 km from the profile. Profile locations and abbreviations are shown in Figs. 2.1 and 2.10.

## 2.8 DISCUSSION

### 2.8.1 Geometry of the Border Range Fault System

Our integrated 2D gravity-magnetic models suggest that the concealed BRFS is a northwest-dipping, high-angle fault between the Peninsular and Chugach Terranes. Two strong potential field gradients that bound anomaly highs are associated with the BRFS (Figs. 2.4 and 2.6). The eastern gradient corresponds with a major fault located along the Chugach and Kenai Mountain fronts (Fig. 2.9). This interpretation is consistent with previous geophysical models (e.g., Bruns, 1982; Fisher and von Huene, 1984; Green, 2003) and geological cross-sections (Wilson et al., 2009). The western gradient may be another branch of the main fault or represents normal reactivation of the fault that is related to Late Cretaceous or Neogene uplift of the accretionary complex (Arkle, 2011).

The dip angle of the BRFS is controversial due to insufficient geophysical data to image its deeper geometry. Our modeling results shown in profiles A-A' to D-D' (Fig. 2.10) suggest the fault dips steeply (~$70^{o}$) toward the northwest-west and penetrates to at least 12 km based on 2D gravity and magnetic cross-section profiles (Fisher and von Huene, 1984) and seismic tomography models (Fuis et al., 1991). Due to the inherent non-uniqueness of modeling gravity and magnetic data, we tested an alternative (Aa-Aa', Fig. 2.12) for the BRFS with a dip of $50^{o}$ toward the northwest along Profile A-A' based on a magnetotelluric (MT) model presented by Green (2003). This model of the BRFS also provided a reasonable result with acceptable misfit errors, as shown in Fig 2.12. Thus, we cannot choose between these models without further geologic or geophysical constraints.

It is also difficult to constrain the distance that the faults penetrate into the lower crust. Based on the seismic models of Fisher and von Huene (1984), the dip angle of the BRFS seems to decrease with depth to become a décollement at ~16 km depth with many steeply dipping fault branches. According to our 2DGAM results, the BRFS cuts through ultramafic rocks and serves as the structural boundary

between serpentinized and unaltered rocks. Another possibility is that the BRFS penetrates steeply to the base of the crust and lies along the western edge of the BRUMA. However, no recent geophysical data support this interpretation.

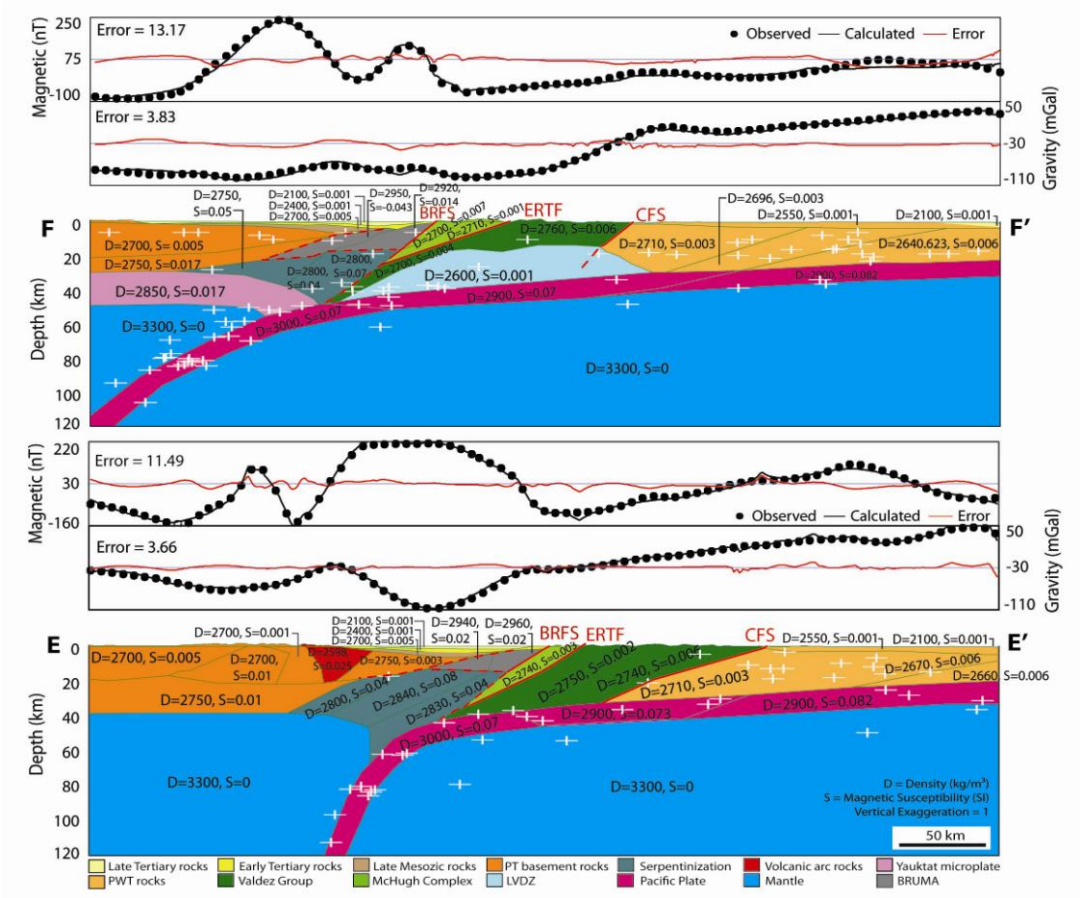


Figure 2.12: Upper) 2DGAM Model Aa-Aa' presents an alternative model with a more gentle dip of 50$^{o}$ for the BRFS and ERTF along the same profile as shown in model A-A'. An inset cross-section W-W' indicates the BRFS location (Fig. 2.2) from the MT interpretation (modified from Green, 2003). Lower) 2DGAM Model Ab-Ab' presents another alternative model with a shallow magnetic source (S = 0.027 SI) and a deeper serpentinized body along the same profile as shown in Model A-A'. The fault locations, map descriptions, and abbreviations are shown in Figs. 2.3, 2.5, 2.9, and 2.10.

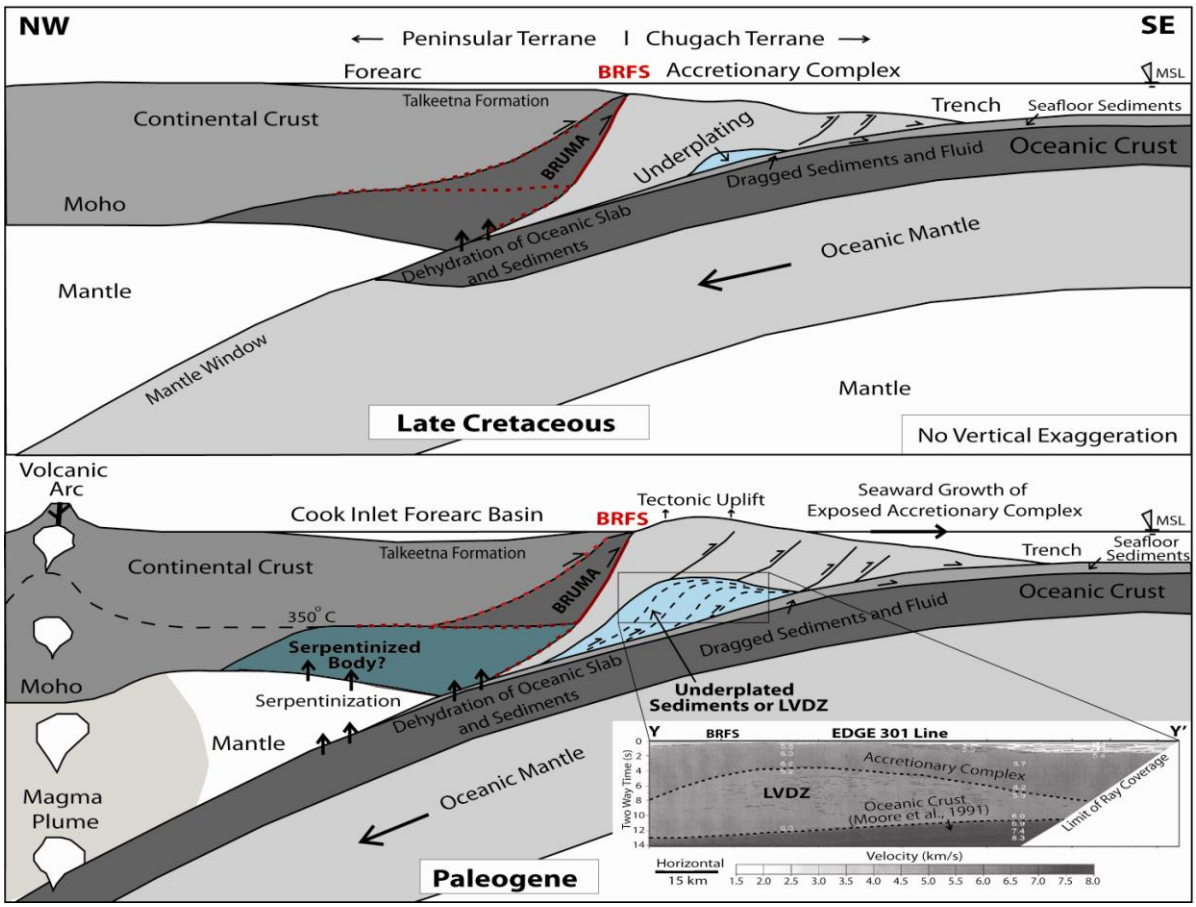


Figure 2.13: Cartoon cross-sections without vertical exaggeration showing how ongoing subduction between Late Cretaceous and Paleogene may have led to formation of a serpentinized crust from Jurassic oceanic arc materials associated with the BRUMA and underplating sediments led to a thick low velocity-density zone (LDVZ) (modified from Plafker et al., 1994; Hyndman and Peacock, 2003; Park et al., 2010; Pavlis et al., 2012). An inset cross-section Y-Y' shows the location of the LVDZ on a velocity model/line drawing based on seismic reflection data along EDGE 301 line (Fig. 2.1) (modified from Moore et al., 1991; Ye et al., 1997).

### 2.8.2 Serpentinized Body

All 2DGAM models show that materials with high magnetic susceptibilities lie between depths of ~16 and ~34 km beneath CIB support the south Alaska magnetic high. Hyndman and Peacock (2003) and Blakely et al. (2005) suggested that the fluidization process of forearc mantle and crust causes abnormal magnetic highs. The subducting slab drags down sediments and fluid during formation of the accretionary wedge. When the slab reaches a temperature of ~350$^{o}$ C at depth, a large volume of fluid is released and rises toward the surface (Fig. 2.13). At these temperatures, the released fluid reacts with pre-existing ultramafic rocks and alters them to form hydrous minerals. Serpentinization produces a residual iron oxide, typically magnetite (Hyndman and Peacock, 2003). The magnetite typically imparts a strong magnetic susceptibility to serpentinites, where its value is proportional to the degree of serpentinization and amount of iron derived from source rocks (Toft et al., 1990).

The serpentinized body interpreted in our 2DGAM models corresponds to a region of conductivity highs from MT profiles (Green, 2003) and low P-wave velocities from seismic tomography models (Eberhart-Phillips et al., 2006). The tops of the conductivity highs shallow and reach the surface at the Knik arm anomaly, which suggests that both the serpentinized body and ultramafic rocks of the BRUMA are associated with the source of the magnetic high (Saltus et al., 2007). P-wave velocity analyses are often used to estimate a degree of the fluidization. Based on studies by Coleman (1971) and Carson (2003), P-wave velocity lows of ~6.2 m/s associated with the regional serpentinized body at depth of 16-34 km correspond to about 40% serpentinization. This result is greater than 20% serpentinization calculated by Hyndman and Peacock (2003) based on seismic tomographic data in the subducted forearc located south of our study area, but close to ~50% serpentinization formed in the forearc of the Cascadia subduction zone (Bostock et al., 2002).

Two hypotheses could explain the deep source (>15 km) of the apparent serpentinization: 1) forearc mantle of the recent subducting slab (Hyndman and Peacock, 2003; Haeussler and Saltus, 2011)

or 2) forearc mantle of the accreted Jurassic oceanic arc (Pavlis and Roeske, 2007). We suggest that the serpentinized body is most easily explained as altered Jurassic forearc mantle in the basement of the Peninsular Terrane (Fig. 2.10). These rocks are observed as fault slices within the BRUMA and must extend beneath the CIB because the basin has behaved as a relatively stable block since Early Jurassic time. A serpentinized body formed from the recent forearc mantle model is less plausible because the top layer of the serpentinized body appears to lie at ~16 km depth, which is much shallower than the estimated Moho depth of 34 km based on the receiver function studies of Romero (2011). Admittedly, it is not obvious what a Moho seismic discontinuity represents in this tectonic setting, but in the broader context of the entire geophysical data set the "lower crust" from depths of 16-34 km could represent altered mafic rocks, serpentinized ultramafic rocks, or both.

Saltus et al., (2007) suggested that Mesozoic, volcanic, and volcaniclastic rocks of the Talkeetna Formation and associated plutonic rocks, lying at depths of ~6 km beneath the eastern CIB and exposed in the northern Chugach Mountain fronts, and the basement rocks of the Peninsular Terrane, could be a shallow source for the south Alaska magnetic high. We tested this alternative (Ab-Ab', Fig. 2.12) by increasing the magnetization of these Late Mesozoic rocks and the basement rocks up to a value of 0.27 SI (Saltus et al., 2007), while keeping other parameters (e.g. densities and geometries) fixed at the same values and decreasing the magnetization of the serpentinized body until a minimum misfit was obtained. The resulting alternative model still requires a magnetic susceptibility of 0.04-0.08 SI (compared to values of 0.07-0.13 SI for our preferred model in Fig. 2.10) for the deeper serpentinite body (Ab-Ab', Fig. 2.12). This lower value corresponds to the value used in the magnetic cross-section models of Saltus et al., (2007). We also note that if the magnetic highs were solely related to rocks of the Talkeetna Formation we would expect to observe the magnetic highs to increase at the northeastern edge of the CIB within Matanuska Valley where this formation outcrops (Figs. 2.5 and 2.9). Consequently,

these results suggest the south Alaska magnetic high is a complicated feature related to both shallow and deep sources.

### 2.8.3 Underplating of Sediments

Our 2DGAM models (Profiles C-C' and D-D' on Fig. 2.10) present one possible model to support the abnormal gravity lows beneath the central Chugach Mountains. The shallow upper crustal rock itself cannot be the source of the gravity lows due to the dense nature of these accreted rocks and the continuity of surface exposures of the homogeneous rock assemblage, the Valdez Group (Mankhemthong et al., 2012). Thus, to fit the gravity data we need to add a lower density material, here termed a low velocity-density zone (LVDZ), beneath the Chugach Terrane and above the subducting slab (Fig. 2.13). The modeled LVDZ is consistent with P-wave velocity lows observed in the original gridded velocity-depth model obtained by Eberhart-Phillips et al. (2006) in their seismic tomography study and seismic refraction cross-section models (Byrne, 1986; Ye et al., 1997) in the Alaska-Aleutian subduction zone, as well as in other subduction zones around the world such as the Cascadia (Calvert et al., 2011), Makran (Kopp et al., 2000), and Nankai subduction zones (Park et al., 2010).

We suggest that an underplated sediment model explains the LVDZ features observed over the metamorphosed accretionary assemblages. The underplated sediments formed the base of the uplifting accretionary assemblage that was associated with the subduction process in south-central Alaska (e.g., Pavlis and Bruhn, 1983; Moore et al., 1991). The subduction caused shortening of the accretionary wedge during Cretaceous (Moore et al., 1991) with later rapid lateral growth trenchward during the Paleogene. Presumably the underplated sheets are relatively young and had to be stacked to form simple duplex structures in order to maintain a stable taper in the accretionary wedge (Fig. 2.10) (Ye et al., 1997), and underplating is consistent with evidence to the east and south that extensive sediment subduction is associated with the Yakutat Terrane collision (Pavlis et al., 2012). Due to less compaction of mixed fluid and seafloor sediment, turbidite fan, and small continental fragment lithology, the

underplated sediments are expected to have lower densities (Kopp et al., 2000; Park et al., 2011) that match the observed density and velocity lows over the metamorphosed accretionary assemblages (Figs. 2.9 and 2.13).

The fluidization process also may decrease the densities of underplated formations (Park et al., 2011), as happened in the accreted Jurassic oceanic arc. Differentiation from serpentinization process, fluidization does not increase the magnetic susceptibility of underplated formations and the accretionary complex because the complex has minimal ferromagnesian minerals that can be altered to produce magnetite-rich rocks (Housen, 1997; Blakely et. al., 2005). Magnetic anomaly lows from the low-pass-filtered magnetic analysis shown on Fig. 2.7 support the idea that the hydrous underplated sediments are less magnetic originally (Housen, 1997).

Arkle (2011) suggested that underplating is the principal mechanism driving deformation and exhumation in the western Chugach Mountains (Fig. 2.13). New thermochronometry age dating techniques used to address the Tertiary exhumation history of the accreted terranes indicate that this terrane complex has had more than one episode of uplift since ~44 Ma in the western Chugach Mountains (Arkle, 2011). The Border Ranges fault system and Contact fault system may control the locus of this first phase of exhumation at 10-20 Ma (Enkelmann et al., 2008). Pavlis et al. (2012) studied the exhumation in the St. Elias orogen and suggested that uplift due to thrust duplex structures may be related to shortening of the subducting Yakutat microplate. Due to the northwestward subduction of the Yakutat microplate underneath the Chugach Mountains, we suggest that the Yakutat microplate carried its cover beneath the margin and these sediments were underplating in Late Neogene time, contributing to the observed uplift and exhumation event at 3-6 Ma (Enkelmann et al., 2008; Arkle, 2011). However, the relationship between the occurrence of underplated sediment and regional tectonic processes of the subducting slab and Yakutat microplate are still too poorly understood to draw any more firm conclusions.

## 2.9 CONCLUSIONS

We provide detailed 2D integrated forward models for the Border Ranges fault system (BRFS) and related geologic structures based on new gravity data with constraints from existing aeromagnetic, seismic, and well log data. These integrated models show that Cenozoic and Mesozoic sedimentations filled the CIB with ~6 km (northern basin) to ~10 km (central basin) of sedimentary rock overlying the Peninsular Terrane basement. The large gravity lows and magnetic highs over the basin may correlate with deep serpentinized body (16 to 34 km) or/and shallow Mesozoic sedimentary rocks of Talkeetna Formation and mafic rock assemblages of the Peninsular Terrane basement (6 to 20 km). We suggest that altered forearc mantle beneath an accreted Jurassic oceanic arc that comprises the basement of the Peninsular Terrane is a source of the fluid serpentinization. The eastern boundaries of the CIB are characterized by gravity-magnetic highs that are related to a 5-15-km wide slice of the emplaced Border Range ultramafic and mafic assemblages (BRUMA). The BRUMA may be related to the formation of serpentinized rocks that comprise a Jurassic oceanic arc.

The eastern gradient of the BRUMA anomaly along the Kenai-Chugach Mountain fronts is interpreted as the primary location of the BRFS. According to our 2DGAM models, the BRFS represents a buried geologic structure separating the Chugach Terrane and the overthrusted BRUMA. One 2DGAM model suggest the BRFS dips steeply (~$70^{o}$) toward the west-northwest. However, a more gently dipping (~$50^{o}$) BRFS is an alternative model that also fits our observations. The BRFS may cut through the ultramafic assemblages and serve as the structural boundary between serpentinized and unaltered ultramafic rocks or penetrate steeply to the base of the crust along the eastern edge of the BRUMA.

Gravity lows are locally observed over the western Chugach Mountains where the accretionary complex of Chugach Terrane is observed at the surface. A model with underplated sediment at the base of the accretionary complex (12 to 40 km) and above the subducted slab is one explanation for this low

and appears to be associated with a low velocity zone imaged in previous seismic tomography studies. Thus we term this body the low velocity-density zone. The proposed underplated sediments may have formed rapidly to maintain a stable taper at the base of the accretionary complex and drove deformation and exhumation of the accretionary complex.

## 2.10 ACKNOWLEDGMENTS

We are grateful to Baker, M., Kaip, G., Eslick, B., Jones, S., and Budhathoki, P. for helping collect gravity data in 2009, 2010, and 2011. We thank Haeussler, P. for discussions related to the geological background and geophysical modeling of the Cook Inlet forearc basin and the Border Ranges fault system and for housing the field crews during the 2010 and 2011 field seasons. We thank Hussein, M., Patlan, E., and Montana C. for advice regarding the modeling techniques and resolving modeling software problems. This research was funded through the American Chemical Society's Petroleum Research Fund (grant no. 48312-AC8) to Doser, D.I.

## 2.11 REFERENCES

Alaska Earthquake Information Center, 2011, AEIC earthquake database search, accessed September 10, 2012 (http://www.aeic.alaska.edu/html_docs/db2catalog.html).

Alaska Oil and Gas Conservation Commission, 2002, Digital well log files, accessed July 1, 2011 (http://doa.alaska.gov/ogc/DigLog/diglogindex.html).

Altstatt, A.A., Saltus, R.W., Bruhn, R.L., and Haussler, P.J., 2002, Magnetic susceptibilities measured on rocks of the upper cook inlet, Alaska: U.S. Geological Survey Open-File Report 02-139, 18 p.

Amato, J.M., and Pavlis, T.L., 2010, Detrital zircon ages from the Chugach Terrane, southern Alaska, reveal multiple episodes of accretion and erosion in a subduction complex: Geology, v. 38, p. 459-462.

Arkle, J., 2011, Focused exhumation in the southern Alaska syntaxis: New insights from apatite and zircon thermochronology [M.S. thesis]: Fullerton, California State University, Fullerton, 132 p.
Biddle, K.T., 1977, Preliminary study of heavy minerals from the Beluga and Sterling Formations exposed near Homer, Kenai Peninsula, Alaska: U.S. Geological Survey Open-File Report 77-874, 12 p.

Blakely, R.J., 1995, Potential theory in gravity and magnetic applications: Cambridge, the United Kingdom, Cambridge University Press, 136 p.

Blakely, R.J., Brocher, T.M., and Wells, R.E., 2005, Subduction zone magnetic anomalies and implications for hydrated forearc mantle: Geology, v. 33, no. 6, p. 445-448.

Bostock, M.G., Hyndman, R.D., Rondenay, S., and Peacock, S.M., 2002, An inverted continental Moho and serpentinization of the forearc mantle: Nature, v. 417, p. 536-538.

Burger, R H., Sheehan, A.F., Jones, C.H., 2006, Introduction to applied geophysics: Exploring the shallow subsurface: New York, W.W. Norton & Inc, 554 p.

Burns, L.E., 1982, Gravity and aeromagnetic modeling of a large gabbroic body near the Border Ranges Fault, southern Alaska: U.S. Geological Survey Open-File Report 82-0460, 66 p.

Burns, L.E., Pessel, G.H., Little, T.A., Pavlis, T.L., Newberry, R.J., Winkler, G.R., and Decker J. , 1991, Geology of the northern Chugach Mountains, south central Alaska: State of Alaska, Division of Geological and Geophysical Surveys, Professional Report 94, 63 p., 2 plate.

Byrne, T. 1986, Eocene underplating along the Kodiak Shelf, Alaska: Implications and regional correlations: Tectonics, v. 5, p. 403-421.

Calvert, A.J., Preston, L.A., and Farahbod, A.M., 2011, Sedimentary underplating at the Cascadia mantle-wedge corner revealed by seismic imaging: Nature Geoscience, v. 4, p. 545-548.

Carlson, R.L., and Miller, D.J., 2003, Mantle wedge water contents estimated from seismic velocities in partially serpentinized peridotites: Geophysical Research Letters, v. 30, p. 1250-1253.

Christensen N.I., 1966, Elasticity of ultrabasic rocks: Journal of Geophysical Research, v. 71, p. 5921-5931.

Clift, P.D., Pavlis, T., DeBari, S.M., Draut, A.E., Rioux, M., Kelemen, P.K., 2005, Subduction erosion of the Jurassic Talkeetna-Bonanza arc and the Mesozoic accretionary tectonics of western North America: Geology, v. 33, p. 881-884.

Coleman, R.G., 1971, Petrologic and geophysical nature of serpentinites: Geological Society of America Bulletin, v. 82, p. 897-918.

DeBari, S.M., and Coleman, R.G., 1989, Examination of the deep levels of an island arc, the Tonsina Ultramafic-Mafic Assemblage, Tonsina, Alaska: Journal of Geophysical Research, v. 94, p. 4373-4391.

Eberhart-Phillips, D., Christensen, D.H., Brocher, T.M., Hansen, R., Ruppert, N.A., Haeussler, P.J., Abers, G. A., 2006, Imaging the transition from Aleutian subduction to Yakutat collision in central Alaska, with local earthquakes and active source data: Journal of Geophysical Research, v. 111, B11303, 31 p.

Ehm, A., 1983, Oil and gas basins map of Alaska: Alaska Division of Geological & Geophysical Surveys Special Report 32, 1 sheet, scale 1:2,500,000.

Enkelmann, E., Garver, J.I., Pavlis, T.L., 2008, Rapid exhumation of ice-covered rocks of the Chugach-St. Elias orogen, SE-Alaska: Geology, v. 36, p.915-918.

Fisher, M.A., and Magoon, L.B., 1978, Geologic framework of lower Cook Inlet, Alaska: American Association of Petroleum Geologists Bulletin, v. 62, p. 373-402.

Fisher, M.A., and von Huene, R., 1984, Geophysical investigation of a suture zone: The Border Ranges Fault of southern Alaska: Journal of Geophysical Research, v. 89, p. 11,333-11,351.

Fuis, G., and Plafker, G., 1991, Evolution of deep structure along the Trans-Alaska Crustal Transect, Chugach Mountains and Copper River Basin, southern Alaska: Journal of Geophysical Research, v. 96, p. 4229-4253.

Gardner, G.H.F., Gardner, L.W., and Gregory, A.R., 1974, Formation velocity and density – The diagnostic basics for stratigraphic traps: Geophysics, v. 39, p. 770-780.

Gesch, D., Oimoen, M., Greenlee, S., Nelson, C., Steuck, M., and Tyler, D., 2002, The National Elevation Dataset: Photogrammetric Engineering and Remote Sensing, v. 68, p. 5-11.

Gesch, D.B., 2007, The National Elevation Dataset, *in* Maune, D., ed., Digital Elevation Model technologies and applications: The DEM users manual, 2nd Edition: Bethesda, Maryland, American Society for Photogrammetry and Remote Sensing, p. 99-118.

Godfrey, N.J., and Klemperer, S.L., 1998, Ophiolitic basement to a forearc basin and implications for continental growth: The Coast Range/Great Valley ophiolite, California: Tectonics, v. 17, p. 558-570.

Godson, R.H., 1984, Composite magnetic anomaly map of the United States, Part B - Alaska and Hawaii: U.S. Geological Survey Geophysical Investigations Map, Report GP-954-B, 8 p., 2 sheets, scale 1:2500000.

Grantz, A., Zeitz, I., and Andreasen, G.E., 1963, An aeromagnetic reconnaissance of the Cook Inlet area Alaska: U.S. Geological Survey Professional Paper 316-G, p. 117-134.

Green, A.M., 2003, Magnetotelluric crustal studies in Kenai, Alaska [M.S. thesis]: Golden, Colorado School of Mines, 78 p.

Haeussler, P.J., and Anderson, R.S., 1997, The "Twin Peaks Fault"; not tectonic or seismogenic structure, *in* Dumoulin, J.A., and Gary, J.E., eds., U.S. Geological Survey Professional Paper, v. 1574, p. 93-99.

Haeussler, P.J., Bruhn, R.L., and Pratt, T.L., 2000, Potential seismic hazards and tectonics of upper Cook Inlet basin, Alaska, based on Pliocene and younger deformation: Geological Society of America Bulletin, v. 112, p. 1414-1429.

Haeussler, P.J., and Saltus, R.W., 2011, Location and extent of Tertiary structure in Cook Inlet basin, Alaska, and Mantle Dynamics that focus deformation and subsidence, *in* Dumoulin, J.A., and Galloway, J.P., eds., Studies by the U.S. Geological Survey in Alaska 2008-2009: U.S. Geological Survey Professional Paper, v. 1776-D, 26 p.

Hill, M., Morris, J., and Whelan, J., 1981, Hybrid granodiorite intruding the accretionary prism, Kodiak, Shumagin, and Sanak Islands, southwest Alaska: *Journal of Geophysical Research*, v. *86*, p. 10, 569-10, 590.

Housen, B.A., 1997, Magnetic anisotropy of Barbados prism sediments, *in* Shipley, T.H., Ogawa, Y., Blum, P., and Bahr, J.M., eds., Proceedings of the Ocean Drilling Program Scientific Results, v. 156, p. 97-105.

Hyndman, R.D., and Peacock, S.M., 2003, Serpentinization of the forearc mantle: Earth and Planetary Science Letters, v. 212, p. 417-432.

Lim, E., Eakins, B.W., and Wigley, R., 2009, Coastal Relief Model of southern Alaska, National Geophysical Data Center, NESDIS, NOAA.

Little, T.A., and Naeser, C.W., 1989, Tertiary tectonics of Border Ranges fault system, Chugach Mountains, Alaska: deformation and uplift in a forearc setting: Journal of Geophysical Research, v. B4, p. 4333-4359.

Nettleton, L.L., 1939, Determination of density for reduction of gravimeter observations: Geophysics, v. 4, p. 8176-8183.

MacKevett, E.M., Jr., and Plafker, G., 1974, The Border Ranges Fault in south-central Alaska; U.S. Geological Survey Journal of Research, v. 2, p. 323-329.

Mankhemthong, N., Doser, D.I., Baker, M.R., 2012, Practical estimation of near surface bulk density variations across the Border Ranges fault system, central Kenai Peninsula, Alaska: Journal of Environmental & Engineering Geophysics, v.17, p. 9-12.

Moore, J.C., Diebold, J.B., Fisher, M.A., Sample, J.C., Brocher, T.M., Talwani, M., Ewing, J.I., von Huene, R., Rowe, C., Stone, D., Stevens, C., and Sawyer, D.S.,1991, EDGE deep seismic reflection transect of the eastern Aleutian arc-trench layered lower crust reveals under-plating and continental growth: Geology, v. 19, p. 420-424.

Nokleberg, W.J., Plafker, G., Lull, J.S., Wallace, W.K., and Winkler, G.R., 1989, Structural analysis of the southern peninsular, southern Wrangellia, and northern Chugach Terranes along the Trans-Alaska Crustal Transect, northern Chugach Mountains, Alaska: Journal of Geophysical Research, v. *94*, p. 4297-4320.

Parasnis, D.S., 1952, A study of rock densities in English Midlands: Geophysical Journal International, v. 6, p. 252-271.

Park, J., Fujie, G., Wijerathne, L., Hori, T., Kodaira S., Fukao, Y., Moore, G.F., Bangs, N.L., Kuramoto, S., Taira, A., 2010, A low-velocity zone with weak reflectivity along the Nankai subduction zone: Geology, v. 38, p. 283-286.

Pavlis, T.L., 1982, Origin and age of the Border Ranges Fault of southern Alaska and its bearing on the Late Mesozoic tectonic evolution of Alaska: Tectonics, v. 1, p. 343-368.

Pavlis, T.L., and Bruhn, R.L., 1983, Deep-seated flow as a mechanism for the uplift of broad forearc ridges and its role in the exposure of high P/T metamorphic terranes: Tectonics, v. 2, p. 473-497.

Pavlis, T.L., and Roeske, S.M., 2007, The Border Ranges fault system, southern Alaska, *in* Ridgway, K.D., Trop, J.M., Glen, J.M.G., and O'Neill, J.M., eds., Tectonic growth of a collisional continental margin: Crustal evolution of southern Alaska: Geological Society of America Special Paper 431, p. 95-128.

Pavlis, T.L., Bruhn, R.L., Ridgway, K., Worthington, L.L., Gulick, S.P.S., Spotila, J., 2012, Structure of the actively deforming fold-thrust belt of the St. Elias orogen with implications for glacial exhumation and three-dimensional tectonic processes: Geosphere, v. 8, p. 991-1019.

Plafker, G., Nokleberg, W., and Lull, J., 1989, Bedrock geology and tectonic evolution of the Wrangellia, Peninsular, and Chugach Terranes along the Trans-Alaska Crustal Transect in the Chugach Mountains and southern Copper River Basin, Alaska: Journal of Geophysical Research, v. 94, p. 4255-4295.

Plafker, G., Moore, J.C., and Winkler, G.R., 1994, Geology of the southern Alaska margin, *in* Plafker, G. and Berg, H.C., eds., The geology of Alaska: Boulder, Colorado, Geological Society of America: The Geology of North America, v. G1, p. 389-449.

Reger, R.D., and Pinney, D.S., 1997, Last major glaciations of Kenai lowland, i*n* Karl, S.M., Vaughn, N.R. and Ryherd, T.J., eds., 1997 Guide to the geology of the Kenai Peninsula, Alaska: Alaska Geological Society, p. 54-67.

Romero, O., 2011, Seismological studies in south central Alaska and northern Mexico [Ph.D. thesis]: El Paso, University of Texas at El Paso, 105 p.

Saltus, R.W., and Simmons, G.C., 1997, Composite and merged aeromagnetic data for Alaska: A website for distribution of gridded data and plot files: U.S. Geological Survey Open-File-Report 97-520 (http://geology.cr.usgs.gov/pub/open-file-reports/ofr-97-0520/).

Saltus, R.W., Haeussler, P.J., Bracken, D.E., Doucette, J.P., Jachens, R.C., 2001, Anchorage urban region aeromagnetics (AURA) Project-Preliminary Geophysical Results: U.S. Geological Survey Open-File Report 01-0085, 21p.

Saltus, R.W., and Haeussler, P.J., 2004, Magnetic properties of Quaternary deposits, Kenai Peninsula, Alaska - Implications for aeromagnetic anomalies of Upper Cook Inlet: U.S. Geological Survey Open-File Report 2004-1202, 26 p.

Saltus, R.W., Blakely, R.J., Haeussler, P.J., Wells, R.E., 2005, Utility of aeromagnetic studies for mapping of potentially active faults in two forearc basins: Puget Sound, Washington, and Cook Inlet, Alaska: Earth, Planets and Space, v. 57, p. 781-793.

Saltus, R.W., Hudson, T.L, and Wilson, F.H., 2007, The geophysical character of southern Alaska-implications for crustal evolution, *in* Ridgway, K.D., Trop, J.M., Glen, J.M.G., and O'Neill, J.M., eds., Tectonic growth of a collisional continental margin: Crustal evolution of southern Alaska: Geological Society of America Special Paper 431, p. 1-20.

Sanger, E.A., and Glen, J.M.G., 2003, Density and magnetic susceptibility values for rocks in the Talkeetna Mountains and adjacent region, south-central Alaska: U.S. Geological Survey Open-File Report 03-268, 42 p.

Shellenbaum, D.P., Gregersen, L.J., and Delaney, P.R., 2010, Top Mesozoic unconformity depth map of the Cook Inlet basin, Alaska: Report of Investigations RI 2010-2, Alaska Division of Geological & Geophysical Surveys Report of Investigation 2010-2, 1 sheet, scale 1:500000.

Swenson, R.F., 1997, Introduction to Tertiary tectonics and sedimentation in the Cook Inlet basin, *in* Karl, S.M., Vaughn, N.R., and Ryherd, T.J., eds., 1997 Guide to the geology of the Kenai Peninsula, Alaska: Alaska Geological Society, p. 18-27.

Toft, P.B., Arkani-Hamed, J., Haggerty, S.E., 1990, The effects of serpentinization on density and magnetic susceptibility: a petrophysical model: Physics of the Earth and Planetary Interiors**,** v. 65, p. 137-157.

Wilson, F.H., Hults, C.P., Schmoll, H.R., Haeussler, P.J., Schmidt, J.M., Yehle, L.A., and Labay, K.A., 2009, Preliminary geologic map of the Cook Inlet region, Alaska: U.S. Geological Survey Open-File Report 2009-1108 (http://pubs.usgs.gov/of/2009/1108/).

Ye, S., Flueh, E.R., Klaeschen, D., and von Huene, R., 1997, Crustal structure along the EDGE transect beneath the Kodiak shelf off Alaska derived from OBH seismic refraction data: Geophysical Journal International, v. 130, p. 283-302.

# SECTION 3

## Constraints on the Structure of the Border Ranges Fault System, Kenai Peninsula, Alaska, from testing a simple block model technique on the 3D Inversion of Gravity Data

*Niti Mankhemthong[1], Diane I. Doser[1], Mark Baker[2], Rolando Cardenas[3]*
*[1]Department of Geological Sciences, University of Texas at El Paso, El Paso, TX 79968-0555*
*[2]Geomedia Research and Development, 6040 Strahan, El Paso, TX 79932, USA.*
*[3]Program in Computational Science, University of Texas at El Paso, El Paso, TX 79968, USA.*

### 3.1 ABSTRACT

We tested plausible initial 3D density models across the eastern Cook Inlet basin using an inversion method based on updated gravity data to constrain the geometry of the Border Ranges fault system (BRFS) and associated structures of the Border Range ultramafic and mafic assemblages (BRUMA). The BRFS forms the structural boundary between the forearc and accretionary terranes of the Aleutian subduction zone in southern Alaska. The BRUMA is a part of the forearc basement rocks that were sliced and thrust upward along the BRFS during the Late Mesozoic. We used 2D density cross-sections as starting models to constrain the 3D inversion block model. We computed the theoretical gravity based on the inversion and compared it to the observed gravity. Gravity differences are generally less than 2 mGal, except the area where the BRUMA is exposed where gravity differences are greater than 4 mGal. Thus, the first applied *"a priori"* model lacks the greater densities required to match observed gravity highs over the BRUMA region. We then computed surface density models from the inversion routine and compared density results and modeling uncertainties to the *"a priori"* density information. The best fit density for the five layers show calculated density distributions that match *"a priori"* models to within 10-100 kg/m$^3$. This might suggest uncertainties on *"a priori"* densities (100-300 kg/m$^3$) or gravity values (1-5 mGal) may be too low so that the inversion may not be allowed to search the entire solution space. Higher misfits occur at contacts between geologic units in regions of complex geology. Lastly, we applied horizontal density gradient analysis to the density solution models

in order to estimate the extent of the BRFS and BRUMA structures. The BRFS appears to dip gently toward the northwest ($50^o$ -$70^o$) along the central Kenai Mountains and steeply ($70^o$- $80^o$) along the northern Chugach Mountain front. This suggests strike-slip faulting occurred along the northern BRFS. The BRUMA belt is modeled as a trapezoidal shaped feature formed by thrusting slices lower crust mantle material. The BRUMA is poorly resolved in the northern Kenai Peninsula due to poor gravity coverage. The region of poor resolution may reflect the poor coverage or to segmentation of the fault system.

## 3.2 INTRODUCTION

The Border Ranges Fault System (BRFS) serves as the structural boundary between the forearc basin of Cook Inlet and the accretionary complex of the Kenai and Chugach mountains. The BRFS has played a major role in the development of the forearc basin system and collisional orogenesis of south-central Alaska since the Jurassic Period Pavlis and Roeske, 2007 (Fig. 3.1). We know little about the subsurface structure of the fault system or how it has influenced the past and present day tectonics of the forearc region. Surface exposure of the BRFS is limited and only a few geophysical surveys have been previously conducted across it (e.g., Burns, 1982; Fisher and von Huene, 1984).

A new dense set of gravity data has been used to help build and test subsurface models of regional geology. With better gravity constraints, density contrasts between adjacent rock units may help us define geologic contacts, including the plausible geometry for the inferred BRFS. We have collected ~1400 gravity points from surveys conducted in 2009-2011 that span the region between the eastern Cook Inlet basin and the topographically higher Kenai and Chugach Mountains. Gravity interpretations and 2D density modeling show high density contrasts of geologic bodies across the BRFS, where the maximum gravity highs and lows reflect shallow ultramafic assemblages and basin deposits, respectively. There is a limitation to modeling geologic bodies along 2D density profiles due to lack of data constraints and the complexity of geologic structures. Thus, the oriented structure of the BRFS is

still poorly resolved in the subsurface (Mankhemthong et al., in press). Since the 3D inversion technique is based on using a sequence of gridded geologic and topographic surfaces, it is feasible to develop software to help build and invert the highly complex geologic models.

Our study applied a geologically constrained inversion method to test a simple block model structure using these results we can then build a sufficiently detailed model to an arbitrary depth. We present a 3D gravity model for the eastern Cook Inlet basin and related structures that uses an inversion approach developed by Baker and Crain (2001). This approach, which has been modified by Cardenas (2011), starts by directly calculating free air gravity using estimated density, geology, and topography. We assumed the misfit between the observed and calculated gravity corresponds to misinterpreted gravity effects from near surface topography and geology that need to be corrected. Topography from integrated DEMs is used to constrain gridded gravity positions. Density and depth constraints from a simplified version of surface geology maps and 2D density modeling interpretations (Mankhemthong et al., in press) are used to guide the building of the 3D density models. In this study, we used a simple structural block as our "*a priori"* model and estimated its uncertainties. We interpreted the BRFS and the BRUMA geometries based on the best resulting density model obtained from the inversion process.

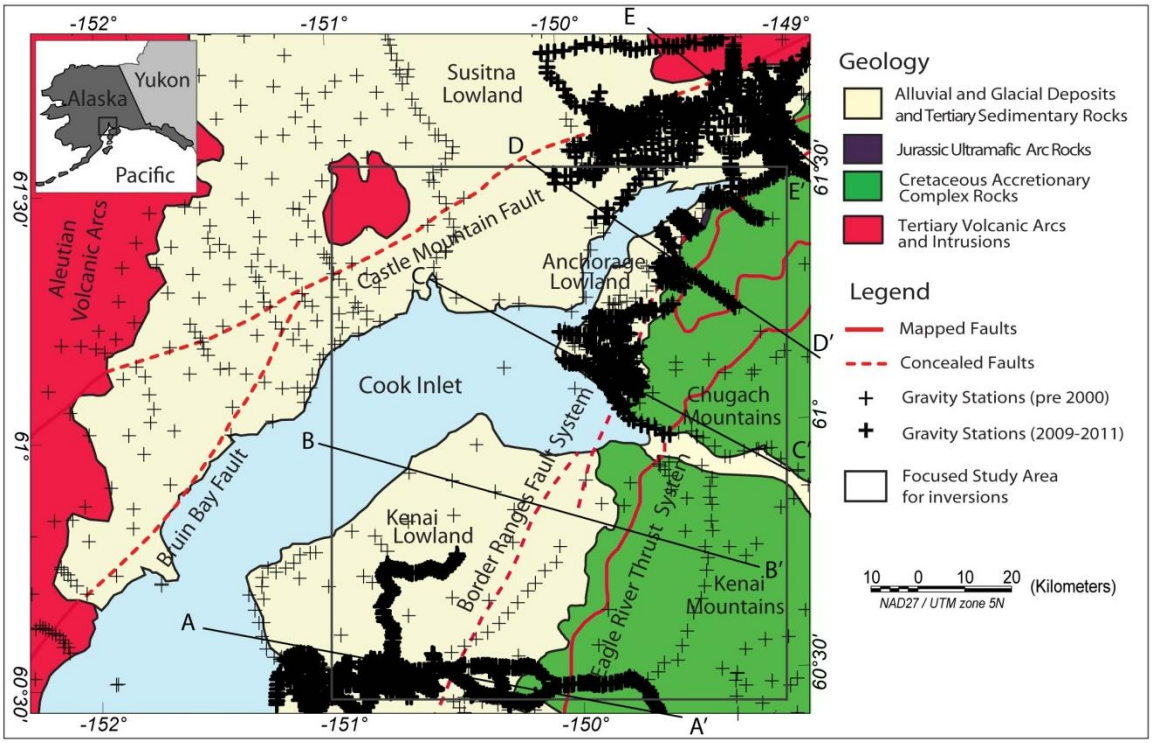


Figure 3.1: Geologic map of the central Kenai Peninsula showing locations of gravity measurements (geology simplified from Wilson et al., 2009). The 2D gravity cross-sections used for building the geologic models lie along A-A' to E-E'. Fault data are digitized from Haeussler et al. (2000).

## 3.3 BACKGROUND GEOLOGY

The study area spans a region marked by a pronounced change in topography from the Kenai and Anchorage Lowlands and Matanuska Valley of the Cook Inlet Basin to the Kenai and Chugach Mountains, south-central Alaska. In our study area, no strong geologic evidence indicates the position of the surface location of the BRFS, especially along the mountain front of the central Kenai Peninsula. Previous geophysical studies suggest that the buried location of the BRFS forms a 2-10 km wide zone (e.g., Burns, 1982; Fuis and Plafker, 1991) and that the BRFS separates the western edge of the Peninsular Terrane from the Chugach Terrane (Nokleberg et al., 1989). The BRFS dips steeply ($50^{o}$-$70^{o}$) to vertically toward the Cook Inlet Basin and may penetrate to the base of the lower crust (Fisher and von Huene, 1984; Mankhemthong et al., in press).

In the Alaska-Aleutian subduction zone, the Cook Inlet basin represents a Cenozoic forearc basin system separating the accretionary complex of the Kenai and Chugach Mountains from the modern volcanic arc of the Alaska-Aleutian Range (Fig. 3.1). The Cook Inlet basin is filled within the 18-45 m deep brackish sea of Cook Inlet (Gatto, 1976) and Quaternary glacial and recent fluvial material that form the Kenai and Anchorage Lowlands and the base of Cook Inlet. The geology of the Cook Inlet basin mainly consists of 6000 to 10000-m-thick non-marine and shallow marine sedimentary rock facies ranging from Late-Cretaceous to Quaternary which extend well east of the present Cook Inlet basin across the trailing edge of the Peninsular Terrane (Mankhemthong et al., in press). Volcanic and volcaniclastic rock assemblages of the late Triassic to Early Jurassic Talkeetna Formation and the intrusive assemblages of the Peninsular Terrane basement lie underneath this sedimentary section (e.g., Clift et al., 2005).

The Border Ranges Ultramafic and Mafic Assemblage (BRUMA) is a sequence of dense basement rocks that stratigraphically underlies younger sedimentary sequences to the east of the Cook Inlet basin (DeBari and Coleman 1989; Plafker et al., 1989). The BRUMA is gabbro to tonalite in

composition with local occurrences of ultramafic rocks (e.g., Burns, 1982; Plafker et al., 1994) and is interpreted as a fragmented crustal section of an Early Jurassic oceanic arc system (Plafker et al., 1989; Pavlis and Roeske, 2007). Pavlis et al. (1988) and Pavlis and Roeske (2007) suggested the BRUMA may represent the upper mantle roots of a serpentinized arc assemblage overlain by lower-crustal mafic rocks grading upward to a volcanic cover of lower-Jurassic volcanic rocks (e.g., Pavlis and Roeske, 2007). Previous geophysical potential field studies and outcrop exposures in the northern Chugach Mountains have confirmed the shallow occurrence of the BRUMA along the western Kenai and Chugach Mountains (e.g., Burns, 1982).

East of the BRUMA and Cook Inlet basin, the geology is related to collisional orogeny and subduction of a succession of oceanic slabs occurring since the Jurassic (e.g., Plafker et al., 1989; Little and Naeser, 1989). The Kenai and Chugach Mountains formed as parts of an uplifted Cretaceous accretionary terrane that is comprised of low-grade metamorphic mélange and metasedimentary assemblages (Plafker et al., 1994). To the west of the Cook Inlet basin, the Alaska-Aleutian Range forms a part of a young volcanic arc (Trop and Ridgway, 2007). The arc rocks are dominated by plutons interpreted as the massive deeper roots of subvolcanic intrusions. These arcs have been formed since mid-Jurassic, but the main episode of arc magmatism occurred later during the Late Cretaceous and Late Paleogene (Trop and Ridgway, 2007).

### 3.4 GRAVITY OBSERVATION

The observed gravity values that serve as input data into the inversion are comprised of ~1400 of new gravity observations acquired from 2009-2011. About ~3000 existing regional gravity data were acquired and .processed from the U.S. Geological Survey and University of Texas at El Paso databases that were collected before 2000 (Fig. 3.1). The new gravity measurements were collected by a Lacoste & Romberg Model G gravimeter with associated reading errors estimated to be <0.1 mGal. Associated elevation and location control information for the new data were collected by a GB-100 GPS receiver

with processing implemented in steps to achieve less than 0.2 m (~0.08 mGal) elevation control and 0.04 m horizontal control (~0.0001 mGal). Thus, we estimate a combined acquisition error of <0.2 mGal for our new data. We estimated the acquisition error for the pre-existing data collected before 1997 with inaccurate elevation control to be around 2 mGal. In order to produce the free air anomaly, which is a residual gravity after the corrections, we have applied drift and tidal, latitude, and free air corrections to the gravity measurements. The free air anomaly represents the effects of the earth's mass from the topographic surface to the reference datum. Surface topography and density effects are then incorporated in the 3D forward and inverse modeling process.

## 3.5 GRID SET OF DATA CONSTRAINTS

Building a gridded data set of *"a priori"* information is necessary to constrain the inversion process and helps address the problem of non-uniqueness. The inversion technique is based on a generalized, nonlinear formulation using a least-squares criterion. The *"a priori"* constraints are essential in order to guide the algorithm to compute models that are consistent with the geology of the region (Cardenas, 2011). In this test, we approximated the 3D geologic model by a series of multiple blocks, but geologic bodies can be defined by gridded upper and lower subsurfaces of arbitrary shapes depending on how the "a priori" models are set up.

As a starting point we fixed the 3D geology, treating it as a geologic hypothesis by making a simple block model. This means more geologically plausible contacts and body shapes are truncated in the *"a priori"* model to make them fit block shapes. We do not allow the geologic contacts and surface depths to vary during the inversion process. Two data sets are used to constrain the "*a priori*" ground surface of the model (Fig. 3.2). The onshore surface topography is based on the National Elevation Dataset (NED), a raster terrestrial elevation data set with 60-m grid spacing and less than a cm vertical resolution, updated by Gesch et al. (2002) and Gesch (2007). Geologic contacts on flattened surfaces

were interpreted based on the 2D models of Mankhemthong et al., (in press) and are more poorly constrained, especially in areas located between the 2D modeling profiles.

In this study, we ran the inversion using fixed block model technique and then simply determined the subsurface location and geometry of the BRUMA based on how rapidly the resulting densities in the block model changed. The initial density model has been built with five surfaces consisting of ground level, and tops at depths of 5, 10, 15 km, 25 km, which cover the BRFS and BRUMA structures (Fig. 3.3). The *"a priori"* uncertainties assigned to these densities were around 100-300 kg/m$^3$ based on physical bounds, our knowledge of the surrounding geology, and the quality of the gravity survey data and topographic information (Cardenas, 2011). All input data were interpolated using the Kriging gridding method available on the Geosoft Oasis montaj software package with a 1,000-meter square grid (~0.01 degree). The standard coordinate system we used was a projected UTM-NAD27 with ellipsoid height in meters. We extended the model 10 km beyond the study area. This extension area will be increased to around one degree (~100 km) for the next approach in order to better minimize the gravity edge effects at the rim of the study area (Khatun et al., 2007).

As an initial step in building the 3D model, we tested the inversion by using only one *"a priori"* density model. Major geologic units were assigned to the bodies enclosed by grouped surfaces and giver *"a priori"* densities (Table 3.1). We only used the separate densities: A density of 2100 kg/m$^3$ for average surface sediments, a density of 2730 kg/m$^3$ for accretionary complex rocks, and a density of 1000 kg/m$^3$ for the water body (Fig. 3.3). A greater density value was not assigned to rocks of the BRUMA in order to see if the inversion would require denser values over the BRUMA to match the observed gravity.

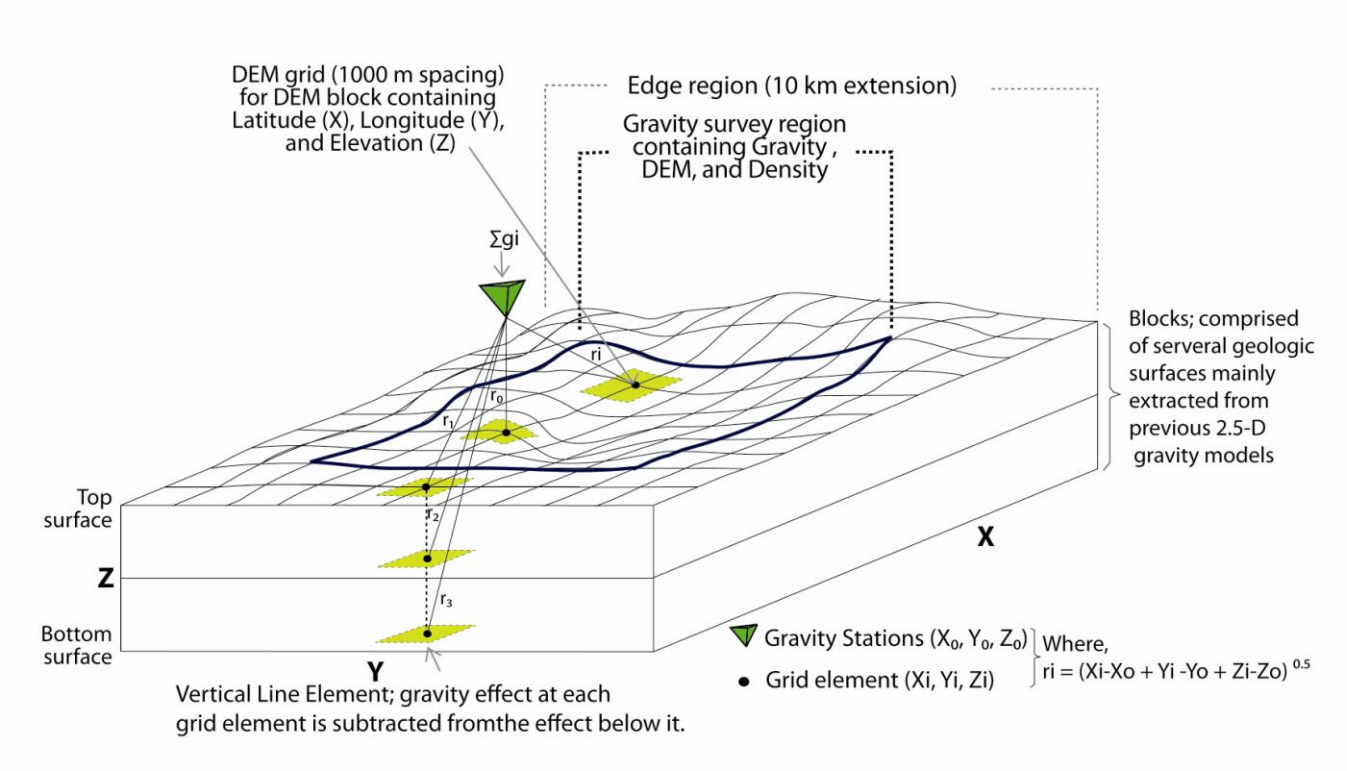


Figure 3.2: Illustration of grid element configuration consisting of multiple surface block models (e.g., topography, bathymetry, and basin surface). Each grid element yields a gravitational contribution that is summed over the region to calculate the overall gravity effect for a individual gravity station (modified from Cardenas, 2011). The theoretical gravity (g) of each grid element gravity is calculated based on the Euclidean distance (r) from a gravity source (X0, Y0, Z0) to an expected density block (Xi, Yi, Zi) and estimated density (ρ). The i-th step is demonstrative of the sum of gravitational effects for a single grid element.

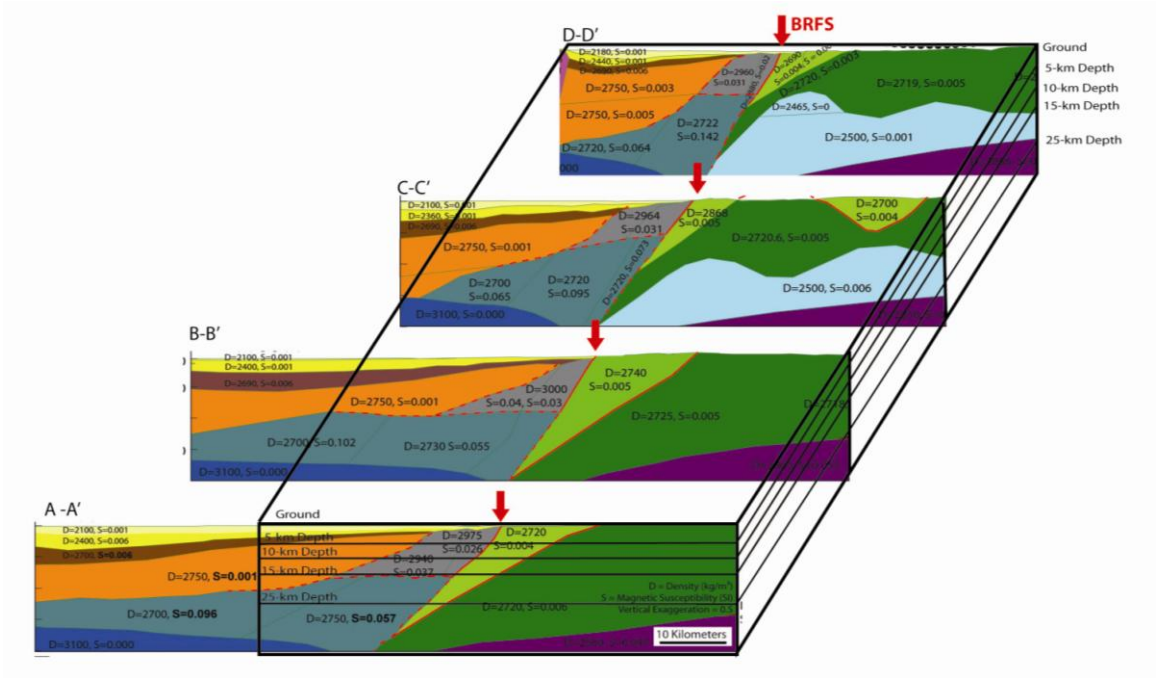


Figure 3.3: Four density profiles: A-A' to D-D' modified from the 2D Gravity cross-section models that were used for *"a priori"* density and geologic constraints in the 3D density block model (bold black rectangles). Black lines indicate the intersection of the top and bottom of five surfaces with the density model. D is density in kg/m$^3$. S is a Magnetic susceptibility in SI. Profile locations are shown in Figure 3.1.

Table 3.1: Densities used in the *"a priori"* models

| **Model bodies** | **Densities*** **(kg/m$^3$)** | **Uncertainties** **(kg/m$^{3)}$** |
|---|---|---|
| Water | 1000 | 0 |
| Basin Sediments | 2100 | 100-300 |
| Peninsular Basement Rocks | 2750 | 100-300 |
| Accretionary Complex rocks | 2730 | 100-300 |

* Based on Mankhemthong et al. (2012) and Mankhemthong et al. (in press)

## 3.6 FORWARD AND INVERSE MODELING METHODS

We started with a forward modeling technique to compute the theoretical free air gravity at the surface based on estimated densities in the subsurface from the inversion technique and see how closely it matches the gravity observation. The forward algorithm we used was originally developed by Baker and Crain (2001) and modified by Cardenas (2011). The algorithm uses vertical line elements to approximate the gravitational attraction of bodies within the mode (Fig. 3.2). A calculation of total gravity contributions ($\sum g_i$) simply known as "calculated gravity" in the inversion is a volume integral of all gravitational grid elements over multiple layered blocks in all dimensions (Boulanger and Chouteau, 2001). It is important to note the length of the vertical line element is theoretically infinite. The subtraction process eliminates the infinite part of the line element (Khatun, 2007). To test our model, we computed a residual anomaly obtained by subtracting the model contributions from the free air observations which ideally should be close to zero.

The gravity observation uncertainties that may cause of a misfit between observed calculated and gravity are included in an *"a priori"* covariance matrix ($C_g$) (Cardenas, 2011). We gave this matrix default values small uncertainties (1-5 mGal) depending on the quality of gravity data collected by various surveys. The causes of the uncertainties can be categorized in three main areas consisting of the procedure of the forward model.

In this study, we used a 3D gravity inversion method to test the "*a priori"* density models. The inversion approach is based on a generalized, nonlinear inversion scheme introduced by Tarantola and Valette (1982). The matrix $C_\rho$ in this inversion approach represents the "*a priori"* uncertainties on the unknown density (Cardenas, 2011). We assumed the level of certainty of density value to be fairly high with approximate values of 100-300 kg/m$^3$.

The estimated density (ρ) from the original *"a priori"* model is then iteratively adjusted to ensure an adequate minimization of the residual anomaly, thus yielding a plausible density model. We

assumed that residuals may reflect an ignored topographic terrane effect, uninterrupted shallow subsurface geology, underestimations or overestimations of densities of the model densities, or data errors (Crain, 2006). The tested inversion model that maintaining plausible density values was judged to be the best hypothesis for the 3D density distributions of each surface layer.

## 3.7 RESULTS AND DISCUSSION

### 3.7.1 Total Gravity Contribution Interpretations and Analyses of Forward Modeling

We show three gravity results in Figure 3.4: 1) the observed gravity anomaly obtained from the gravity reduction process, 2) the calculated (theoretical) gravity contributions of the free air gravity from the forward modeling technique, and 3) the residual free air gravity which is the difference between the calculated and the observed gravity models. Ideally, the residual gravity should be close to zero. However, in practice, this is highly unlikely due to data uncertainties, computational errors, sparse gravity data coverage, and the truncation of geologic bodies used to derive the block model.

The observed free air gravity anomaly shows broad gravity lows (-130 to -100) within the Cook Inlet basin and the Turnagain Arm (TA in Fig. 3.4) regions. Strong gravity gradients are observed in the surrounding areas, generally indicating the basin boundary. Maximum gravity gradients are observed along the Chugach and Kenai Mountain fronts on the eastern basin rim. Gravity highs (-60 to 20 mGal) are found within the surrounding mountain ranges, and the maximum gravity highs (-10 to 0 mGal) appear in a belt of anomalies along the eastern margin of the Cook Inlet basin. These likely represent higher density arc and accreted rocks where the maximum anomalies may be associated with the exposed and shallow concealed rocks of the BRUMA (Burns, 1982; Pavlis and Roeske, 2007).

The free air gravity (Fig. 3.4b) computed by inverting the *"a priori"* simple block model inversion looks fairly similar to the observed free air gravity with differences of less than 0.2 mGal. However, larger misfits (~0.45 mGal) are observed locally over a region where the BRUMA is exposed

at the surface. These misfit highs show that a simple geologic interpretation that excludes the BRUMA is not capable of representing the complexity of the gravity field in that region. In addition, there are edge effects visible (pink bulls eye anomalies of 0.4 mGal in Fig. 3.4c) at contacts between two density bodies that reflect the misestimate of densities at edges of the geologic rock contacts. The positive differences between observed and calculated gravity indicate the *"a priori"* density model is too low in the region of the BRUMA (Fig. 3.4c).

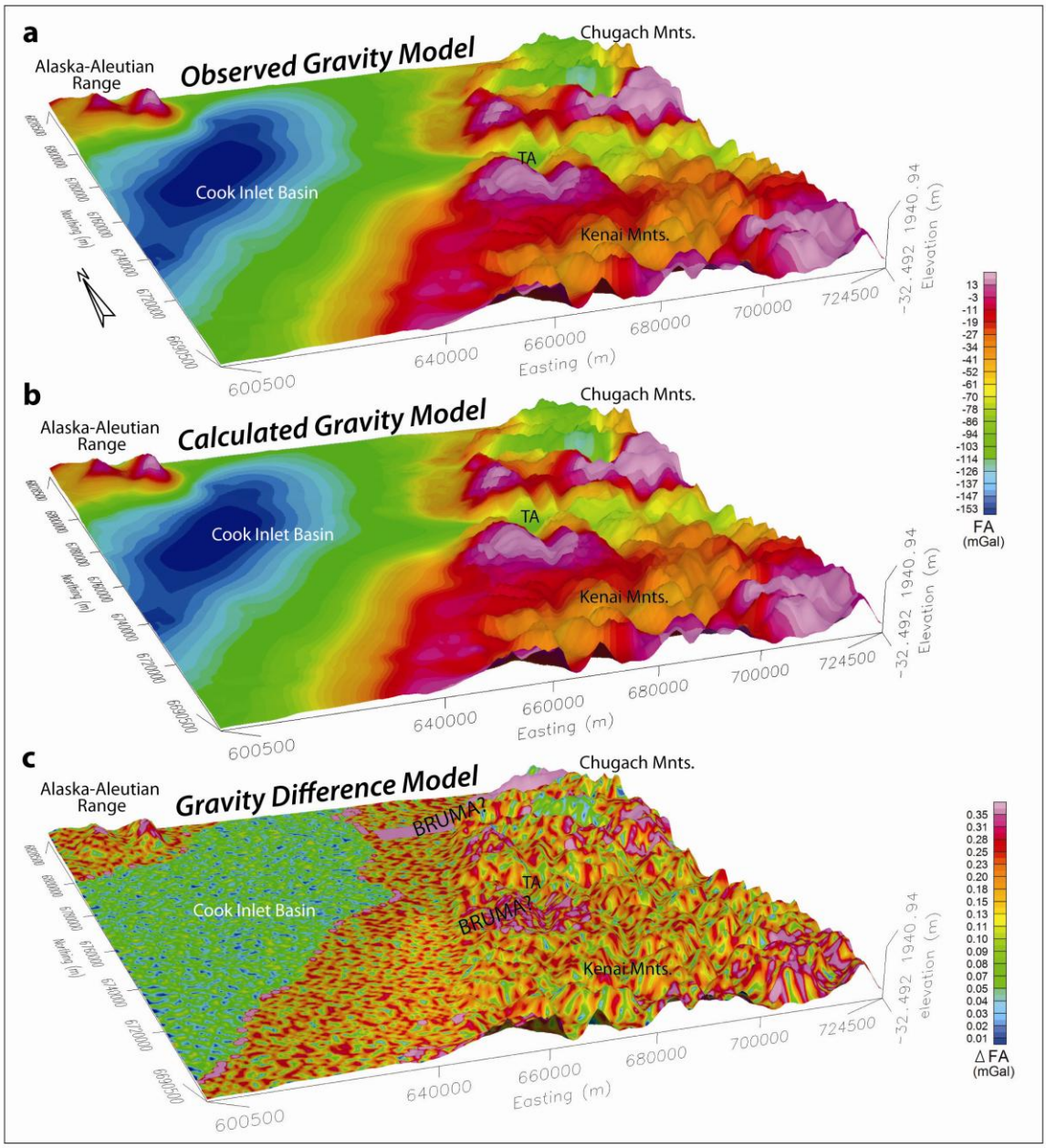


Figure 3.4: a) Free air anomaly model from observations, b) Calculated free air anomaly model from the "a priori" starting model, and c) Differences between observed and calculated gravities. TA is the Turnagain Arm.

### 3.7.2 3D Density Solution Models from Inversion

Figure 3.5 shows gridded density solution models computed from the inversion method. The density solution models are compared to *"a priori"* density models determined from gridded models of the 2D density cross-section models (Mankhemthong, et al., in press). These model comparisons help us to determine how density misfits between the *"a priori"* and final density models may be related to specific subsurface features. Figure 3.5 shows density distributions for *"a priori*" inversion models and residuals for the five surfaces extending from the topographic ground surface (a) to horizontal surface layers with tops at 5-km (b), 10-km (c), 15-km (d), and 25-km (e) depths below sea level.

The Figure 3.5a *"a priori"* model shows the mapped surface geology consisting of water (blue), surface sediments (yellow), and accretionary complex rocks (orange/red). All calculated misfits between the *"a priori"* and calculated models give positive values that reflect the greater densities calculated from inversion. We divided the misfits into two ranges; misfit lows (10–50 kg/m$^3$) and misfit highs (100–150 kg/m$^3$). The density solutions with misfit lows are observed over topographi highs. However, higher misfit values are observed on some topographically high regions of the accretionary complex terrane (Fig. 3.5a). The higher misfit over the Turnagain Arm region may be caused by very high density contrasts (1000 and 2730 kg/m$^3$) or misestimated densities along the geological contacts. The higher misfits over the Kenai-Chugach Mountains and Alaska-Aleutian Ranges may be more related to the heterogeneous lithology of the mountain rocks that are covered with glacial deposits and weathered sediments that the inversion tends to misinterpret. In addition, the BRUMA along the western Chugach Mountains front exposure (Pavlis and Roeske, 2007) that was ignored in the *"a priori"* model may cause the density misfit highs over this region.

Results of density solution models shown in Figures 3.5b-3.5d at depths of 5, 10, and 15 km are similar with four main density units: basin sediments, basement rocks, the BRUMA, and accretionary complex rocks. The calculated BRUMA density is ~3200 kg/m$^3$ which is greater than computed

densities of surrounding geologic units of the accretionary complex and the Peninsular Terrane basement rocks. The density misfits of the accretionary complex and the Peninsular Terrane basement rocks show positive values with small ranges (100-120 kg/m$^3$). The greater misfits over the Cook Inlet basin rocks may reflect varying density of sediments or misapproximation of basin shape. The maximum misfit densities in these depth slices are observed over the BRUMA belt and appear as bull's eye features that may be caused by an interpolation limitation used in the process of the constructing "*a priori"* density models. Figure 3.5e shows density solutions at a depth of 25 km. The *"a priori"* model consisted of three density units of serpentinized basement, the Peninsular Terrane basement, and accretionary complex rocks, whose density solutions are slightly different (<300 kg/m$^3$) and are close to our estimated *"a priori*" uncertainties (200 kg/m$^3$) of the density mismatches. The larger mismatch may reflect decreasing density resolution with increasing distance from the ground surface.

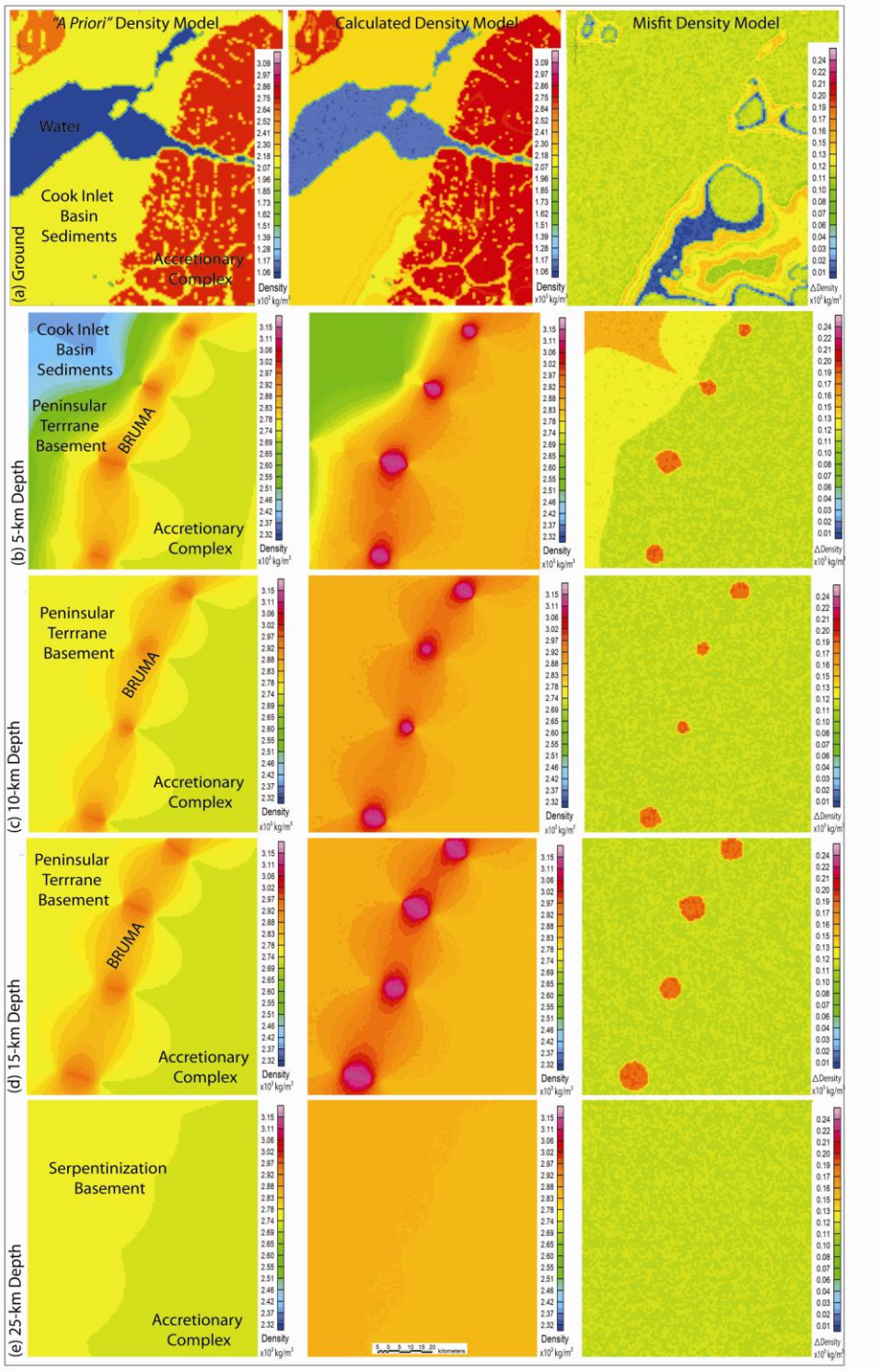


Figure 3.5: Model comparisons between *"a priori"* density (left), calculated density (middle), and density misfit (right) at ground surface (a) and horizontal surfaces at depths of 5 (b), 10 (c), 15 (d), and 25 (e) km. The densities/misfit densities are in g/cm$^3$.

### 3.7.3 Structures on the Border Ranges Fault and the Border Ranges Ultramafic and Mafic Assemblage

We applied a horizontal gradient grid analysis in a northwest direction, which is generally perpendicular to the strikes of the BRUMA and BRFS structures, to the three surface density solution models at depths of 5, 10, and 15 km,. The strongest positive gradients (pink anomalies on Figs. 3.6b-d, and 3.7b-d) indicate where abrupt density changes occur across the geologic contact from the accretionary complex (~2730 kg/m$^3$) to the BRUMA (~2950 kg/m$^3$). The negative gradients (blue anomalies on Figs. 3.7b-d) are abrupt density changes across the geologic contact from the BRUMA to Peninsular basement rocks (2750 kg/m$^3$).

The approximate location of the maximum positive gradient for each depth slice is projected to the surface to indicate the BRFS traces (Figs. 3.6). The gradient analysis shows an approximate dip of 50$^o$-80$^o$ for the BRFS. A major segment of the BRFS appears to dip moderately (50$^o$-70$^o$) along the central Kenai Mountains front and more steeply (70$^o$-80$^o$) along the northern Kenai-Chugach Mountains front. The northern segment of the BRFS with almost vertical dip supports previous geophysical models of BRFS structure (e.g. Burns 1982; Green, 2003) and evidence for strike-slip motion along the mapped surface fault scraps in the northern Chugach Mountains (Pavlis and Roeske, 2007).

A similar technique was used to determine locations for the BRUMA. Its bounds are drawn based on the strongest positive and negative horizontal gradients at depths of 5, 10, and 15 km and projected to surface (Fig. 3.7). The BRUMA belt is constrained to be ~10 km wide at 5-km depth and to increase in width to 15-20 km at 15-km depth (Fig. 3.7a). The BRUMA belt seems consistent with mapping studies of ultramafic exposures in the northern Chugach Mountain region (Pavlis and Roeske, 2007). In addition, the BRUMA is modeled as having a trapezoidal shape (Inset, Fig. 3.7) associated with its formation from fragmented upper mantle rots and the Jurassic arc that was sliced and thrust upward during Late - Mesozoic and Early Cenozoic times (e.g., Burns, 1982).

The green circle drawn on Figures 3.6a and 3.7a indicates a region where we could not constrain the structures of the BRFS and BRUMA based on horizontal gradient grid analysis because we lack sufficient gravity constraints. The abnormally shifted patterns of the BRFS and BRUMA in the region may be related to lack of gravity data constraints (Fig. 3.1). A discontinuity between the northern and southern BRFS and BRUMA is another possible reason for this abnormal pattern. However, without additional gravity information, we could not draw any firm conclusions on the geometry of geologic structures beneath the circled region.

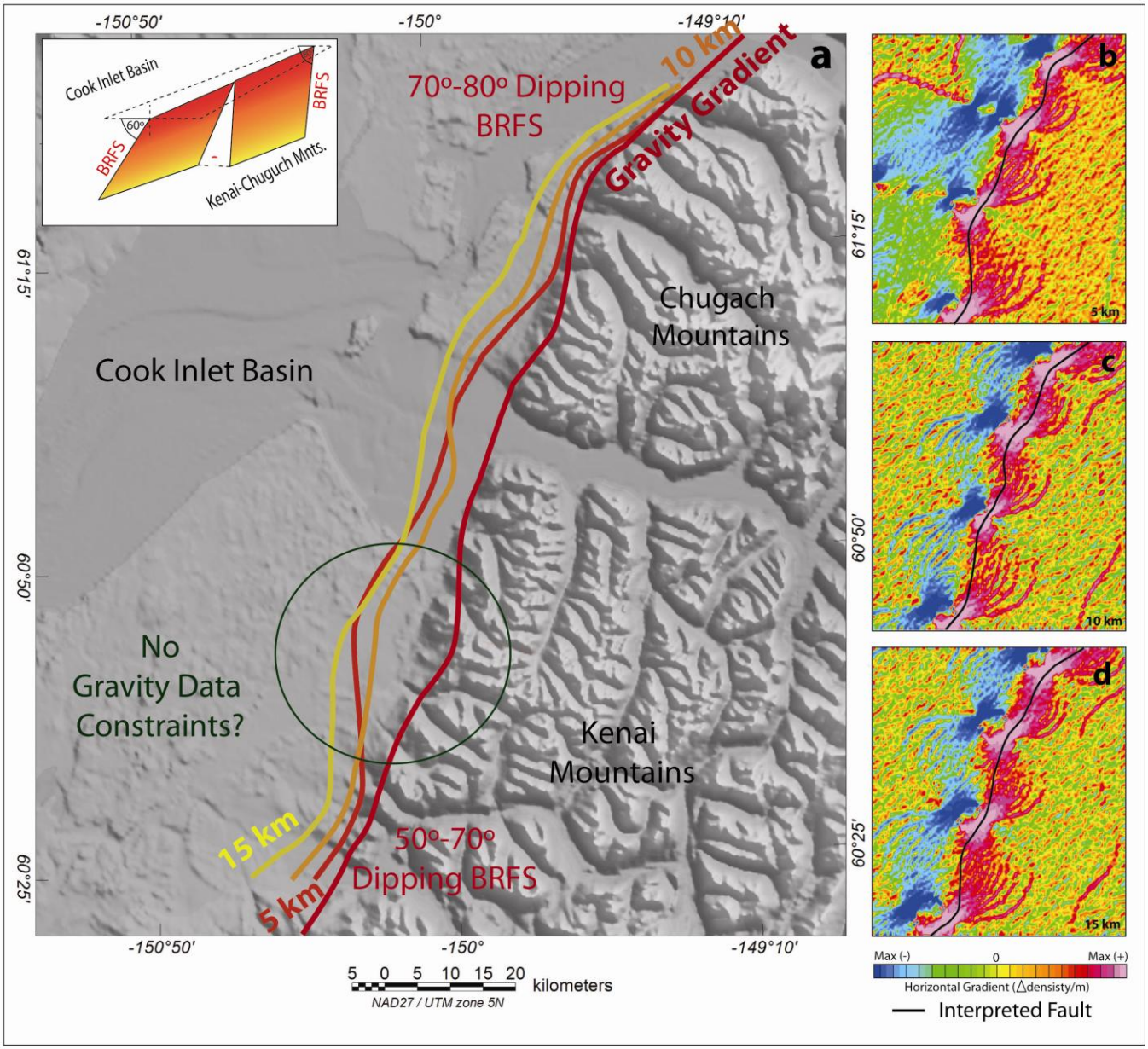


Fig. 3.6: a) Structural constraints on the Border Ranges fault system (BRFS) based on horizontal gradient analysis of the inversion results at depths of 5-km (b), 10-km (c), and 15-km (d). Top inset is a 3D cartoon showing structure of the BRFS based on these gradient analysis results.

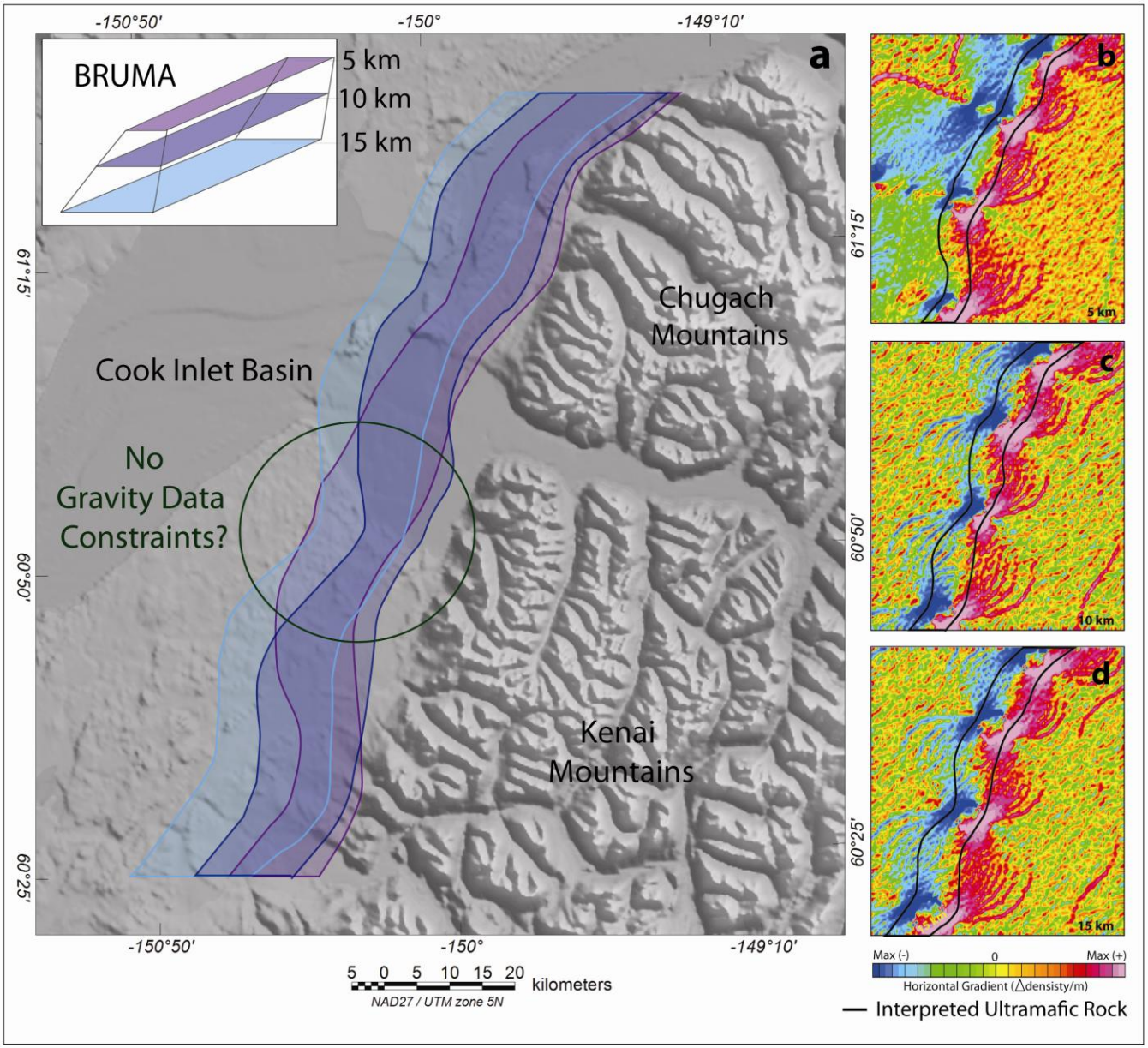


Fig. 3.7: a) Structural constraints on the Border Ranges ultramafic and mafic assemblage (BRUMA) bounds based on horizontal gradient analysis of the inversion results at the depths of 5-km (b), 10-km (c), and 15-km (d). Top inset is a cartoon showing 3D perspective model of the BRUMA based on the results of the gradient analysis.

## 3.8 CONCLUSIONS

Results of this study show the 3D inversion of new gravity data is capable of constraining the simple shape of the structures beneath the Border Ranges Fault System (BRFS) and Border Ranges ultramafic and mafic assemblages (BRUMA) using a block model technique. The calculated total gravity contribution reflects estimated surface densities used in the inversion for the entire study area and has a misfit less than 0.2 mGal, except in the region where the BRUMA is locally exposed. The calculated density distributions have uncertainties that correspond to their geologic constraints with the density misfits around 10-100 kg/m$^3$. Regions containing higher misfit densities (>100 kg/m$^3$) are related to miscalculated densities along geologic terrane boundaries that ignored more heterogeneous density distributions, more complicated 3D structures or multiple layered rock units, or truncated geologic shapes due to approximating geology with a block model. When horizontal grid analysis is applied to the computed density solution models the approximate shape of the structures of the BRFS and BRUMA can be estimated. The BRFS dips toward the northwest with a steeper dip (70$^o$ to 80$^o$) along the northern section that correlates well with previous geologic and geophysical studies that suggest strike-slip motion occurred along the BRFS in this region. The gradient analysis suggests a trapezoidal shape for the BRUMA with 10-km wide top at 5 km depth and a 20-km wide bottom at 15 km depth that corresponds to its formation as slivers of oceanic crust and mantle thrust upward during Late Mesozoic time. In one region where gravity coverage is poor a reversal of dip/structure is suggested. This may reflect lack of data or segmentation of the system.

## 3.9 FUTURE WORK

The models presented in this study were computed from averaged theoretical block models where the extent of real geologic surfaces and bodies were approximated and often cut off or ignored. These density models tended to misinterpret the true geologic geometry. For example, the depth of the Cook Inlet basin was cut off at 5 km (Circle in Fig. 3.8 left) compared to the more reasonable depths of

6-10 km interpreted from the 2D gravity modeling (Circle in Fig. 3.8 right). Thus, the inversion solutions may contain unexpected highly errors because of the smearing and interpolation problems found in the starting model.

In our next step, we will construct an *"a priori"* density model based on more realistic structural surfaces that are allowed to have arbitrary shapes instead of the block interpolations of bodies at flat lying depths (Fig. 3.8). We will include the surfaces consisting of the bathymetry surface of Cook Inlet, the bottom of basin sediments (based on well log and seismic estimates), the top and bottom of the BRUMA, the bottom of the crustal basement (or Moho), and the top of the accretionary complex that assumed to be the same surface of the BRFS fault plane (Fig. 3.9). The *"a priori"* densities will be as same as those used previously (Table 3.1). We would go to uncertainties of at least ±500 kg/m$^3$ which include more reasonable uncertainties to allow inversion to search wide space.

We expect to achieve more accurate and reasonable density solution models with this approach. We will produce several alternative starting models by varying the body proportions (depths) or/and densities. For example, the BRFS could be extended to base of crust or become listric at 15 km depth or a block of the BRUMA could be added to the "*a priori"* ground surface density model.

.

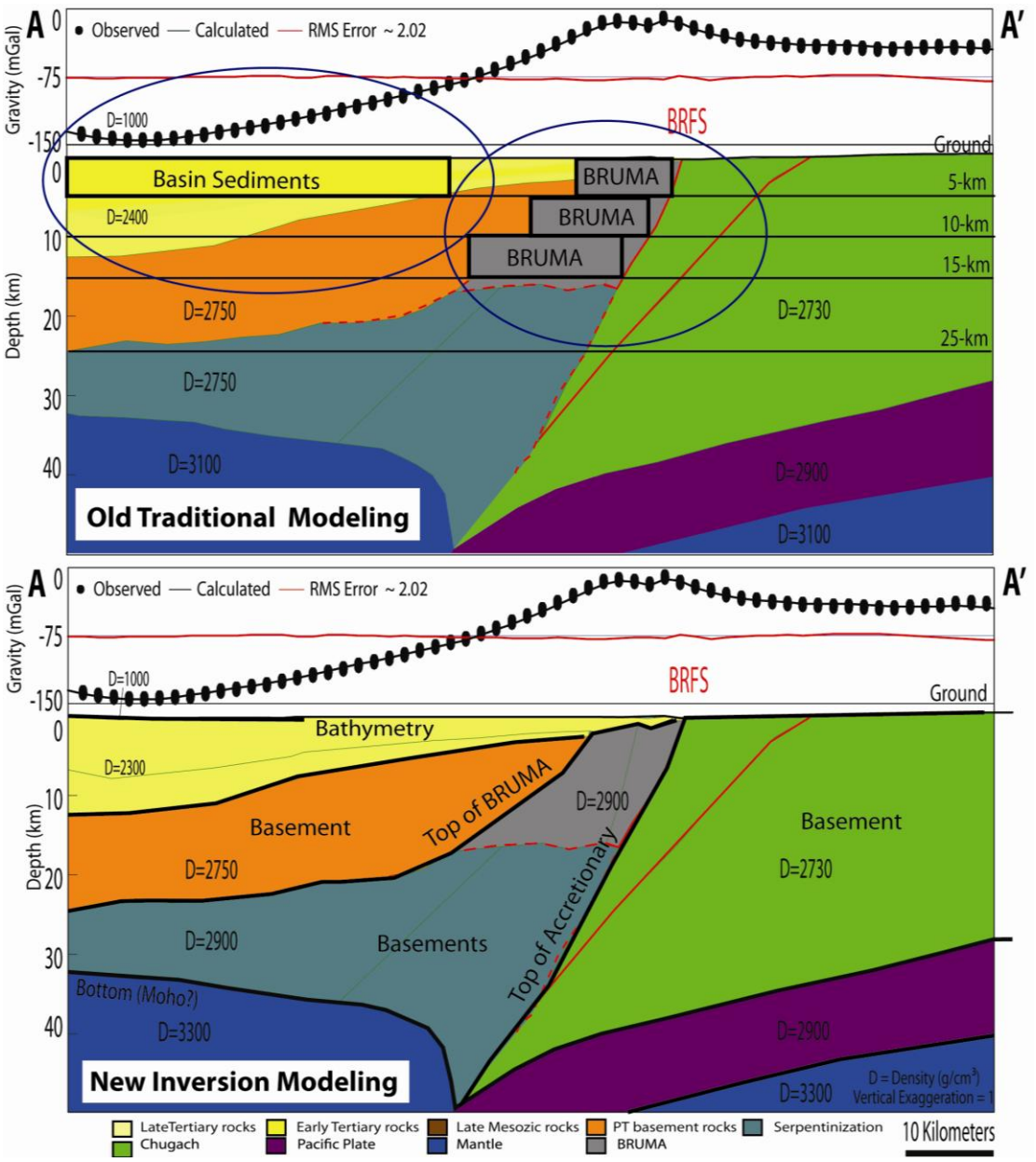


Figure 3.8: Comparison showing how the "a priori" model was built from the original 2D models in two different techniques. An old traditional inversion model was from simple block models with flat layers (bold solid rectangles in a top figure) and subsequent inversion models will be based on real geologic surfaces (bold lines in the bottom figure). Blue circles show true geologic structures were truncated by the block interpolation technique.

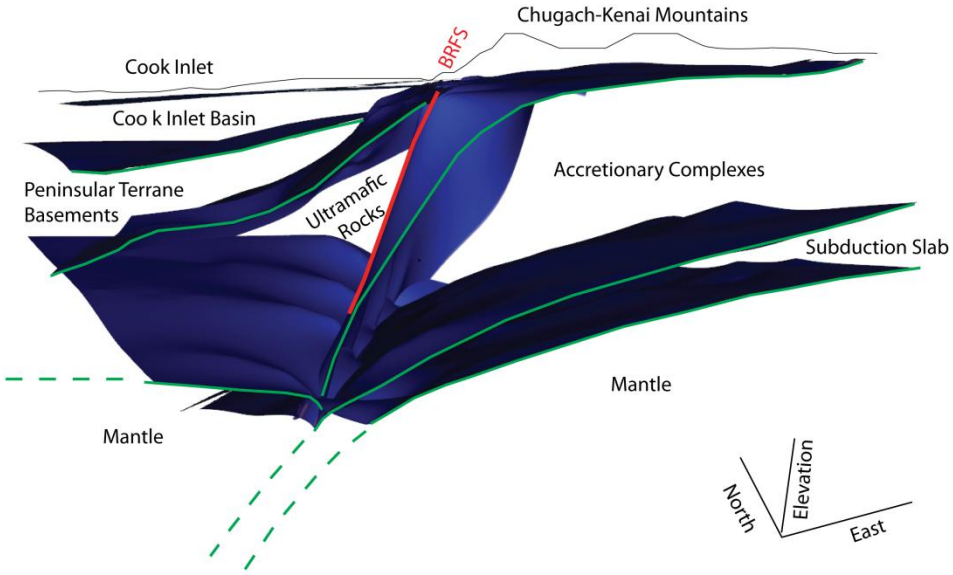


Figure 3.9: 3D perspective of multiple surfaces illustrating the topography, bathymetry, shape of the bottom of the Cook Inlet bottom, top and bottom of the BRUMA, and Moho. These will be used for "a priori" depth constraints in the next stage of 3D inversion modeling.

## 3.10 ACKNOWLEDGEMENTS

We are grateful to G. Kaip, B. Eslick, S. Jones, and P. Budhathoki for helping collect gravity data in 2009- 2011. We acknowledge P. Haeussler and T. Pavlis for discussions related to the geological background and geophysical modeling of the study area and P. Haeussler and K. Haeussler for housing the field crews during the 2010 and 2011 field seasons. We thank L. Sandoval, E. Patlan, and C. Montana for advice regarding the modeling techniques and resolving modeling software problems. This research was funded through the American Chemical Society's Petroleum Research Fund (grant no. 48312-AC8) to D. Doser.

## 3.11 REFERENCES


Backus, G, and Gilbert, F., 1970. "Uniqueness in the inversion of inaccurate gross Earth data", Philosophical Transactions of the Royal Society of London: Series A, Mathematical and Physical Sciences, Vol. 266, No. 1173, pp. 123-192.

Baker, M.R., Crain, K., 2001. SURFGRAV html user's guide, Unpublished document, Geomedia Research and Development, El Paso, Texas, 20 pp.

Boulanger, O. and Chouteau, M., 2001. Constraints in 3D gravity inversion. Geophysical Prospecting, 49: 265–280. doi: 10.1046/j.1365-2478.2001.00254.x

Burns, L.E., 1982. Gravity and aeromagnetic modeling of a large gabbroic body near the Border Ranges fault, southern Alaska. U.S. Geol. Survey Open File Rep. 82-0460, 66 pp.

Cardenas, R, 2011. Software development for a 3-D gravity inversion and application to study of the Border Ranges fault system, south-central Alaska [M.S. proposal]: El Paso, University of Texas at El Paso, 59 pp.

Clift, P.D., Pavlis, T., DeBari, S.M., Draut, A.E., Rioux, M., Kelemen, P.K., 2005. Subduction erosion of the Jurassic Talkeetna-Bonanza arc and the Mesozoic accretionary tectonics of western North America. Geology, 33, 881–884.

Crain, K., 2006. Three dimensional gravity inversion with a priori and statistical constraints. Ph.D. dissertation, The University of Texas at El Paso, United States -- Texas. Retrieved July 29, 2012, from Dissertations & Theses @ University of Texas - El Paso.(Publication No. AAT 3242138).

DeBari, S.M., and Coleman, R.G., 1989. Examination of the deep levels of an island arc, the Tonsina Ultramafic-Mafic Assemblage, Tonsina, Alaska. Journal of Geophysical Research, 94, 4373-4391.

Fisher, M.A., and von Huene, R., 1984. Geophysical investigation of a suture zone: The Border Ranges fault of southern Alaska. Journal of Geophysical Research, 89, 11,333-11,351.

Fuis, G., and Plafker, G., 1991. Evolution of deep structure along the Trans-Alaska Crustal Transect, Chugach Mountains and Copper River Basin, southern Alaska. Journal of Geophysical Research, 96, 4229-4253.

Gatto, L.W., 1976. Baseline data on the oceanography of Cook Inlet, Alaska. U.S. Army Corps of Engineers, CRREL Rept, 76-25, 81.

Gesch, D., Oimoen, M., Greenlee, S., Nelson, C., Steuck, M., and Tyler, D., 2002. The National Elevation Dataset. Photogrammetric Engineering and Remote Sensing, 68, 5-11.

Gesch, D.B., 2007. The National Elevation Dataset, in Maune, D., ed., Digital Elevation Model technologies and applications: The DEM Users Manual, 2nd Edition: Bethesda, Maryland. American Society for Photogrammetry and Remote Sensing, 99-118.

Haeussler, P.J., and Saltus, R.W., 2011. Location and extent of Tertiary structures in Dumoulin, J.A., and Galloway, J.P., ed., Cook Inlet Basin, Alaska, and mantle dynamics that focus deformation and subsidence: in Studies by the U.S. Geological Survey in Alaska 2008–2009: U.S. Geological Survey Professional Paper, 1776-D, 26 pp.

Khatun, S., Doser, D.I., Imana, E.C., and Keller G.R., 2007. Locating Faults in the Southern Mesilla Bolson, West Texas and Southern New Mexico, Using 3-D Modeling of Precision Gravity Data. Journal of Environmental & Engineering Geophysics, 12, 149-161.

Khatun, S., 2003. A precision gravity study of the Southern Mesilla bolson, West Texas. M.S. dissertation, The University of Texas at El Paso, United States -- Texas. Retrieved July 29, 2012, from Dissertations & Theses @ University of Texas - El Paso.(Publication No. AAT EP10570).

Lim, E., Eakins, B.W., and Wigley, R., 2009. Coastal Relief Model of Southern Alaska, National Geophysical Data Center, NESDIS, NOAA.

Little, T.A., and Naeser, C.W., 1989. Tertiary tectonics of Border Ranges fault system, Chugach Mountains, Alaska: deformation and uplift in a forearc Setting. Journal of Geophysical Research, B4, 4333-4359.

Mankhemthong, N., Doser, D.I., Baker, M.R., 2012. An inversion to determine surface bulk density determination variations across the Border Ranges fault system, central Kenai Peninsula, Alaska: Journal of Environmental & Engineering Geophysics, v.17, p. 9-12.

Mankhemthong, N., Doser, D. I., Pavlis, T.L., Interpretation of gravity and magnetic data and development of 2D cross-sectional models for the Border Ranges fault system, south-central Alaska, Geosphere, (in press).

Pavlis, T.L., and Roeske, S.M., 2007. The Border Ranges fault system, southern Alaska, in Ridgway, K.D., Trop, J.M., Glen, J.M.G., and O'Neill, J.M., eds., Tectonic growth of a collisional continental margin: Crustal evolution of southern Alaska: Geological Society of America Special Paper 431, p. 95-128.

Plafker, G., Nokleberg, W., and Lull, J., 1989. Bedrock geology and tectonic evolution of the Wrangellia, Peninsular, and Chugach terranes along the Trans-Alaska Crustal Transect in the Chugach Mountains and southern Copper River Basin, Alaska. Journal of Geophysical Research, 94, 4255-4295.

Plafker, G., Moore, J.C., and Winkler, G.R., 1994. Geology of the southern Alaska margin, in Plafker, G. and Berg, H.C., eds., The geology of Alaska: Boulder, Colorado, Geological Society of America. The Geology of North America, G1, 389-449.

Tarantola, A., and Valette, B., 1982. Generalized non-linear inverse problems solved using least squares criterion: Review of Geophysics and Space Physics, 20, 219-232.

Trop, J.M. and Ridgway, K.D., 2007. Mesozoic and Cenozoic tectonic growth of southern Alaska: A sedimentary basin perspective: in Tectonic growth of a collisional continental margin: crustal evolution of southern Alaska. Geological Society of America Special Paper 431, 55-94.

Wilson, F.H., Hults, C.P., Schmoll, H.R., Haeussler, P.J., Schmidt, J.M., Yehle, L.A., and Labay, K.A., 2009. Preliminary geologic map of the Cook Inlet region, Alaska. US Geol Survey Open-File Rep. 2009-1108.

# SECTION 4

# Appendix

## 4.1 A COVER LETTER

December, 5th, 2012

Dear the editor (s),

Please find the attached manuscript: "Estimation of Near Surface Bulk Density Variations across the Border Ranges Fault System, Central Kenai Peninsula, Alaska" by Mankhemthong et al. (2012), that was recently published in the Journal of Engineering and Environmental Geophysics.

I request a permission to reproduce this paper as a chapter of my PhD dissertation. I am the first author on this manuscript. All my co-authors have seen and agreed using this paper as a chapter of my doctoral dissertation with the content of the manuscript. This paper will not be used in any other publication except my Ph.D. dissertation.

Sincerely yours,

Niti Mankhemthong,

December, 17th, 2012

Dear the editor (s),

Please find the manuscript (Ms. No. GS833R2): "Interpretation of Gravity and Magnetic Data and Development of 2D Cross-Sectional Models for the Border Ranges Fault System, South-Central Alaska" by Mankhemthong et al., that was recently accepted for publication in the Geosphere.

I request a permission to reproduce this paper as a chapter of my PhD dissertation. I am the first author on this manuscript. All my co-authors have seen and agreed using this paper as a chapter of my doctoral dissertation with the content of the manuscript. This paper will not be used in any other publication except my Ph.D. dissertation.

Sincerely yours,

Niti Mankhemthong,

# Vita

Niti Mankhemthong was born in Uttaradit, Thailand in 1981. He started studying Geology at Chiang Mai University and received his Bachelor of Sciences in Geology in 2004. He journeyed to the USA in 2006 and earned his Master of Sciences in Geophysics from the University of Nevada, Reno in 2008. Then in 2009, he joined a doctoral program in Geophysics at the University of Texas at El Paso.

Niti Mankhemthong received a research assistantship and worked as a geophysical research assistant position with Dr. Diane Doser, who was his mentor and advisor, from 2009 to 2010. He has worked as a teaching assistant position since 2010. In addition, he volunteered to co-chair "The 26th Annual UTEP Geological Sciences Colloquium" in 2012.

Nit Mankhemthong has presented his research work at several international geological, geophysical, and science conferences since 2007. He was awarded the best poster presentation from the GRC 31th Annual Meeting, Reno in 2008. He published one publication with the Geothermal Resources Council Transactions in 2008 and with the Journal of Environmental & Engineering Geophysics in 2012.

Niti Mankhemthong's primary research interest is in exploration geophysics. His dissertation is entitled "Constraints on the Structure of the Border Ranges Fault System, South Central Alaska from Integrated 3-D Inversion of Gravity/Magnetic Data".

Niti Mankhemthong will work as a lecturer at Chiang Mai University after graduation.

Permanent address: 91 M.14, Phajuk, Muang Uttaradit, Uttaradit, Thailand 53000

niti.ace@gmail.com

This dissertation was typed by Niti Mankhemthong